Title

Joint Feedback Feedforward Data Driven Control Design and Input Shaping Techniques for Multi Actuator Hard Disk Drives

Author

Shah, Prateek

Publication Date

2020

Peer reviewed|Thesis/dissertation

Joint Feedback Feedforward Data Driven Control Design and Input Shaping Techniques for Multi Actuator Hard Disk Drives

by

Prateek Shah

A dissertation submitted in partial satisfaction of the

requirements for the degree of

Doctor of Philosophy

in

Engineering - Mechanical Engineering

in the

Graduate Division

of the

University of California, Berkeley

Committee in charge:

Professor Roberto Horowitz, Chair
Assistant Professor Mark Mueller
Associate Professor Javad Lavaeiyanesi

Summer 2020

Joint Feedback Feedforward Data Driven Control Design and Input Shaping Techniques for Multi Actuator Hard Disk Drives

Abstract

Joint Feedback Feedforward Data Driven Control Design and Input Shaping Techniques for Multi Actuator Hard Disk Drives

by

Prateek Shah

Doctor of Philosophy in Engineering - Mechanical Engineering

University of California, Berkeley

Professor Roberto Horowitz, Chair

With rapidly rising demand for cloud storage, there is an increasing need for more efficient data storage options. Seagate Technology PLC unveiled the multi actuator drive technology in December 2017, a breakthrough that can almost double the data rate transfer performance of future generation hard disk drives [44].

A standard hard disk drive has a single actuator arm controlling the position of eight read/write heads onto corresponding eight rotating disks. The multi actuator technology will equip drives with two actuator arms operating independently on the same pivot point, controlling four read/write heads each. Each actuator arm has a voice coil motor (VCM) connected in series with a micro actuator (MA). The read/write head is mounted at the edge of the MA. Each actuator arm has two operation modes, first - the track following mode - the actuator arm positions the read/write head onto a data track for data recording. This mode requires precision positioning of the read/write head for the smooth functioning of the hard disk drive. Second - the track seeking mode - the actuator arm sweeps through data tracks to settle onto a new desired track to initiate track following. This operation mode generally generates considerable vibration.

The multi actuator drive technology has induced new control challenges. Since, two actuator arms are operating independently on the same pivot timber, the control forces and torques generated by one actuator arm can adversely affect the performance of the other actuator arm. In this dissertation, feedforward data driven control design methodologies are presented to suppress the vibration imparted by the neighboring track seeking actuator arm onto a track following actuator arm. Also, joint feedback-feedforward data driven control design methodologies are presented to stabilize the closed loop system of the track following actuator, minimize the position error of the read/write head and, suppress the imparted vibration by a neighboring actuator arm.

Traditionally, in the model based design approach, models are fitted to frequency response measurements and, controllers are designed based on these models. In the data driven control design methodology, controllers are obtained directly based on the frequency response measurements of the system, avoiding model mismatch. Multiple frequency response measurements of the system and the imparted vibration are considered simultaneously in the design process, ensuring robustness of the control design.

Mixed $H_2 - H_\infty$ norm control design optimization problems, in the frequency domain, are formulated to obtain the feedforward and feedback controllers for the multi actuator drive. H_2 norm conditions are transformed into a locally convex objective function requiring an initial stabilizing controller for minimization. H_∞ norm conditions are transformed into necessary and sufficient convex constraints guaranteeing closed loop stability of the control system and providing an initial stabilizing controller for the H_2 norm minimization.

Application of input shaping techniques as an add-on feedforward suppression scheme for multi actuator drives is also discussed in this dissertation. Input shaping is used to suppress resonant frequencies of the coupling vibration from the excitation signal, minimizing the resultant vibration. The input shaping tool along with the data driven feedforward controller suppress up to 90 percent of the imparted vibration.

Contents

List of Figures

List of Tables

Acknowledgments

My journey at UC Berkeley has been an exciting one and it would not have been possible without my personal army of people. It is important for me to appreciate these amazing people who played vital roles in completion of this dissertation.

First and foremost I would like to express my gratitude to Prof. Roberto Horowitz for allowing me to be part of his team and guiding my research. He believed in me, encouraged me to further my research interests and inculcated skills to be a persistent researcher. His constant support has been a cornerstone during my graduate studies at UC Berkeley and I will be forever grateful for this chance to learn from him. Thank you!

I would like to thank the entire Controls group at UC Berkeley. I am indebted to my dissertation committee and qualification exam members Professor Javad Lavaei and Professor Mark Mueller for their help and advice. I am grateful to Professor Fai Ma and Professor Paul Grigas for serving on my qualification exam committee. I would especially like to thank Professor Andrew Packard who energized my research interests in the field of Controls. I must also express my gratitude to Professor Kameshwar Poolla for giving me the opportunity to serve as his teaching assistant.

My research would not have been possible without the support of the data storage industry. I sincerely thank the Advance Storage Research Consortium, Western Digital Corporation and Hitachi Global Storage Technologies for their support and guidance. I am extremely grateful to Dr. Richard Conway for aiding my research through the Western Digital - UC Berkeley collaboration. I would also like to thank Dr. Fred Hong, Dr. Kevin Tzou, Mr. Hidehiko Numasato and Mr. Shrey Khanna at Western Digital Corporation for their counsel during my internship.

I would like to thank my labmates at Computer Mechanics Laboratory - Servo Group, Omid Bagherieh, Jinwen Pan, Zhi Chen, Matthew Wright, Ruolin Li and Nikhil Potu Surya Prakash, who have assisted me throughout my research. I am especially thankful to Omid Bagherieh - my work with him is key in my realization of this research. I am grateful to Jinwen Pan for his assistance in my formative years and to my classmate Zhi Chen for sharing this journey with me.

I would like to dedicate this dissertation to my grandfather Mr Ashok Bagi. He sparked in me an interest in engineering as a child - setting me on the path that eventually led here. I am lucky to have had unconditional love from my grandmothers Mrs Jayshree Shah and Mrs Nandini Bagi and cherish their blessings and guidance.

My parents Mr Bhushan Shah and Mrs. Bharati Shah have been my lifelong pillars and cheerleaders. Thank you - everything I am today is a result of your support, efforts and sacrifices. I am also grateful for the blessings and love of my in-laws Dr Jayant Upadhye and Dr Jayshree Upadhye. I am glad to have shared this with my partner Aboli Upadhye and appreciate her encouragement and love.

Finally, I would also like to thank friends who stood by me. Niladri Chaterji, Archit Gupta, Srimukh Prasad, Chirag Modi and Kush Bhatia have been my constants at Berkeley. They have witnessed and shared all ups and downs over these years. Many thanks to

Soovadeep Bakshi, Devashish Kulkarni, Ishan Deshpande, Chinmay Kulkarni, Rahul Moghe and Sourabh Katti for all the good times - you have helped keep my spirits up.

Thank you everyone - I wouldn't be here without you.

Chapter 1

Introduction

1.1 Introduction

The demand for cloud storage is ever increasing and insatiable today [55]. The supply of data storage is falling short of the demand considerably, requiring more efficient storage options. Today, hard disk drives (HDDs) and solid state drives (SSDs) are the most widely used data storage options. HDDs are generally used in data centers, whereas, SSDs are more common in personal computing systems [29].

The structure of a hard disk drive is explained in chapter 2. The first commercial hard disk drive was manufactured and sold by IBM in 1956 [37]. And ever since, the design for HDD has evolved to increase the data storage density. A HDD comprises of an actuator arm that positions a read/write head onto a rotating disk. With an increase in the data storage density, there arises a need to develop precision positioning of the read/write head onto the rotating disk. The actuator arm is made up of two or three actuators connected in series. First we have a voice coil motor (VCM) which is the actuator with a larger stroke. Each voice coil motor is connected with a micro actuator (MA) in series. A HDD with a dual actuator setup is called a dual stage HDD [3, 14, 33]. Some hard disk drives have another micro actuator or a thermal actuator (TA) connected in series to the dual stage setup. These hard disk drives are called triple stage HDDs.

In December 2017, Seagate unveiled the 'Multi Actuator Technology', a break through that can double the data performance of the future hard disk drives at hyper-scale data centers [44]. This technology will equip drives with two independent actuator arms operating on the same pivot point. These actuator arms can either be a dual stage actuator or a triple stage actuator. Currently in the industry, we have dual stage multi actuator drives, hence, we shall present our methodologies and results for multi actuator drives with dual stage actuator arms.

In HDD Controls, we have two classes of HDD operation modes. Track following mode is when the read/write head follows a particular track on the rotating disk. This mode is when the HDD is actually reading or writing data on the rotating data disk. Feedback track

following controllers are used to stabilize the actuator arm and follow the data track with precision [59]. The data storage density of the disk is a function of the precision of these track following controllers.

Whereas, track seeking mode is when the read/write head sweeps across multiple tracks to settle onto the desired data track to initiate track following at the new desired data track. The seeking process is designed such that the track following process can be started as soon as possible while minimizing the vibration and jerk being excited by the seeking process. A minimum jerk trajectory was presented for the track seeking actuator in [41]. A model predictive control design methodology was presented to obtain the track seeking controllers in [39]. The advantages of the model predictive control design approach is that hard constraints can be used to ensure the stability of the actuator arms. But, model predictive control algorithm requires high online computation which a hard disk drive cannot offer.

The multi actuator drive technology has introduced new control design challenges. In a multi actuator drive we have two actuator arms operating independently along the same pivot timber. The control forces and torques generated by one actuator arm can affect the operation of the other actuator arm. The vibration interaction between the two actuator arms can be categorized into three scenarios. First, the vibration interaction when both the actuators are in track following mode. Second, the vibration interaction when both the actuators are in the track seeking mode. Finally, the vibration interaction when one actuator is in the track following mode and the other actuator is in track seeking mode.

The track seeking process generates a lot of vibration. Considerable vibration interaction is expected in the second and third scenario. In the third scenario, vibration disturbances will be imparted by the track seeking actuator onto the track following actuator, affecting it's performance drastically. Traditional "passive" vibration compensation techniques in large scale mechanical systems like vehicles were discussed in [20, 10, 38, 24, 30]. In this dissertation we focus on "active" vibration suppression techniques. In the past, active vibration suppression techniques were discussed in [51, 48]. Active vibration techniques are based on the simple idea of superposition of signals first published in [32].

In chapter 3, we propose data driven feedforward control design methodologies to suppress the imparted broadband vibration by the track seeking actuator to the track following actuator. Traditionally, adaptive feedforward control algorithms are used to suppress active vibration in hard disk drives [42, 50, 49, 47]. Model based frequency domain design methods were exploited to pose a classical linear quadratic Gaussian (LQG) problem with weighting filters to shape the controller effort in [18, 35, 11]. In data driven control design, the controllers are designed directly based on the frequency response measurements [9, 28, 27].

We present a sequential single-input single-output (SISO) feedforward data driven control design methodology [46] and a single-input multi-output (SIMO) feedforward data driven control design methodology. In sequential SISO design methodology, first we design a feedforward controller for VCM, to suppress the entire imparted vibration. Then, we design a feedforward controller for MA to suppress the residual vibration after VCM's feedforward compensation. Whereas, in SIMO data driven control design methodology we design feedforward controllers for VCM and MA simultaneously, to suppress the imparted vibration.

We shall also compare the performance of the two design algorithms. Dual stage vibration compensation was presented earlier in [16].

The data driven feedforward control design methodologies are based on frequency response measurements of the open-loop VCM and MA. These actuators have resonant modes [60, 6]. The frequency response measurements of the vibration imparted by the track seeking actuator on the track following actuator is also available to the designer. A multiple set of frequency response measurements of the vibration interaction are considered simultaneously to ensure robustness.

In chapter 3, we will consider a pre-designed track following data driven feedback controller obtained using the methods in [8]. A mixed $H_2 - H_\infty$ norm optimization problem is used to obtain feedback controllers for VCM and MA. The design is based on data driven techniques. Multiple frequency response measurements of VCM and MA are considered in the design process. Feedforward controllers for VCM and MA are designed based on the frequency response measurements of the open loop actuators VCM and MA, frequency response measurements of the vibration interaction between the seeking actuator and the track following actuator and the feedback controller of the track following actuator [46].

In robust control theory, dynamic uncertainties are considered in the design process [23, 62]. Multiple seeking scenarios are considered simultaneously in the feedforward control design process to ensure robustness. The vibration excited by the seeking actuator depends on the seek length and the control input of the seeking actuator. Therefore, multiple seek scenarios are simultaneously considered in the design process.

In chapter 5, we present a data driven control design methodologies design feedback and feedforward controllers of the track following actuator in a multi actuator drive. The feedback controller is designed to minimize the position error of the read/write head and stabilize the actuator arm while considering the vibration being imparted by the track seeking actuator, wind disturbances in the drive, measurement noise and runout [19, 21, 8]. Whereas, the feedforward controller is designed to suppress the imparted vibration by the track seeking actuator [47, 42, 46].

We propose two methodologies to design the feedback and feedforward controllers for the track following actuator. First, an alternating iterative data driven control design approach. We iterate alternately between the data driven feedback design and the data driven feedforward design till we achieve convergence for the controllers. Secondly, a joint feedback feedforward data driven control design approach. We simultaneously solve for the feedback and feedforward controllers to stabilize the actuators VCM and MA, minimize the position error of the read/write head and suppress the imparted vibration.

A mixed H_2 - H_∞ norm optimization problem is used to set up the control problem for the feedforward control design as well as the joint feedback feedforward control design problem. H_∞ norm conditions are used to stabilize the closed loop system [28]. H_2 norm condition is used to minimize the position error of the read/write head and suppress the imparted vibration. H_2 condition is also used to pose soft constraints on the stroke of the MA and control input of the VCM [8]. H_∞ norm conditions are posed as constraints whereas, H_2 norm conditions are posed as constraints as well as the objective function to be minimized.

The data driven H_∞ problem for SISO systems was presented in [28], the H_∞ norm condition is transformed into a necessary and sufficient convex condition. The H_∞ norm control design methodology was extended to multi-input multi-output (MISO) systems in [7, 8]. The H_∞ norm control design methodology was extended to multi-input multi-output (MIMO) systems in [27]. The H_2 norm condition was transformed to a locally convex constraint or a locally convex objective in [27, 8, 7].

A dual stage HDD is a MISO system, that is, it has two control inputs, one for each actuator, and one output, that is the position error signal of the read/write head. Therefore, an ideal controller for a MISO system is a SIMO controller as presented in [7, 8].

A mixed $H_2 - H_\infty$ norm data driven optimization problem for feedforward control design was presented in [46]. A data driven $H_2 - H_\infty$ optimization control problem is used to design feedforward controllers for both sequential SISO and SIMO control design methodologies. The application of these feedforward control design methodologies will be discussed in chapter 4.

A data driven mixed $H_2 - H_\infty$ norm optimization problem is also proposed for a joint feedback feedforward control design methodologies. The simultaneous optimization of feedback and feedforward control approaches provide better control performance and help in improving the optimization of the control problem. H_∞ norm necessary and sufficient convex constraints are used to obtain initial feedback and feedforward controllers independently. Then, the optimization problem is merged to minimize the H_2 norm of the position error of the read/write head and suppress the vibration.

An add on input shaping tool is discussed in chapter 7. Input shaping is an open loop time domain tool used to suppress the resonant frequencies from input signals of actuators [54, 40]. Input shapers can be used in the seeking actuator of the multi actuator drive. Seeking actuator of the multi actuator drive generates a lot of vibration during its seeking process affecting the neighboring track following actuator adversely. Input shaper reduces the generated vibration at the source, hence aiding in the feedforward suppression of the vibration signal by the track following actuator. The disadvantage of using an input shaper is that it adds a delay to the seeking process.

We consider two input shaping techniques, a zero vibration (ZV) input shaper and a zero vibration derivative (ZVD) input shaper [54, 40, 57, 61, 53]. Addition of an input shaper adds a delay to the seeking process. ZV input shaper adds a smaller delay but is less robust than the ZVD input shaper. It requires the suppressing resonant frequency to be known precisely. We present a data driven technique to locate the resonant frequency to be suppressed. Multiple frequencies can be suppressed simultaneously using an input shaper. But, each frequency adds a delay to the seeking process.

1.2 Contribution of Each Chapter

Chapter 2: In this chapter, the structure of a standard hard disk drive is first discussed. The standard control problems in the hard disk drive servo design field are also discussed.

The control block diagram of a multi actuator drive used to formulate the control design methodologies in this dissertation is also discussed in detail. The frequency response measurements of the actuators, the frequency response measurements of the coupling vibration and the input signals of the neighboring actuator used to design the feedback and feedforward controllers are shared in this chapter.

Chapter 3: The data driven feedforward control design methodology is presented in this chapter. The H_2 norm and H_∞ norm conditions are translated to a locally convex optimization problem. The design process assumes the feedback controller is already designed for the actuator in question. The feedforward controller is then design to suppress the vibration imparted by a neighboring actuator to the actuator in question. The algorithm chart used to solve the optimization problem in an iterative manner is also discussed in this chapter.

Chapter 4: The application of the data driven feedforward control design methodology from chapter 3 to multi actuator hard disk drives is presented in this chapter. A sequential single-input single-output (SISO) control design methodology and a single-input multi-output (SIMO) control design methodology are presented to obtain feedforward controllers for VCM and MA of the track following actuator. The sequential SISO design first obtains VCM feedforward controller to suppress the entire imparted vibration. Then, the MA feedforward controller is obtained to suppress the residual vibration. Whereas, the SIMO control design obtains VCM and MA feedforward controllers simultaneously. The design results of the two methodologies are also shown and compared in this chapter.

Chapter 5: Two joint feedback - feedforward data driven control design methodologies are presented in this chapter. First - The alternating iterative control design methodology - the feedback control design problem and the feedforward control design problem are iterated alternately. This methodology is useful for actuators being imparted by vibration disturbance for over 30 percent of their operation time, like in a multi actuator hard disk drive. The feedback controller is designed while considering the imparted vibration during the design process. Second - the simultaneous control design methodology - the feedback controller and the feedforward controller are designed simultaneously for all the actuators in the actuator arm. This methodology is more concise and obtains similar results as the alternating iterative control design methodology.

Chapter 6: The application of the joint feedback - feedforward data driven control design methodology to the multi actuator hard disk drive is presented in this chapter. The constraints and objective function for the feedback control design, feedforward control design and the simultaneous feedback - feedforward control design are discussed and compiled for a multi actuator drive. The design results of the two approaches are also compared.

Chapter 7: The application of input shaping technique as an add-on feedforward suppression tool to the data driven feedforward controllers for the multi actuator hard disk drive is discussed in this chapter. The input shaper can only suppress vibration at fixed number of frequencies. A zero vibration input shaper and a zero vibration derivative input shaper are used to suppress the resonant frequencies of the coupling vibration imparting disturbance to the track following actuator. The design results with the feedforward controller and the input shaping tool used simultaneously are also presented in this chapter.

Chapter 8: This chapter concludes the dissertation by summarizing the materials discussed in each chapter and discussing the important results. Some basic ideas to extend the theory presented in this dissertation are also discussed in the future work section.

1.3 Preliminaries

Frequency Response Data

Frequency response is the quantitative measure of the output spectrum of a system or device in response to a sinusoidal stimulus, and is used to characterize the dynamics of the system. It is a measure of the magnitude and phase of the output as a function of frequency, with respect to the input.

Estimating a frequency response for a physical system generally involves exciting the system with an input signal, measuring both input and output time histories, and comparing the two through a process called the Fast Fourier Transform (FFT).

A Fourier transform (FT) is a mathematical transform that decomposes a function (often a function of time, or a signal) into its constituent frequencies. Let, $f(t)$ be is continuous time function of time t. The continuous Fourier transform $F(j\omega)$ of $f(t)$ is given by:

$$F(j\omega) = \int_{-\infty}^{\infty} f(t)e^{-j\omega t}dt \tag{1.1}$$

Fourier transform $F(j\omega)$ is a function of frequency ω, where $\omega \in (-\infty, \infty)$, and provides magnitudes of each frequency comprised in the function $f(t)$. For a discrete time sequence $f(kT_s)$, where T_s is the sampling time, the discrete Fourier transform $F(j\omega)$ is given by:

$$F(j\omega) = \sum_{k=-\infty}^{\infty} f(kT_s)e^{-j\omega kT_s} \tag{1.2}$$

where $\omega \in [-\pi, \pi]$. The inverse discrete Fourier transform is given by:

$$f(kT_s) = \frac{1}{2\pi}\int_{-\pi}^{\pi} F(e^{j\omega})e^{j\omega kT_s}d\omega \tag{1.3}$$

The Fast Fourier Transform (FFT) is an algorithm which evaluates the discrete Fourier transform, Eq. (1.2), or discrete inverse Fourier transform, Eq. (1.3), of time sequences. Fourier analysis is used to convert sequences from time domain to frequency domain.

In this dissertation, data driven control design algorithms based on frequency response measurements are presented. Design methodology directly based on frequency response measurements will not have any model mismatch between the design process and the actual control actuator or device. We will be only considering the frequency response measurements of an actuator $G(j\omega)$ for $\omega \in \Omega$, except for finite number of frequencies that correspond to the poles of $G(z)$, in the z domain.

$$\Omega = \{\omega | -\pi \leq \omega \leq \pi\} \tag{1.4}$$

H_∞ norm

For a stable single-input single-output (SISO) system the H_∞ norm is defined as the peak gain or the largest value of the magnitude of a frequency response. Whereas, for a multi-input multi-output system, the H_∞ norm is defined as the largest singular value across the frequency range Ω.

For a SISO transfer function $H(j\omega)$, the H_∞ norm is defined as:

$$||H(j\omega)||_\infty \triangleq \sup_{\omega\in\Omega} |H(j\omega)| \tag{1.5}$$

For a $m \times n$ MIMO transfer function $H(j\omega)$, the H_∞ norm is defined as:

$$||H(j\omega)||_\infty \triangleq \sup_{\omega\in\Omega} \bar{\sigma}(H(j\omega)) \tag{1.6}$$

Here, $\bar{\sigma}(.)$ denotes the largest singular value of the matrix $H(j\omega)$. Eq. (1.7) presents an example of an H_∞ norm constraint.

$$||W_f(j\omega)S(j\omega)||_\infty \leq \gamma \tag{1.7}$$

Here, $S(j\omega)$ is the frequency response of a transfer function. $W_f(j\omega)$ is a weighting filter, in the frequency domain, used to shape $S(j\omega)$. γ is an upper limit used to set the constraint.

H_2 norm

The H_2 norm is an estimation of the system's energy and is defined as:

$$||H(j\omega)||_2^2 \triangleq \frac{1}{2\pi}\int_\Omega \mathrm{Tr}[H^*(j\omega)H(j\omega)]d\omega \tag{1.8}$$

where $H^*(j\omega) = \bar{H}^*(j\omega)$ is the complex conjugate transpose and Tr(H) is the trace of the matrix H.

According to the Parseval's theorem, H_2 norm can be used to constrain the variance of the output of a system in time domain. In the control algorithms presented in this dissertation, H_2 norm will be used to formulate constraints and objective functions to optimize the variance of signals in the time domain.

Chapter 2

Hard Disk Drive Structure

2.1 Introduction

Hard Disk Drives (HDDs) have been around for over six decades now. The first commercial hard disk drive, the IBM 350, was introduced in 1956 [25, 1]. The disk drive created a new level in the computer data hierarchy, then termed Random Access Storage but today known as secondary storage, less expensive and slower than main memory (then typically drums) but faster and more expensive than tape drives [1, 13].

The storage capacity of hard disk drives has grown exponentially since then. The IBM 350 had storage capacity of 3.75 megabytes, whereas, today's commercial desktop HDDs have a capacity of the order of 6 terabytes. Each generation of disk drives replaced larger, more sensitive and more cumbersome devices.

The spread of the Internet and the ever increasing demand for storage capacity is requiring more efficient storage options. Hard disk drives (HDDs) and solid state drives (SSDs) are the most widely used data storage options today. HDDs are now primarily used at data centers, while SSDs are used in personal computers and portable devices. [29]. Despite the decrease in the personal computing market, the demand for enterprise level hard disk drives will be growing.

In this chapter, the structure of the hard disk drive is discussed. The feedback structure used to obtain controllers is also described. Control block diagram for the new multi actuator technology [44] is introduced.

2.2 Hard Disk Drive

A modern day hard disk drive is a sealed unit containing number of platters in a stack. These platters are mounted on a flexible spindle motor to create more data storage in a smaller space. The platter has a core made up of aluminum or glass substrate, covered with a thin layer of Ferric oxide or cobalt alloy. On both sides of the substrate material, a thin coating is deposited by a special manufacturing technique. This, thin coating where actual data is

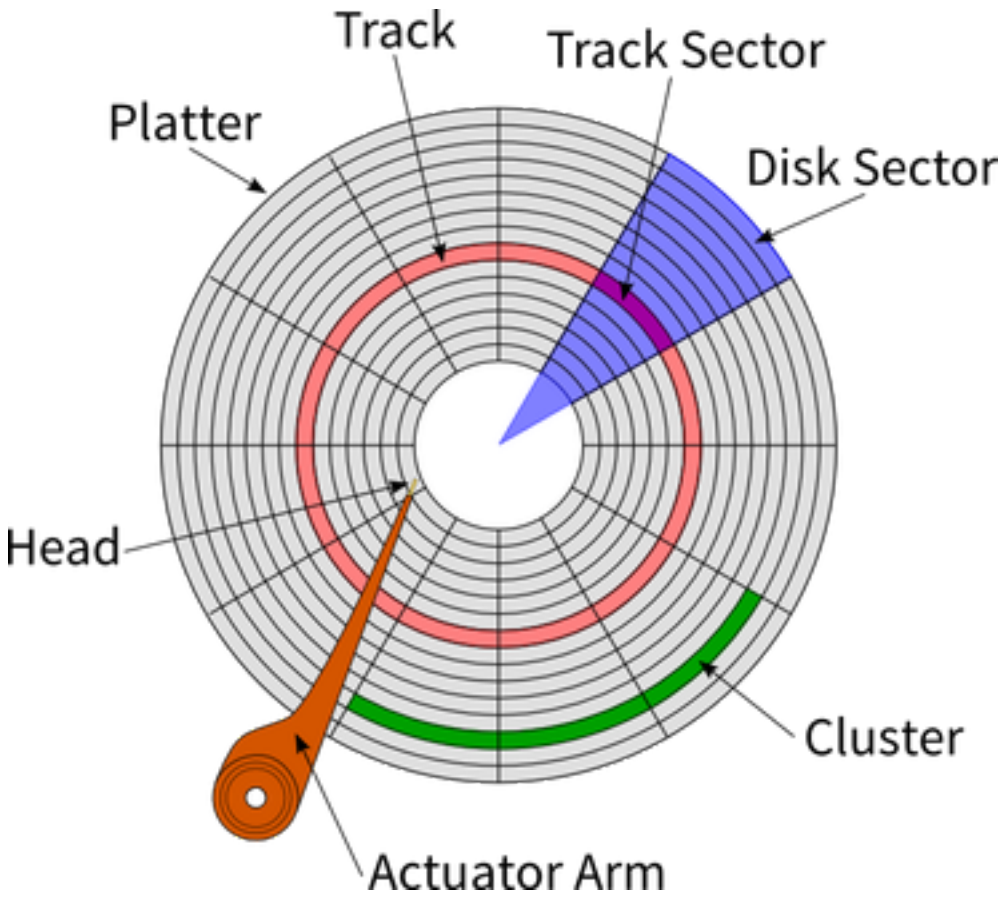

Figure 2.1: Each platter of a hard disk drive is divided into tracks, sectors and clusters. This division helps for organizing data. An actuator arm is used to position the read/write head onto the required track sector. This figure was obtained from [26]

stored is the media layer [2, 58, 17]. When the magnetic media is applied to the surface of the substrate material, a thin lubricating layer is applied to protect the material.

Each disk (platter) is divided into tracks and sectors to organize and compartmentalize data. A track is an annular ring on the disk. Each disk is divided into thousands of concentric circles known as tracks. The outer most ring is track zero, the number of tracks increases as we move towards the inner surface of the disk.

Each platter is further broken down into smaller units called sectors. A sector is the basic unit of data storage on an HDD. A single track typically can have thousands of track sectors and each track sector can hold more than 512 bytes of data. A few additional bytes are required for control structures and error detection and correction. A collection of multiple track sectors is called a cluster. Figure 2.1 shows tracks, sectors and clusters on a platter.

An actuator arm is used to position the read/write head onto the platter. The read/write heads are an interface between the magnetic media where the data is stored and electronic

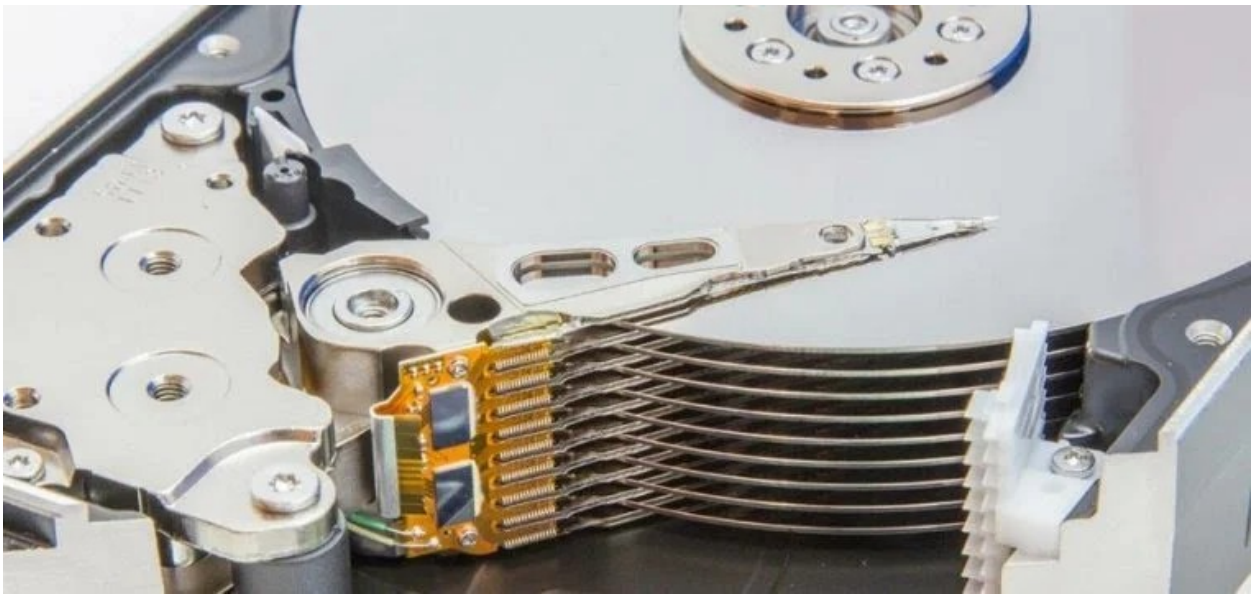

Figure 2.2: An actuator arm is used to position the read/write head onto the platter. A voice coil motor is used for large stroke movements. Whereas, a micro actuator is used for small strokes and high frequency precision. This figure was obtained from [12].

components in the hard disk drive. The heads convert the information, which is in the form of bits to magnetic pulses when it is stored on the platter and reverses the process while reading.

Figure 2.2 shows an actuator arm used to position the read/write heads onto their respective platters. The entire actuator arm is controlled using a voice coil motor (VCM) for large displacements. Whereas, each read/write head has a piezoelectric micro actuator (MA) for small precise displacements [22, 59]. This is a typical two actuator setup currently used in the industry. It is called a dual stage hard disk drive [4, 8].

Similarly, triple stage hard disk drives are being developed. [43, 45, 5]. In triple stage hard disk drives we have two piezoelectric actuators connected in series. Along with the VCM, we have a three actuator control setup to position the read/write head. Some triple stage hard disk drives also use thermal actuators as the third stage actuator [43].

2.3 Dual Stage Hard Disk Drive

With ever increasing data aerial density, there is a need for high precision servo control to achieve this ultra high positioning of the read/write head. In this section we will look at the basic HDD control problems and the control block diagram for a dual stage HDD.

Hard disk drive servo systems have three operation modes. Track following mode is when the read/write head follows a data track. This process requires very high precision. Read

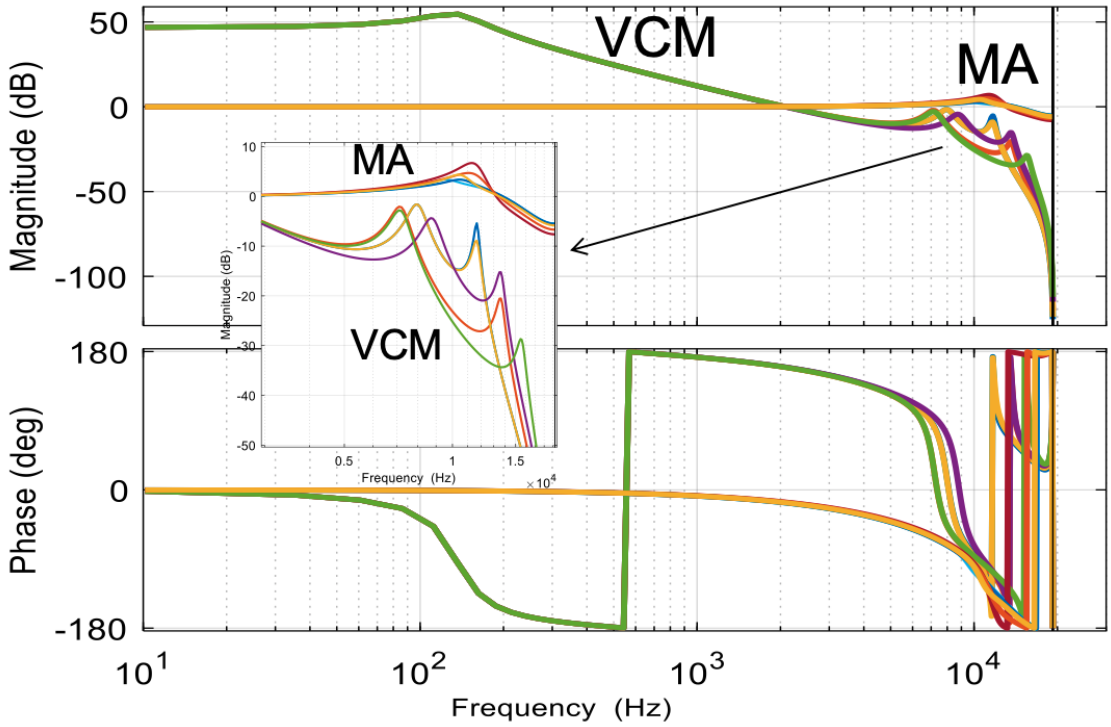

Figure 2.3: Frequency response data measurements of five VCM and MA are plotted. The frequency response measurements are from the control input of the actuators to their corresponding outputs.

and write process occurs during track following. Seeking mode is when the read/write head sweeps through data tracks to locate the desired new data track to begin track following. This process generates a lot of vibration. Finally, settling mode is the transition mode between seeking and track following. The read/write head approaches the desired new track with certain momentum, the objective of the settling mode is to smoothly settle the read/write head onto the new track while minimizing jerk [41].

The read/write head is controlled by the actuator arm. From the perspective of control design the actuator arm comprises of VCM and MA connected in series. VCM has a larger stroke but a smaller bandwidth than MA. VCM is used for low frequency large displacements movements. Whereas, the micro actuator is used for high frequency small displacements movements. The frequency response data measurements of voice coil motor and the micro actuator of five hard disk drives are plotted in Figure 2.3.

Figure 2.4 is the control block diagram of a dual stage hard disk drive. Here, r is the runout, radial noise generated by the spindle motor, a limiting factor for the performance of a HDD. e is the position error of the read/write head from the data track being followed. e is known as the position error signal or simply the PES. n is the measurement noise. w_v and

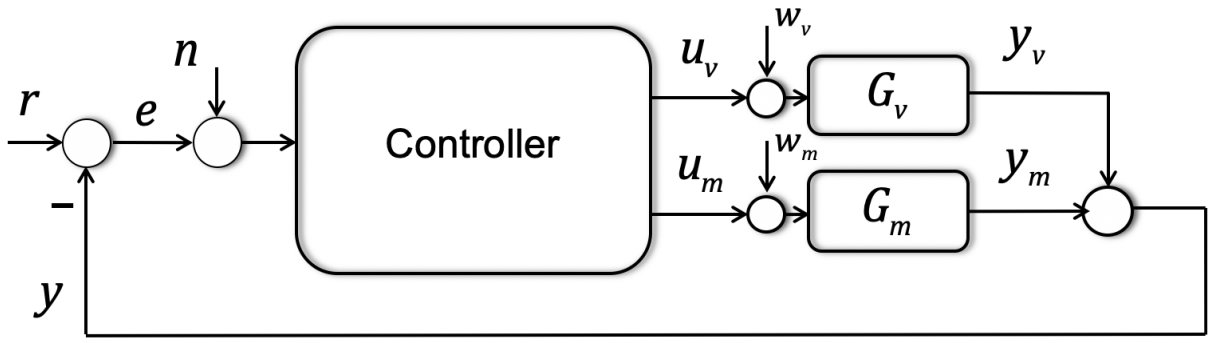

Figure 2.4: Control block diagram of a dual stage HDD is plotted. G_v and G_m are open loop transfer functions of VCM and MA. u_v, u_m are their corresponding control inputs and y_v, y_m are their corresponding outputs. r is the runout, e is the position error signal, n is the measurement noise and, w_v and w_m are wind disturbances.

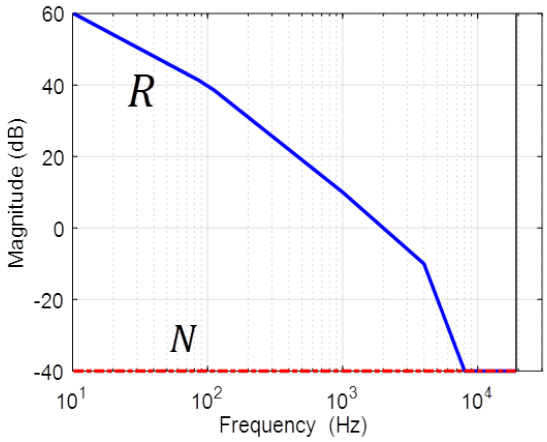

Figure 2.5: The spectrum of runout and measurement noise used for simulations in this dissertation are plotted.

w_m are wind disturbances in the hard disk drive and are commonly referred to as windage. Traditionally, HDDs were filled with air but modern HDDs use Helium to minimize windage [31]. Following the standard practice in the HDD industry, we will assume that w_v and w_m are small enough to be lumped into the runout r and the measurement noise n.

The magnitude of the frequency response of the runout r and the measurement noise n spectrum used for the simulations in this dissertation are as shown in Figure 2.5. It is a good assumption to assume that r is a colored Gaussian random noise, while, n is a white noise.

Here, $G_v(j\omega)$ and $G_m(j\omega)$ are open loop frequency response measurements of the VCM

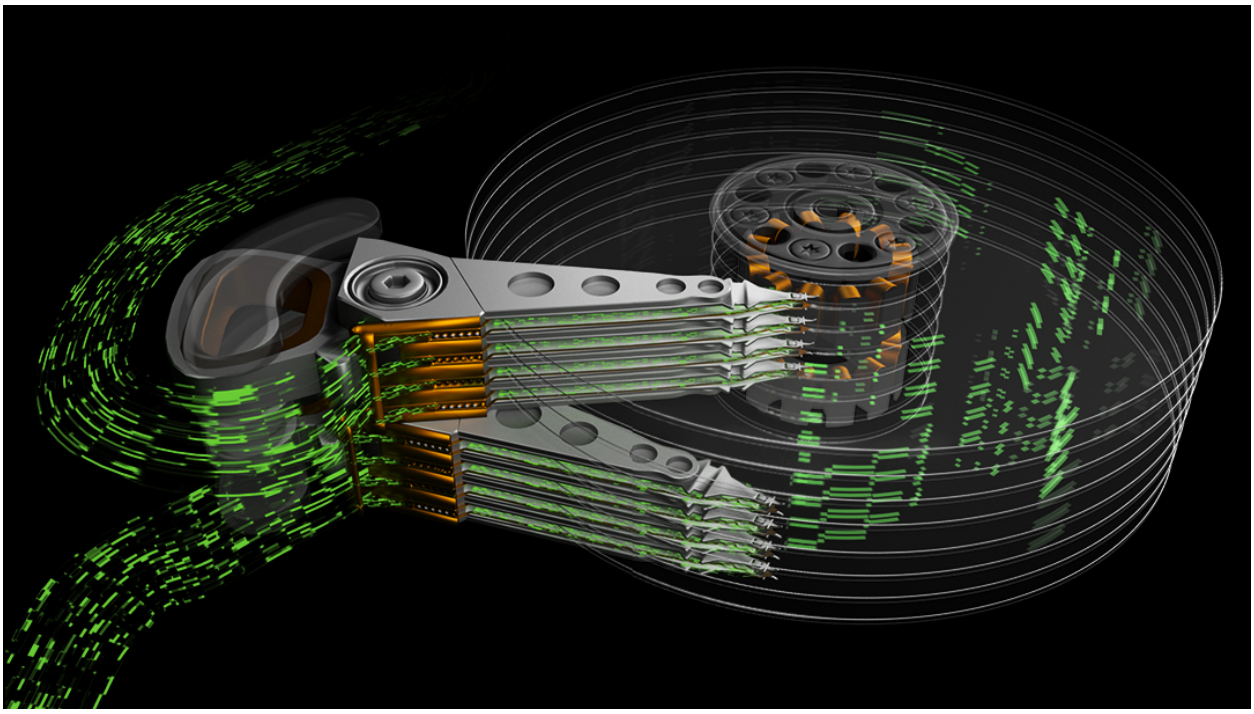

Figure 2.6: The multi actuator technology was unveiled by Seagate in 2017. This picture is taken from the Seagate announcement [44].

and MA respectively as shown in Figure 2.3. u_v and u_m are the corresponding control inputs and y_v and y_m are the corresponding outputs. The objective of the track following control design problem is to design a feedback controller to stabilize the closed loop and minimize the position error signal e [8].

In this block diagram, Figure 2.4, lowercase letters represent discrete time sequences and the uppercase letters represent transfer functions in z domain or the frequency domain.

2.4 Multi Actuator Hard Disk Drive

Multi Actuator Technology was unveiled by Seagate in December 2017 [44]. To increase the performance speed of a hard disk drive multi actuator drives will be equipped with two independently operating actuator arms as shown in Figure 2.6. The independence of the two actuator arms ensures that two read/write heads can simultaneously function. The operation of one multi actuator drive is equivalent to two simultaneous hard disk drives but at lesser power usage.

Multi Actuator technology poses new control problems. The operation of the two actuator arms can interfere with the performance of each other. There are three possible vibration interaction scenarios between the two actuator arms. First, the two actuator arms can be

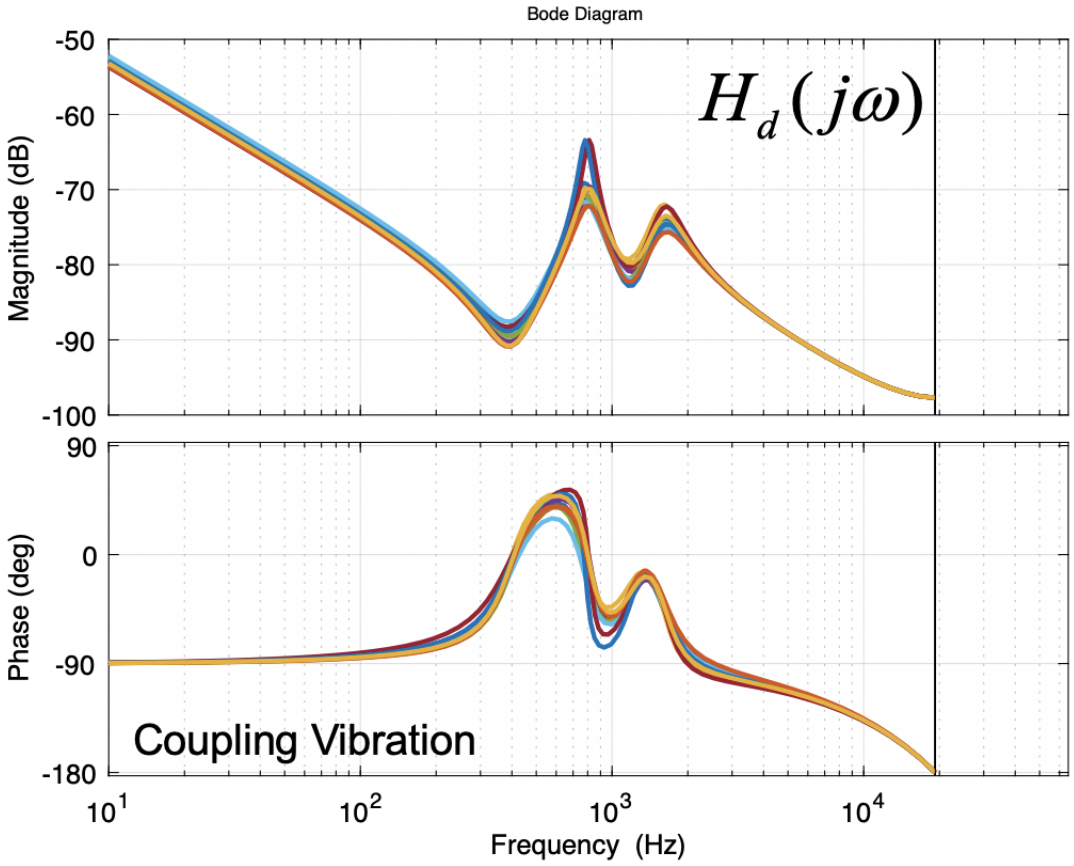

Figure 2.7: Frequency response data measurements of the coupling transfer function between the track seeking actuator arm and the track following actuator arm are shown. Data measurements are modeled based on actual frequency response measurements observed by the industry to represent the behavior but do not reveal the true data.

operating in the track following mode. Second, the two actuator arms can be operating in the track seeking mode. Third, one actuator arm can be track seeking while, the other actuator arm is track following. It is expected that scenario two and three will involve considerable vibration interaction between the two actuator arms.

In scenario two, the two actuators arms are track seeking. The vibration interaction does not result in an impaired drive read/write performance. But, in scenario three, one actuator arm is track following, the vibration interaction can adversely affect the read/write performance of this actuator arm. In this dissertation, we will focus on scenario three. We will present control design tools to suppress the vibration being imparted by the track seeking actuator arm to the track following actuator arm.

Multiple frequency response measurements of the imparted vibration will be simultaneously considered. The coupling transfer function imparting the vibration is denoted as

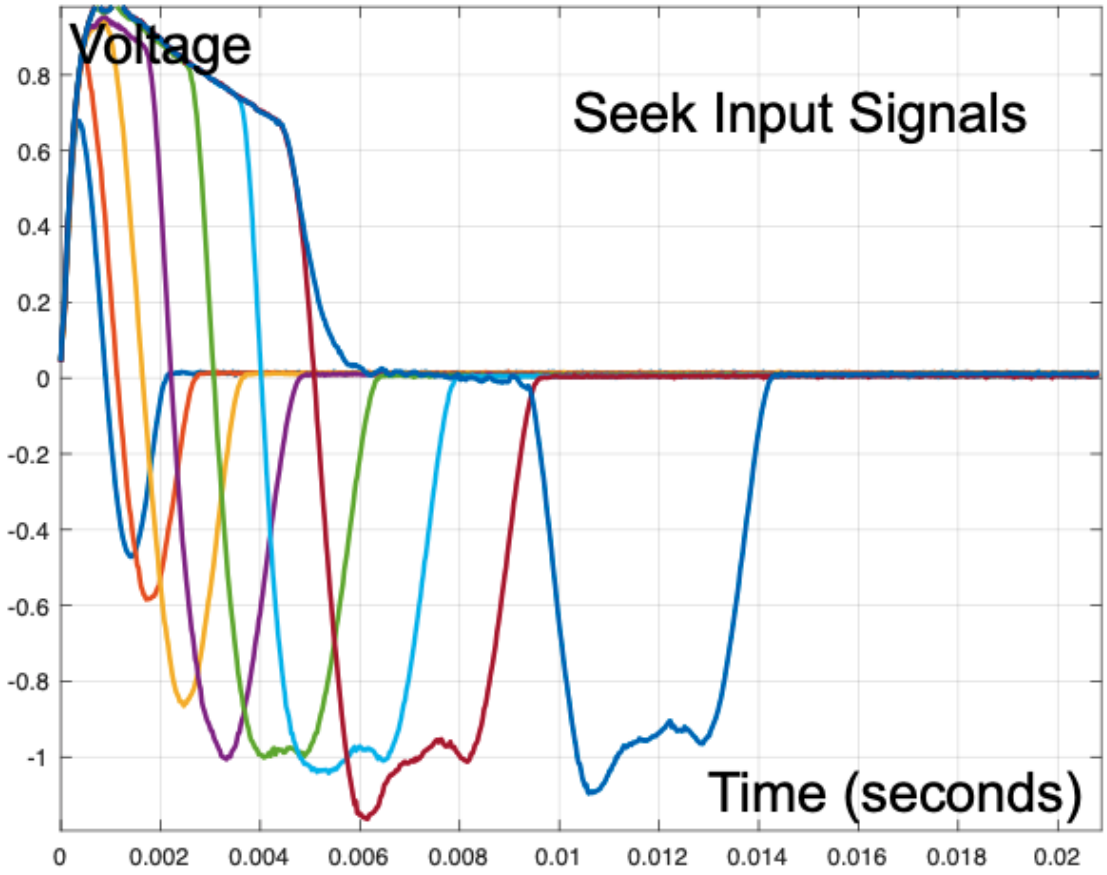

Figure 2.8: Typical seeking input signals $u_{seek}(t)$ of the seeking actuator arm are shown. These input signals when passed through the actuator arm will generate vibration which adversely affect the performance of the track following actuator.

$H_d(j\omega)$. We consider multiple measurements simultaneously to ensure robustness of the design process. Figure 2.7 plots the frequency response data measurements of the coupling transfer function. Data in Figure 2.7 is modeled based on actual frequency response measurements observed by the industry to represent the behavior but not reveal the true data.

Our objective is to design feedforward controllers for the VCM and MA of the track following actuator to suppress the imparted vibration by the track seeking actuator. A data driven control design methodology is presented to obtain these feedforward controllers. The data driven control design methodology obtains controllers directly based on the frequency response measurements of the vibration interaction (Figure 2.7) and the frequency response measurements of the open loop actuators (Figure 2.3). Multiple frequency response measurements of the actuators and the vibration interaction are considered simultaneously to

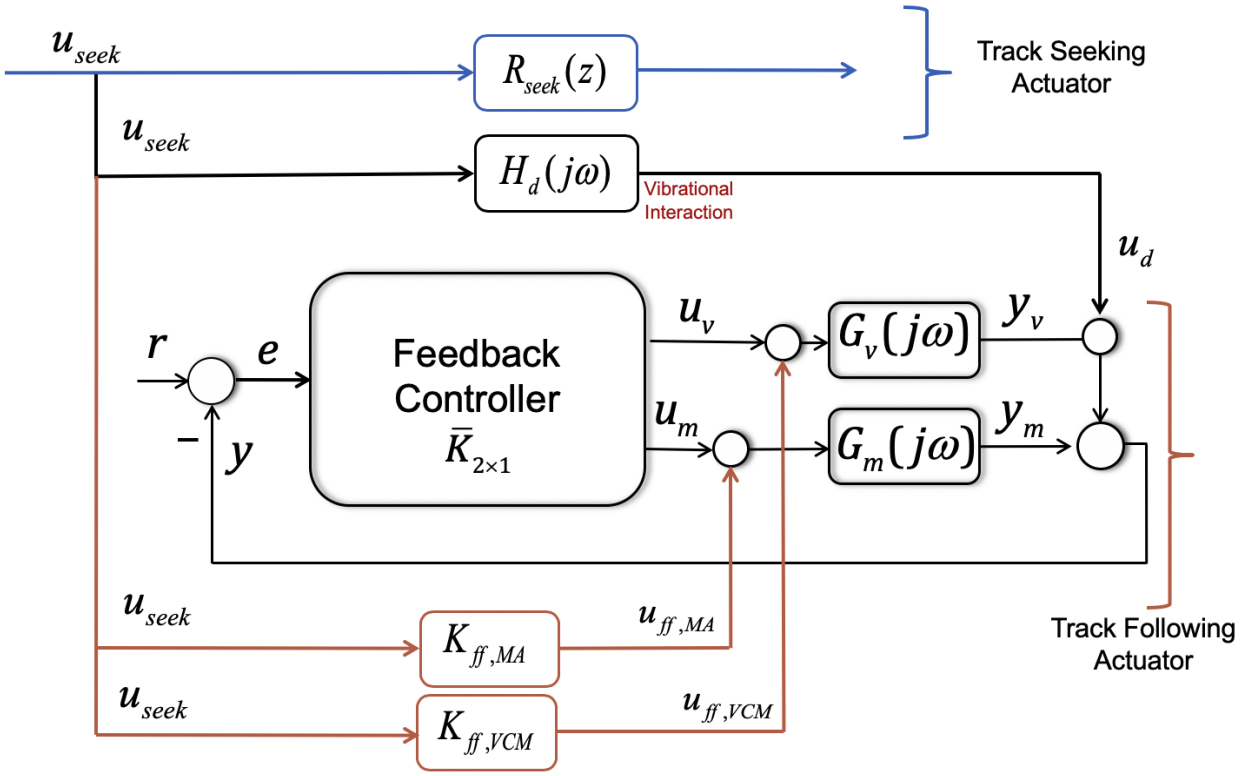

Figure 2.9: The control block diagram of the multi actuator drive is shown.

ensure robustness of the design. The feedforward control design also considers multiple seeking scenarios simultaneously, so that the same feedforward controller could be used for all the seeking scenarios. Figure 2.8 plots the seeking input signals for eight seeking scenarios considered simultaneously during the design process.

2.5 Block Diagram of the Multi Actuator Drive

The control block diagram of a multi actuator drive is shown in the Figure 2.9. $R_{seek}(z)$ is the closed loop transfer function of the track seeking actuator. u_{seek} is the track seeking input signal as shown in Figure 2.8.

The control loop of the track seeking actuator is similar to a dual stage HDD as shown in Figure 2.4. $G_v(j\omega)$ and $G_m(j\omega)$ are VCM and MA respectively. u_v, u_m are their corresponding control inputs, whereas, y_v, y_m are their corresponding outputs. r is the runout, e is the position error signal and n is the measurement noise. $\bar{K}(z)$ is a single-input dual-output track following feedback controller.

The seeking actuator imparts coupling vibration as a disturbance signal u_d to the track

following actuator. The coupling transfer function between the seeking actuator and the track following actuator is as shown in Figure 2.7. Our objective is to design feedforward controllers for VCM ($K_{ff,VCM}(z)$) and MA ($K_{ff,MA}(z)$) to suppress the imparted vibration $H_d(j\omega)$. [46].

We define the following closed loop transfer functions of the track following actuator which will be used in the design process. $E_{r\to e}(j\omega)$ is the closed loop transfer function from runout r to position error signal (PES) e. $E_{u_v\to e}(j\omega)$ is the closed loop transfer function from VCM control input u_v to PES e. $E_{u_m\to e}(j\omega)$ is the closed loop transfer function from MA control input u_m to PES e.

In this block diagram, Figure 2.9, lowercase letters represent discrete time sequences and the uppercase letters represent transfer functions in the z domain or the frequency domain.

Chapter 3

Data Driven Feedforward Control Design

3.1 Introduction

The data driven feedforward control design methodologies used to design feedforward controllers based on frequency response measurements are proposed in this chapter[1]. Traditionally, control design methods fit a model to the frequency response data and design a controller based on the model. But, with the data driven design approach controllers can be designed directly based on the frequency response data.

In this chapter, data driven design methodology in the frequency domain is presented. H_∞ norm and H_2 norm are used to formulate an optimization problem. A data driven methodology for single-input single-output (SISO) systems to design feedback controllers based only on the H_∞ norm conditions was presented earlier in [28]. A data driven approach for multi-input single-output (MISO) systems to design feedback controllers using mixed $H_2 - H_\infty$ norm conditions was presented in [8, 27, 7].

In section 3.2, we will discuss the preliminaries and notations used to set up the design problem. The controller factorization used to obtain the feedforward controllers are discussed in section 3.3. We will discuss the H_∞ norm conditions and the H_2 norm condition in section 3.4. The mixed $H_2 - H_\infty$ norm optimization problem is also formulated in section 3.4.

3.2 Preliminaries

In this section, the block diagram used to obtain the data driven feedforward control design methodology is first discussed. The advantage of considering multiple frequency response

[1]This chapter is part of a peer - reviewed publication:
Shah, P., and Horowitz, R. "Active Vibration Rejection in Multi Actuator Drives: Data Driven Approach." Proceedings of the ASME 2019 Dynamic Systems and Control Conference. Volume 3, October, 2019. V003T17A002. ASME. https://doi.org/10.1115/DSCC2019-8983

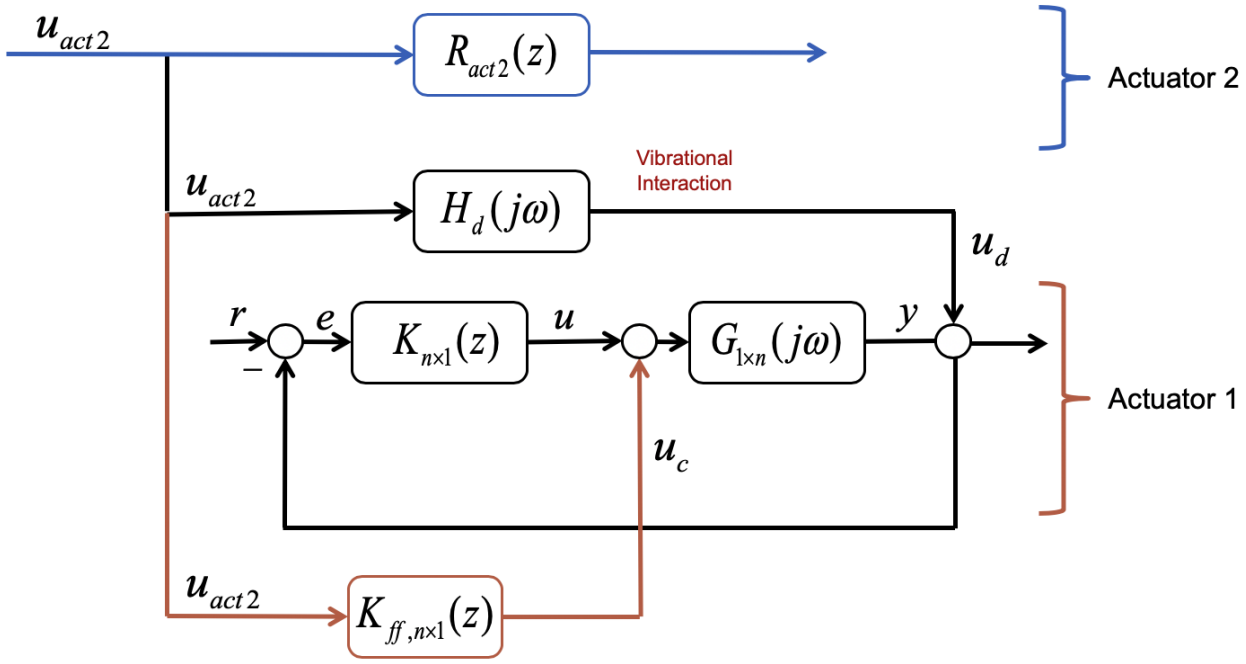

Figure 3.1: The control block diagram used to obtain the data driven feedforward control design methodology is shown. Here, $G_{1\times n}(j\omega)$ is the open loop frequency response measurement of actuator 1. $K_{n\times1}(z)$ is the pre-designed feedback controller. $H_d(j\omega)$ is the frequency response measurement of the coupling transfer function between actuator 2 and actuator 1. $K_{ff,n\times1}(z)$ is the feedforward controller to be designed to suppress the imparted vibration $H_d(j\omega)$. $R_{act2}(z)$ is the closed loop transfer function of actuator 2 and u_{act2} is its corresponding input signal.

measurements is then discussed.

The rise in miniaturization has introduced new control challenges. New products have control systems packed closely together. The compactness is leading to vibration interaction between the neighboring actuators in a control system. Figure 3.1 is a control block diagram for two neighboring actuators operating independently but imparting vibration disturbances to each other. The lower case letters represent discrete time sequences (also loosely referred to as signals). The uppercase letters represent transfer functions either in the z domain or the frequency domain.

In Figure 3.1, $R_{act2}(z)$ is the closed loop of actuator 2. u_{act2} is the control input signal of actuator 2. u_{act2} is available to the designer. In general, we will differentiate between transfer functions that are characterized by an actual model, such as the controller transfer function $K(z)$, and transfer functions that are only characterized by frequency response data, such as the actuator transfer function $G(j\omega)$.

$G_{1\times n}(j\omega)$ is the open loop transfer function of actuator 1 which, as alluded earlier, is only characterized by frequency response measurement data. $G_{1\times n}$ is a multi-input single-output (MISO) system. $G_{1\times n}(j\omega)$ has n dynamic systems connected in series. For example: a dual stage HDD is a 1×2 system. It has two dynamic systems, a voice coil motor and a micro actuator, connected in series.

An ideal feedback controller for $G_{1\times n}(j\omega)$ is a single-input multi-output (SIMO) controller. $K_{n\times 1}(z)$ is a pre-designed feedback controller of actuator 1. u is the feedback control signal and y is the output of the actuator. r is a colored noise for reference and e is the error signal.

$H_d(j\omega)$ is the coupling dynamics transfer function that produces the vibration imparted by actuator 2 to actuator 1. $H_d(j\omega)$ is only characterized by frequency response measurement data. u_d is the imparted disturbance by actuator 2 onto actuator 1.

Our objective is to design a feedforward controller $K_{ff,n\times 1}(z)$ to suppress the imparted vibration disturbance u_d. The designer can choose which frequency response data of actuator 1 are to be used to design the feedforward vibration suppression controller $K_{ff}(z)$. Without loss of generality, we will generally use all n available actuator frequency response data simultaneously in the design process.

Multiple Frequency Response Measurements

As stated earlier, multiple frequency response measurements of the open loop of actuator 1, $G_{1\times n}(j\omega)$ and vibration interaction coupling dynamics $H_d(j\omega)$ will be considered in the design process simultaneously. This ensures the feedforward controllers are robust and will achieve good vibration suppression on the actual system.

Conversely, the vibration interaction experienced on actuator 1 could be divided into clusters of frequency response measurements, and one feedforward controller could be obtained for each cluster with similar frequency responses. The imparted vibration may change as a function of temperature, sometimes the imparted vibration is non linear and can be estimated by a bunch of linear frequency response measurements. The ability to simultaneously consider multiple vibration scenarios is useful for such actuators.

Similarly, non linear actuators can be estimated using a bunch of frequency response measurements for $G_{1\times n}(j\omega)$. A common controller can be designed for multiple actuators simultaneously by considering all the frequency response measurements in the design process.

3.3 Controller Factorization

The stable factorization from [56] are used for the feedforward controller $K_{ff,n\times 1}(z)$ in Figure 3.1.

$$K_{ff,n\times 1}(z) = X_{n\times 1}(z)Y_{1\times 1}^{-1}(z) \tag{3.1}$$

where $X_{n\times 1} \in \mathbb{RH}_\infty^{n\times 1}$, $Y_{1\times 1} \in \mathbb{RH}_\infty^{1\times 1}$ are asymptotically stable rational proper transfer functions. The factorization are for frequency domain and the z domain. The stable factorization can be transformed to frequency domain simply by substituting z by $e^{j\omega}$. We will factorize the controller $K_{ff,n\times 1}(z)$ using finite impulse response filters (FIRs), with all poles at the origin.

$$\begin{aligned} X_{n\times 1}(z) &= \frac{1}{z^p}\begin{bmatrix} x_{1,p}z^p + x_{1,p-1}z^{p-1} + \cdots + x_{1,1}z + x_{1,0} \\ \vdots \\ x_{n,p}z^p + x_{n,p-1}z^{p-1} + \cdots + x_{n,1}z + x_{n,0} \end{bmatrix} \\ Y_{1\times 1}(z) &= \frac{z^p + y_{p-1}z^{p-1} + \cdots + y_1 z + y_o}{z^p} \end{aligned} \tag{3.2}$$

where p is the controller order and the controller parameters $\{y_{p-1}, \cdots, y_o\} \in \mathbb{R}^{1\times 1}$ and $\{x_{i,p}, \cdots, x_{i,0}\} \in \mathbb{R}^{1\times 1} \forall i \in \{1 \dots n\}$ are to be determined.

For simplicity, the poles of the stable factorization are chosen to be at the origin, but they can be placed anywhere inside the unit circle. The stable factorization can be written in terms of the controller coefficients and filter terms:

$$X_{n\times 1}(z) = \rho_x F_x(z) \tag{3.3}$$
$$Y_{1\times 1}(z) = \rho_y F_y(z) \tag{3.4}$$

where ρ_x and ρ_y are given by:

$$\rho_x = \begin{bmatrix} x_{1,p}, & \dots, & x_{1,1}, & x_{1,0} \\ & & \dots & \\ x_{n,p}, & \dots, & x_{n,1}, & x_{n,0} \end{bmatrix} \tag{3.5}$$

$$\rho_y = \begin{bmatrix} y_{1,p}, & \dots, & y_{1,1}, & y_{1,0} \end{bmatrix} \tag{3.6}$$

and the filter terms $F_x(z)$ and $F_y(z)$ are given by:

$$F_x(z) = \frac{1}{z^p}\begin{bmatrix} z^p & \dots & z^1 & z^0 \end{bmatrix}^\top \tag{3.7}$$

$$F_y(z) = \frac{1}{z^p}\begin{bmatrix} z^p & \dots & z^1 & z^0 \end{bmatrix}^\top \tag{3.8}$$

3.4 Data Driven Control Design

The data driven feedforward control design methodology is presented in this section. First, a simplified control block diagram is obtained using the closed loop transfer functions to formulate the control design problem. Then, the control objectives of the feedforward data driven methodology are discussed. Finally, an optimization problem is formulated and the algorithm is discussed.

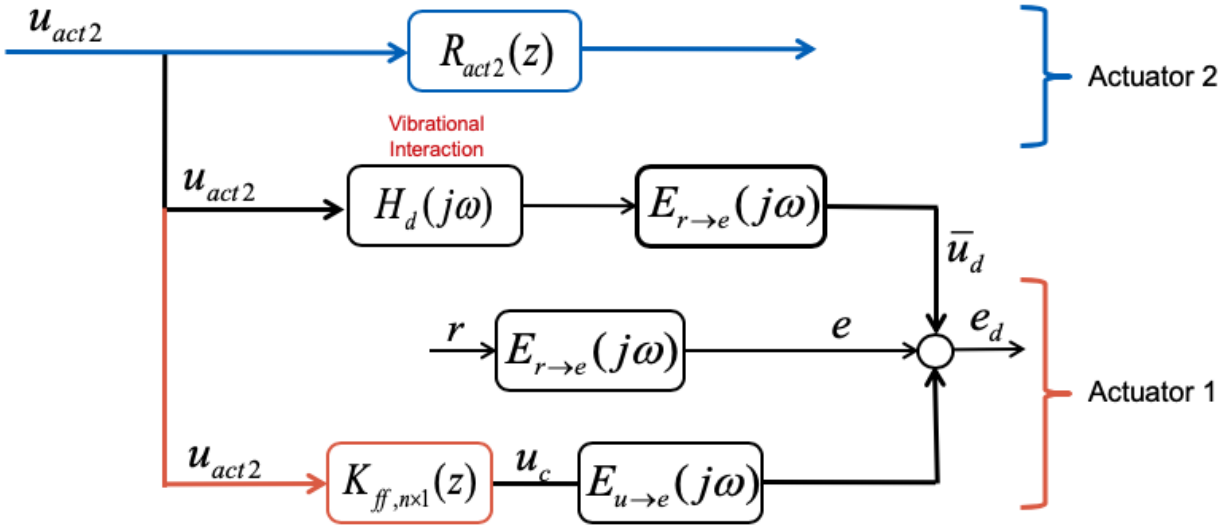

Figure 3.2: Simplified Control Block Diagram obtained by defining closed loop transfer functions in Figure 3.1. $E_{r\to e}(j\omega)$ is the closed loop transfer function from r to e in Figure 3.1. $E_{u_c\to e}(j\omega)$ is the closed loop transfer function from u_c to e in Figure 3.1.

Simplified Control Block Diagram

In Figure 3.1, define closed loop transfer function from r to e as $E_{r\to e}(z)$. Similarly, the closed loop transfer function from u_c to e is defined as $E_{u_c\to e}(z)$.

As the feedback controller $K_{n\times 1}(z)$ and the open loop actuator $G_{1\times n}(j\omega)$ are available to the designer, the closed loop transfer functions, in the frequency domain, $E_{r\to e}(j\omega)$ and $E_{u_c\to e}(j\omega)$ are deterministic. The frequency response of the feedback controller $K_{n\times 1}(z)$ can be simply obtained by replacing z by $e^{j\omega}$. $E_{r\to e}(j\omega)$ is a 1×1 frequency response, whereas, $E_{u_c\to e}(j\omega)$ is a $1\times n$ frequency response.

Now, in Figure 3.2, $R_{act2}(z)$ is the closed loop transfer function of actuator 2. u_{act2} is the control input signal of actuator 2. The control input signal is available to the designer. $H_d(j\omega)$ is the frequency response of the coupling dynamics that generates the vibration disturbance being imparted by actuator 2 to actuator 1.

$E_{r\to e}(j\omega)$ is the frequency response of the closed loop transfer function from the runout r, which is a colored noise, to e, the error signal. $\bar{u_d}$ is the disturbance signal after the vibration is imparted to the closed loop system $E_{r\to e}(j\omega)$. $\bar{u_d}$ is the disturbance added to the error signal e.

The objective is to design feedforward controller $K_{ff,n\times 1}(z)$ to suppress the vibration $H_d(j\omega)$. The frequency response of $K_{ff,n\times 1}(z)$ can be obtained by replacing z by $e^{j\omega}$ to get $K_{ff,n\times 1}(j\omega)$. The feedforward control signal enters the system through the closed loop transfer function $E_{u_c\to e}(z)$. The frequency response of the closed loop transfer function from

the control input u_c to the error signal e is given by $E_{u_c \to e}(j\omega)$.

e_d is the error signal in presence of the vibration coupling dynamics $H_d(j\omega)$ and the feedforward controller $K_{ff,n\times 1}(z)$. Whereas, e is the original error signal in absence of any vibration interaction or any feedforward action. Ideally, we want the error signal e_d to be equal to error signal e implying total vibration suppression.

The frequency response measurements of $E_{r\to e}(j\omega)$, $E_{u_c\to e}(j\omega)$ and $H_d(j\omega)$ are considered for $\omega \in \Omega$, except for the finite frequencies that correspond to the poles of actuator 1 and the vibration interaction $H_d(j\omega)$.

$$\Omega = \left\{ \omega | -\frac{\pi}{T_s} \leq \omega \leq \frac{\pi}{T_s} \right\} \tag{3.9}$$

where, T_s is the sampling time of the frequency response measurements.

Control Objectives

Let, R be the frequency spectrum of the colored runout r. The frequency spectrum of u_{act2} can be obtained using Fast Fourier Transform, Eq. (1.2). Let U_{act2} be the frequency spectrum of u_{act2}.

Let, $E(j\omega)$ be the frequency spectrum of error signal e and $E_d(j\omega)$ be the frequency spectrum of error signal e_d.

The frequency spectrum of error signal e is given by:

$$E(j\omega) = E_{r\to e}(j\omega)R \tag{3.10}$$

The frequency spectrum of the error signal e_d, in presence of vibration $H_d(j\omega)$ and feedforward action is given by:

$$E_d(j\omega) = E_{r\to e}(j\omega)R + E_{r\to e}(j\omega)H_d(j\omega)U_{act2} + E_{u_c\to e}(j\omega)K_{ff,n\times 1}(j\omega)U_{act2} \tag{3.11}$$

Our objective is to minimize the difference between the frequency spectrum of the ideal error signal, $E(j\omega)$, and the frequency response of the actual error signal, $E_d(j\omega)$.

H_2 Norm

H_2 norm of a $m \times n$ MIMO system with a frequency response $H(j\omega)$ is defined as:

$$||H(j\omega)||_2^2 \triangleq \frac{1}{2\pi}\int_\Omega \mathrm{Tr}[H(j\omega)^* H(j\omega)]d\omega \tag{3.12}$$

where $H^*(j\omega) = \bar{H}^*(j\omega)$ is the complex conjugate transpose and Tr(H) is the trace of the matrix H.

H_2 norm is an estimate of the energy of the system. Here, H_2 norm of $H(j\omega)$ provides us a measure of the energy stored in the system represented by the frequency response $H(j\omega)$.

According to Parseval's theorem [52], the energy of the system evaluated in the time domain and the frequency domain should be the same. For a time signal $x(t)$, with Fourier transform given by $X(j\omega)$, we have:

$$\int_{-\infty}^{\infty} |x(t)|^2 dt = \frac{1}{2\pi} \int_{-\infty}^{\infty} |X(j\omega)|^2 d\omega \tag{3.13}$$

For a discrete time sequence $x(k)$ with the discrete time Fourier transform $X(k)$, we have:

$$\sum_{k=0}^{N} |x(k)|^2 = \frac{1}{N} \sum_{k=0}^{N} |X(k)|^2 \tag{3.14}$$

According to Eq.(3.14), the H_2 norm of a transfer function can be used to constrain the variance of the output of the transfer function in the time domain.

For our design process, we want to constrain the difference between the actual error signal e_d with disturbance and feedforward action and the ideal error signal without any disturbance or feedforward action e.

$$||e_d - e||_2^2 = ||E_d - E||_2^2 \tag{3.15}$$

Therefore, according to Parseval's theorem [52], minimizing the H_2 norm of the difference between E_d and E constrains the variance of the difference between the time sequences e_d and e.

$$\min ||E_d - E||_2 \tag{3.16}$$

Substituting E and E_d from Eq.(3.10) and Eq.(3.11) respectively, we have

$$\min_{X,Y} ||E_{r\to e}(j\omega)H_d(j\omega)U_{act2} + E_{u_c\to e}(j\omega)K_{ff}(j\omega)U_{act2}||_2^2 \tag{3.17}$$

Here, the dimension of the controller $K_{ff}(j\omega)$ is dropped for simplicity. The controller factorization from Eq.(3.1) will be used. Therefore, on substituting the controller factorization, we have:

$$\min_{X,Y} ||E_{r\to e}(j\omega)H_d(j\omega)U_{act2} + E_{u_c\to e}(j\omega)\frac{X(j\omega)}{Y(j\omega)}U_{act2}||_2^2 \tag{3.18}$$

The data driven methodology can obtain a feedforward controller for multiple actuator data, multiple coupling dynamics vibration data and multiple control signals of actuator 2 simultaneously. p frequency response measurements of the closed loop measurements of actuator 1 $E_{r\to e,i}(j\omega)$ and $E_{u_c\to e,i}(j\omega)$, where i represents the i^{th} measurement, are considered. v frequency response measurements of the imparted coupling dynamics vibration $H_{d,l}(j\omega)$, where l represents the l^{th} measurement, and s control input signals $u_{act2,m}$, where m represents the m^{th} excitation signal, are also considered simultaneously. The average difference

between the actual error signal E_d and the ideal error signal E will be given by:

$$\min_{X,Y} \sum_{i=1}^{p} \sum_{l=1}^{v} \sum_{m=1}^{s} ||E_{(d),i,l,m} - E_i||_2^2 =$$
$$\min_{X,Y} \sum_{i=1}^{p} \sum_{l=1}^{v} \sum_{m=1}^{s} ||E_{r\to e,i}(j\omega)H_{d,l}(j\omega)U_{act2,m} + E_{u_c\to e,i}(j\omega)\frac{X(j\omega)}{Y(j\omega)}U_{act2,m}||_2^2 \quad (3.19)$$

Eq.(3.19) is only a function of $X(j\omega)$ and $Y(j\omega)$. But, Eq.(3.19) is not a convex function in X and Y. A convex upper limit for the H_2 norm in Eq.(3.19) was obtained using the following result from [27].

Theorem 1 *Given 'p' frequency response data of the plant (actuator 1), where the i^{th} closed loop plant measurements $E_{r\to e,i}(j\omega)$ and $E_{u_c\to e,i}(j\omega)$ are given over the frequency region Ω, given 'v' frequency response data of the imparted vibration, where the l^{th} vibration measurement $H_{d,l}(j\omega)$ is given over the frequency region Ω, given 's' input signals of actuator 2, where the frequency spectrum of the m^{th} control input signal $U_{act2,m}$ is given, and an initial stabilizing controller $K_{ff,k-1}(z) = X_{k-1}(z)Y_{k-1}(z)^{-1}$ is given, an upper bound on the average variance defined in Eq.(3.18) can be computed as follows:*

$$\min_{X_k,Y_k} \sum_{i=1}^{p} \sum_{l=1}^{v} \sum_{m=1}^{s} ||E_{(d),i,l,m} - E_i||_2^2 \quad \leq \quad \min_{X_k,Y_k,\Gamma} \sum_{i=1}^{p} \sum_{l=1}^{v} \sum_{m=1}^{s} \int_{\Omega} \Gamma_{i,l,m}(j\omega)d\omega \quad (3.20)$$

$\forall i \in 1,\dots p,\ \forall l \in 1,\dots v,\ \forall m \in 1,\dots s$ *and* $\omega \in \Omega$*:*

$$\begin{bmatrix} \Gamma_{i,l,m} & (E_{r\to e,i}H_{d,l} + E_{u_c\to e,i}X_k)U_{act2,m} \\ ((E_{r\to e,i}H_{d,l} + E_{u_c\to e,i}X_k)U_{act2,m})^* & Y_k^*Y_{k-1} + Y_{k-1}^*Y_k - Y_{k-1}^*Y_{k-1} \end{bmatrix}(j\omega) \geq 0 \quad (3.21)$$

The upper bound on Eq.(3.19) is given by Theorem 1. The upper bound in Eq.(3.20) and the constraint in Eq.(3.21) are convex in X_k, Y_k and Γ. By minimizing the upper bound, we can minimize the H_2 norm in Eq.(3.19).

Notice that, the linear matrix inequality in Eq.(3.21) is an iterative solution and depends on a stabilizing controller $K_{ff,k-1(z)}$ from the previous iteration, as given in Eq.(3.22). Here, 'k' is the current iteration. Overall, we have a locally convex optimization problem in Eq.(3.20) and Eq.(3.21).

$$K_{ff,k-1}(z) = \frac{X_{k-1}}{Y_{k-1}} \quad (3.22)$$

The stabilizing controller from the previous iteration as shown in Eq.(3.22) has the controller factorization given in Eq.(3.2).

H_∞ norm

H_∞ norm is used in control theory to achieve stabilization with guaranteed performance. For a stable single-input single-output (SISO) system the H_∞ norm is defined as the peak gain or the largest value of the magnitude of a frequency response. Whereas, for a multi-input multi-output system, the H_∞ norm is defined as the largest singular value across the frequency range Ω.

For a SISO transfer function $H(j\omega)$, the H_∞ norm is defined as:

$$||H(j\omega)||_\infty \triangleq \sup_{\omega\in\Omega} |H(j\omega)| \tag{3.23}$$

For a $m \times n$ MIMO transfer function $H(j\omega)$, the H_∞ norm is defined as:

$$||H(j\omega)||_\infty \triangleq \sup_{\omega\in\Omega} \bar{\sigma}(H(j\omega)) \tag{3.24}$$

Here, $\bar{\sigma}(.)$ denotes the largest singular value of the matrix $H(j\omega)$. Eq.(3.25) presents an example of an H_∞ norm constraint.

$$||W_f(j\omega)S(j\omega)||_\infty \leq \gamma \qquad \forall\omega \in \Omega \tag{3.25}$$

Here, $S(j\omega)$ is the frequency response of a transfer function. $W_f(j\omega)$ is a weighting filter, in the frequency domain, used to shape $S(j\omega)$. γ is an upper limit used to set the constraint.

The difference between the actual error signal with vibration and feedforward action, E_d, and the ideal error signal E can be shaped using H_∞ constraints.

$$||W_f(j\omega)(E_d - E)||_\infty \leq \gamma \tag{3.26}$$

On substituting E_d and E in Eq.(3.26), we have:

$$||W_f(j\omega)(E_{r\to e}(j\omega)H_d(j\omega)U_{act2}(j\omega) + E_{u_c\to e}(j\omega)K_{ff}(j\omega)U_{act2}(j\omega))||_\infty \leq \gamma \tag{3.27}$$

Now, as the frequency spectrum of the input signal of actuator 2 is common, we can choose to shape the transfer function excluding this frequency response in Eq.(3.27). The weighting filter $W_f(j\omega)$ can be shaped according to the requirements of the designer. Dropping the $(j\omega)$ argument from the equation for simplicity, we have:

$$||W_f(E_{r\to e}H_d + E_{u_c\to e}K_{ff})||_\infty \leq \gamma \tag{3.28}$$

The controller factorization used for H_∞ norm design are according to the Eq.(3.2).

$$||W_f(E_{r\to e}H_d + E_{u_c\to e}\frac{X}{Y})||_\infty \leq \gamma \tag{3.29}$$

The H_∞ norm condition stated in Eq.(3.29) is not convex in X and Y. Previously, [28] and [8] have presented approaches to transform Eq.(3.29) to convex constraint for feedback design. We have the following theorem to obtain a convex constraint for a feedforward design:

Theorem 2 *Given 'p' frequency response data of the plant (actuator 1), where the i^{th} closed loop measurements $E_{r\to e,i}(j\omega)$ and $E_{u_c\to e,i}(j\omega)$ are given over the frequency region Ω, given 'v' frequency response measurements of the imparted vibration, where the l^{th} measurement $H_{d,l}(j\omega)$ is given over the frequency region Ω and given a positive scalar γ, the following two statements are equivalent:*

I The following H_∞ norm condition is met $\forall i \in 1,\dots,p$ and $\forall l \in 1,\dots,v$:

$$||W_f(E_{r\to e,i}H_{d,l} + E_{u_c\to e,i}K_{ff})||_\infty \leq \gamma \tag{3.30}$$

II There exists controller stable factorization $X_{n\times 1}(z)|_{z=e^{j\omega}}$, $Y_{1\times 1}(z)|_{z=e^{j\omega}}$ according to Eq.(3.2), such that the following convex inequality holds $\forall\omega \in \Omega$, $\forall i \in 1,\dots,p$ and $\forall l \in 1,\dots,v$:

$$\gamma^{-1}\bar{\sigma}\Big(W_f(j\omega)\left(E_{r\to e,i}(j\omega)H_{d,l}(j\omega) + E_{u_c\to e,i}(j\omega)X(e^{j\omega})\right)\Big) \leq Re\{Y(e^{j\omega})\} \tag{3.31}$$

A necessary and sufficient convex constraint is obtained using Theorem 2. Starting with only the controller factorization, stabilizing controllers are obtained. Theorem 2 does not require an initial stabilizing controller to obtain a controller satisfying the H_∞ norm constraint. On the contrary, Theorem 2 can be used to obtain an initial stabilizing controller for Theorem 1. For proof see [7].

Mixed $H_2 - H_\infty$ Norm Optimization

The mixed $H_2 - H_\infty$ norm control optimization problem is characterized by the minimization of the H_2 norm and application of H_∞ norm and/or H_2 norm constraints.

We can combine the locally convex H_2 norm objective function from Eq.(3.20) and Eq.(3.21), and the H_∞ norm constraints from Eq.(3.31) to obtain a mixed $H_2 - H_\infty$ norm locally convex optimization problem.

$$\min_{X_k,Y_k,\Gamma} \sum_{i=1}^{p}\sum_{l=1}^{v}\sum_{m=1}^{s}\int_\Omega \Gamma_{i,l,m}(j\omega)d\omega \tag{3.32}$$

such that $\forall i \in 1,\dots p$, $\forall l \in 1,\dots v$, $\forall m \in 1,\dots s$ and $\omega \in \Omega$:

$$\begin{bmatrix} \Gamma_{i,l,m} & (E_{r\to e,i}H_{d,l} + E_{u_c\to e,i}X_k)U_{act2,m} \\ ((E_{r\to e,i}H_{d,l} + E_{u_c\to e,i}X_k)U_{act2,m})^* & Y_k^*Y_{k-1} + Y_{k-1}^*Y_k - Y_{k-1}^*Y_{k-1} \end{bmatrix}(j\omega) \geq 0 \tag{3.33}$$

$$\gamma^{-1}\bar{\sigma}\Big(W_f(j\omega)\left(E_{r\to e,i}(j\omega)H_{d,l}(j\omega) + E_{u_c\to e,i}(j\omega)X_k(e^{j\omega})\right)\Big) \leq Re\{Y_k(e^{j\omega})\} \tag{3.34}$$

Eq.(3.32), Eq.(3.33) and Eq.(3.34) give us the mixed $H_2 - H_\infty$ norm optimization problem. The stabilizing controller for the first iteration is obtained by solving a feasibility problem with just the H_∞ constraints.

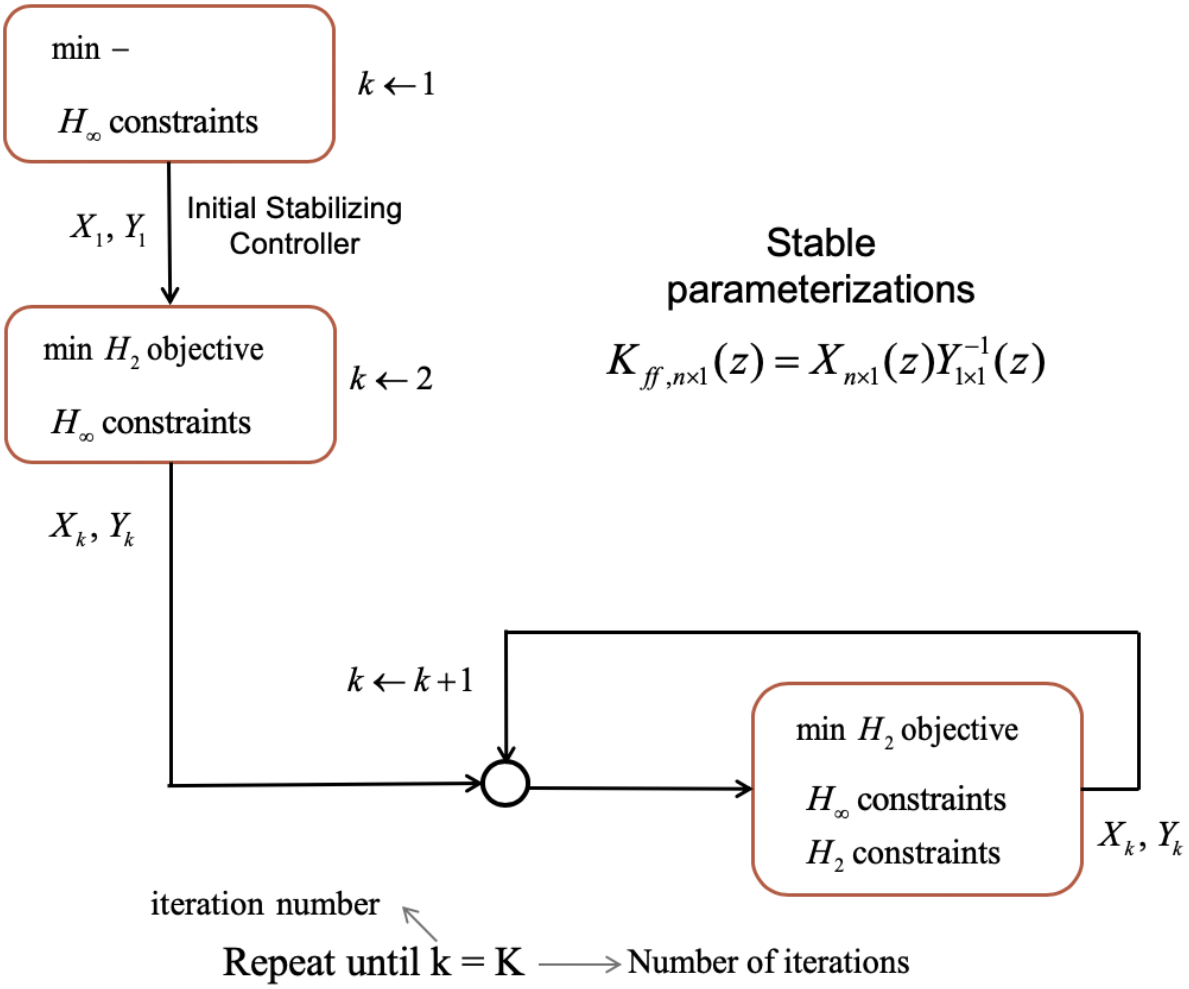

Figure 3.3: The algorithm used to design the data driven feedforward controller is shown in this figure. The H_∞ norm feasibility problem is solved to obtain initial stabilizing controller. The mixed $H_2 - H_\infty$ norm control design optimization problem is solved to obtain the feedforward controller suppressing the imparted vibration disturbance.

Algorithm

The algorithm used to obtain the feedforward controller $K_{ff,n\times1}(z)$ is shown in Figure 3.3. The H_∞ norm feasibility problem is solved to obtain an initial stabilizing controller. The mixed $H_2 - H_\infty$ norm control design optimization problem is solved to obtain the feedforward controller that suppresses the imparted vibration disturbance.

This problem is iterated till the stopping condition is reached. The stopping condition can be chosen by the designer. An example of a good stopping condition is to have E_d

within five percent of E. The solver MOSEK [36] on MATLAB [34] is used to solve the locally convex iterative optimization problem.

Chapter 4

Application of Data Driven Feedforward Control Design to Multi Actuator Drives

4.1 Introduction

Hard disk drive servo systems have three operation modes. Track following mode is when the read/write head follows a data track. This process requires very high precision. Read and write processes occur during track following. Seeking mode is when the read/write head sweeps through data tracks to locate the new desired new data track to initiate track following. This process generates a lot of vibration. Finally, settling mode is the transition mode between seeking and track following. The read/write head approaches the desired new track with certain momentum, the objective of the settling mode is to smoothly settle the read/write head onto the new track while minimizing jerk [41].

Multi actuator drives present new design challenges. A multi actuator drive has two actuator arms operating independently off a same pivot timber. The control forces and torque generated by one actuator arm can affect the operation of the other actuator arm. The control block diagram for a multi actuator drive is presented in section 4.2[1].

The vibration interaction between the two actuator arms can be categorized into three scenarios. First, the two actuator arms are operating in the track following mode. Second, the two actuator arms are operating in the track seeking mode. Third, one actuator arm is track seeking while, the other actuator arm is track following. It is expected that scenario two and three will involve considerable vibration interaction between the two actuator arms.

In scenario two, the two actuators arms are track seeking. The vibration interaction does

[1]This chapter is part of a peer - reviewed publication:
Shah, P., and Horowitz, R. "Active Vibration Rejection in Multi Actuator Drives: Data Driven Approach." Proceedings of the ASME 2019 Dynamic Systems and Control Conference. Volume 3, October, 2019. V003T17A002. ASME. https://doi.org/10.1115/DSCC2019-8983

not result in an impaired read/write performance. But, in scenario three, with one actuator arm track following, the vibration imparted by the tracking seeking actuator arm can adversely affect the read/write performance of this actuator arm. In this chapter, we present data driven feedforward control design methodologies to suppress the vibration imparted by the track seeking actuator onto the track following actuator.

In chapter 3, the data driven control design algorithm was presented to obtain feedforward controllers to suppress the vibration imparted by one actuator arm onto the other. In section 4.4, a sequential single-input single-output (SISO) control design methodology and a single-input multi-output (SIMO) control design methodology is presented to obtain feedforward controllers for the voice coil motor (VCM) and the micro-actuator (MA) using the data driven algorithm. The controller factorization used for the data driven problem are presented in section 4.3. The design results for the sequential SISO design and SIMO design methodologies are discussed in section 4.5.

4.2 Block Diagram of a Multi Actuator Drive

Figure 2.9 shows the control block diagram of a multi actuator drive. In this section, we simplify the block diagram using the closed loop transfer functions of the track following actuator. Figure 4.1 shows a simplified control block diagram of a multi actuator drive.

In Figure 4.1, $R_{seek}(z)$ is the closed loop transfer function of the track seeking actuator. u_{seek} is the control input signal of the track seeking actuator. The seeking process generates vibration which affects the performance of the neighboring track following actuator. The seeking control input signals are shown in Figure 2.8.

$H_d(j\omega)$ is the frequency response measurement of the coupling dynamics between the track seeking actuator and the track following actuator. The vibration is imparted as a disturbance signal u_d to the track following actuator. Multiple measurements of $H_d(j\omega)$ are considered simultaneously during the design process, as shown in Figure 2.7.

$E_{r\to e}(j\omega)$ is the closed loop transfer function from runout r to position error signal (PES) e, in the frequency domain. Similarly, $E_{u_v\to e}(j\omega)$ is the closed loop transfer function from the control input signal of VCM u_v to the PES e, in the frequency domain. $E_{u_m\to e}(j\omega)$ is the closed loop transfer function from the control input signal of MA u_m to the PES e, in the frequency domain.

Here, e is the ideal position error signal in the absence of any vibration or any feedforward control signal. e_d is the actual position error signal in the presence of vibration and feedforward compensation. Our objective is to design feedforward controllers for VCM ($K_{ff,VCM}$) and MA ($K_{ff,MA}$) to suppress the vibration imparted by the coupling dynamics $H_d(j\omega)$. $u_{ff,VCM}$ and $u_{ff,MA}$ are the feedforward compensation signals.

The data driven H_2. $- H_\infty$ norm optimization methodology presented in chapter 3 is used to design the feedforward controllers for VCM and MA. In this chapter, two control design methodologies are presented to obtain these feedforward controllers. First, a sequential single-input single-output (SISO) data driven control design methodology. In this approach,

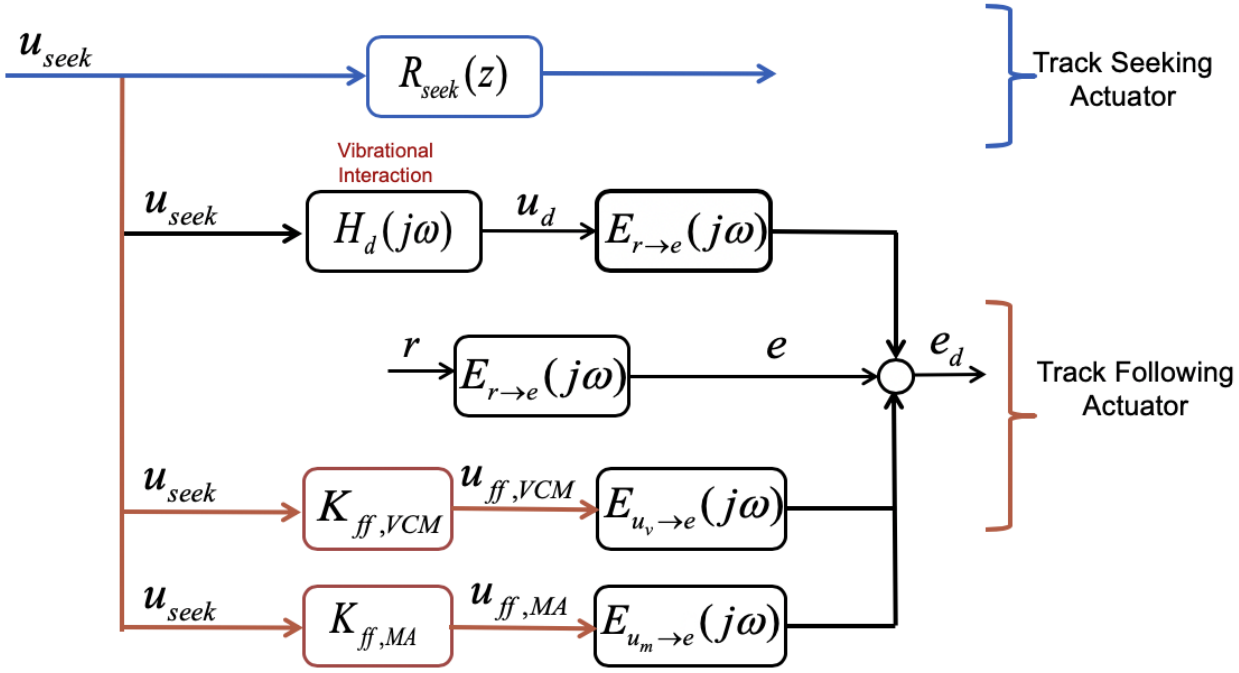

Figure 4.1: Control block diagram of a multi actuator drive is shown in this figure. Closed loop transfer functions of the track following actuator are used to simplify the representation of the control problem.

we first design $K_{ff,VCM}$, the feedforward controller for VCM, to suppress the entire imparted vibration. Then, the feedforward controller for MA, $K_{ff,MA}$ is designed to suppress the residual vibration. The second approach presented is the single-input multi-output (SIMO) data driven control design methodology. In this approach, the feedforward controllers $K_{ff,VCM}$ and $K_{ff,MA}$ are simultaneously designed to suppress the vibration $H_d(j\omega)$.

4.3 Controller Factorization

The stable factorization from [56] are used for the feedforward controllers $K_{ff,VCM}$ and $K_{ff,MA}$ of Figure 4.1. The controller factorization used are according to the $H_2 - H_\infty$ norm data driven methodology presented in chapter 3, Eq.(3.1). We will consider the same order of the controller for both VCM and MA.

$$K_{ff,VCM}(z) = X_{VCM}(z)Y_{VCM}^{-1}(z) \quad (4.1)$$
$$K_{ff,MA}(z) = X_{MA}(z)Y_{MA}^{-1}(z) \quad (4.2)$$

where $X_{VCM} \in \mathbb{RH}_\infty^{1\times1}$, $Y_{VCM} \in \mathbb{RH}_\infty^{1\times1}$, $X_{MA} \in \mathbb{RH}_\infty^{1\times1}$ and $Y_{MA} \in \mathbb{RH}_\infty^{1\times1}$ are all asymptotically stable rational proper transfer functions. The factorization are for frequency domain and the z-domain. The stable factorization can be transformed to frequency domain simply by substituting z by $e^{j\omega}$. In this chapter, we will factorize the controller $K_{ff,VCM}(z)$ and $K_{ff,MA}(z)$ using finite impulse response filters (FIRs), with all poles at the origin.

$$\begin{aligned} X(z) &= X_p z^p + X_{p-1} z^{p-1} + \cdots + X_o \\ Y(z) &= z^p + Y_{p-1} z^{p-1} + \cdots + Y_o \end{aligned} \tag{4.3}$$

where p is the controller order and the controller parameters $\{Y_{p-1}, \cdots, Y_o\} \in \mathbb{R}^{1\times1}$ and $\{X_p, \cdots, X_o\} \in \mathbb{R}^{1\times1}$ are to be determined.

4.4 Data Driven Feedforward Control Design

The data driven feedforward control design methodology is used to obtain feedforward controllers $K_{ff,VCM}(z)$ and $K_{ff,MA}(z)$ for VCM and MA respectively. Two methodologies, sequential SISO methodology and SIMO methodology, are presented to obtain the feedforward controllers for the track following actuator of the multi actuator drive. In the sequential SISO methodology, first $K_{ff,VCM}(z)$ is designed to suppress the entire imparted vibration by the coupling dynamics $H_d(j\omega)$. Then, $K_{ff,MA}(z)$ is designed to suppress the residual vibration from the VCM feedforward control design. Whereas, in the SIMO methodology, feedforward controllers $K_{ff,VCM}(z)$ and $K_{ff,MA}(z)$ are designed simultaneously to suppress the imparted vibration by the coupling dynamics $H_d(j\omega)$.

Sequential SISO Feedforward Control Design

The servo assembly of a track following actuator arm consists of a voice coil motor (VCM) and a micro actuator (MA) attached in series. VCM has a larger stroke but a smaller bandwidth than MA. Figure 4.2 shows the frequency response measurements of VCM and MA for a set of five actuator arms.

The objective is to design feedforward controllers $K_{ff,VCM}(z)$ and $K_{ff,MA}(z)$ to suppress the vibration imparted by the coupling dynamics $H_d(j\omega)$. Multiple sets of frequency response data of $H_d(j\omega)$ are considered simultaneously as shown in Figure 2.7. Multiple input signals u_{seek} for the seeking actuator are also considered simultaneously, Figure 2.8.

In Figure 4.1, e is the ideal position error signal (PES) in absence of any vibration and feedforward action. e_d is the PES in presence of vibration and feedforward action. Let, $E(j\omega)$ be the frequency spectrum of PES e and E_d be the frequency spectrum of PES $E_d(j\omega)$. Our objective is to design feedforward controllers such that the actual frequency spectrum $E_d(j\omega)$ approaches the ideal frequency spectrum $E(j\omega)$.

The control objectives are considered in terms of H_∞ norm constraints, Eq.(3.31), and an H_2 norm objective function, Eq.(3.20), and Eq.(3.21). The H_∞ norm constraints are necessary and sufficient convex constraints in the controller parameterization X, Eq.(4.1),

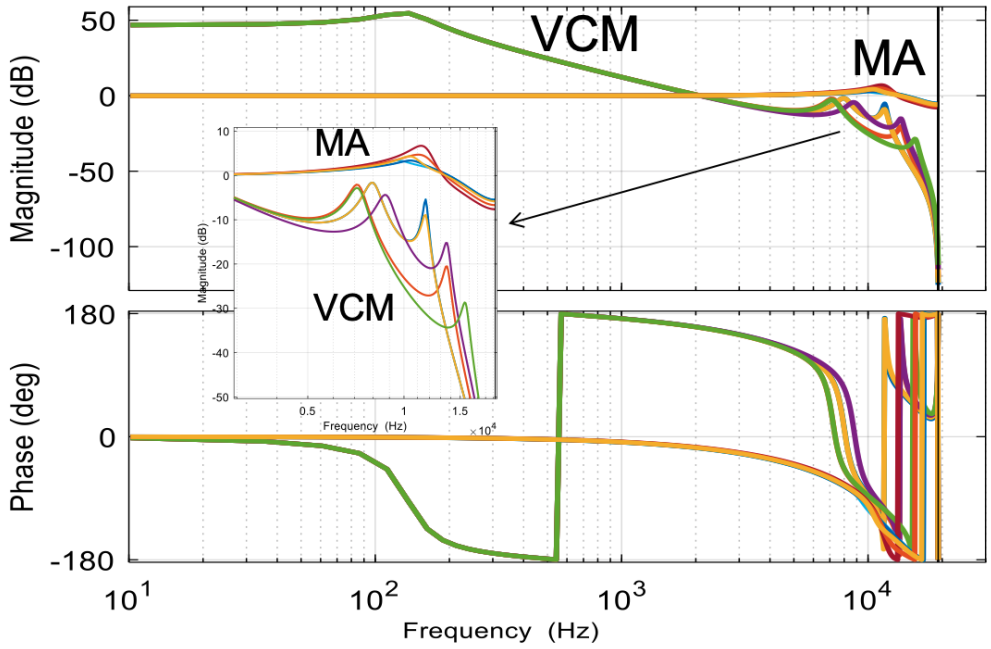

Figure 4.2: The frequency response measurements of VCM and MA for a set of five actuator arms are shown. This figure was also plotted in chapter 2 and is reproduced here as a reference.

and Y, Eq.(4.2). The convexity of the constraint ensures existence and uniqueness of the solution. The H_2 norm condition is only locally convex and requires an initial stabilizing controller to minimize the objective function.

In the first step, the VCM feedforward controller is designed to minimize the difference between E and E_d. In the second step, the MA feedforward controller is designed to suppress the residual vibration after VCM compensation.

VCM Feedforward Control Design

The frequency spectrum E is given by:

$$E(j\omega) = E_{r\to e}(j\omega)R(j\omega) \tag{4.4}$$

Here, $R(j\omega)$ is the frequency spectrum of runout r. $E_{r\to e}(j\omega)$ is the closed loop transfer function from r to e as shown in Figure 4.1. Assuming, we only have the VCM to suppress the vibration imparted by the coupling dynamics $H_d(j\omega)$, the frequency spectrum E_d is given by:

$$E_d(j\omega) = E_{r\to e}(j\omega)R(j\omega) + E_{r\to e}(j\omega)H_d(j\omega)U(j\omega) + E_{u_v\to e}(j\omega)K_{ff,VCM}(j\omega)U(j\omega) \tag{4.5}$$

Here, $U(j\omega)$ is the frequency spectrum of the seeking input signals u_{seek}. $K_{ff,VCM}(j\omega)$ is obtained by replacing z by $e^{j\omega}$ in Eq.(4.1). $E_{u_v \to e}(j\omega)$ is the closed loop transfer function from u_v to e as shown in Figure 4.1. $H_d(j\omega)$ is the coupling dynamics between the track seeking actuator and the track following actuator.

Our objective is to minimize the difference between E_d and E. H_2 norm objective function is used to minimize the difference between E_d and E. The H_2 norm minimization from Theorem 1 requires an initial stabilizing controller. Whereas, the H_∞ norm feasibility problem from Theorem 2 is a necessary and sufficient convex constraint. The convexity of the constraint ensures existence and uniqueness of the solution. Therefore, for the first iteration, only the H_∞ norm feasibility constraints are posed. Once a stabilizing controller is obtained from the H_∞ norm feasibility problem, H_2 norm objective function is introduced and iterated to minimize the difference between E_d and E.

A set of p frequency response measurements of VCM are considered, where i denotes the i^{th} VCM measurements. Also, a set of v frequency response measurements of the coupling dynamics $H_{d,l}(j\omega)$, where l denotes the l^{th} measurement data, and frequency response of s seeking input signals denoted by $U_m(j\omega)$, for the m^{th} frequency response of the seeking signal u_{seek}, are considered.

H_∞ Norm Feasibility Problem

From Theorem 2 the H_∞ norm feasibility problem is given by:

$\forall i \in \{1, \ldots, p\}$, $\forall l \in \{1, \ldots, v\}$ and $\forall \omega \in \Omega$ we have

$$\min_{X_{VCM}, Y_{VCM}} \quad 1 \tag{4.6}$$

$$\gamma^{-1} \left| W_f(j\omega) \left(E_{r \to e,i}(j\omega) H_{d,l}(j\omega) + E_{u_v \to e,i}(j\omega) X_{VCM}(j\omega) \right) \right| \quad \leq \quad Re\{Y_{VCM}(j\omega)\} \tag{4.7}$$

Here, W_f is a weighting filter used to shape the frequency response. Ω is the frequency region given by Eq.(3.9) over which the H_∞ norm constraints are posed. The frequency response of the stabilizing controller obtained from the feasibility problem is given by:

$$K_{ff,VCM}(j\omega) = X_{VCM}(j\omega) Y_{VCM}^{-1}(j\omega) \tag{4.8}$$

Mixed $H_2 - H_\infty$ Norm Optimization Problem

Using Eq.(4.8) as the initial stabilizing controller for the mixed $H_2 - H_\infty$ norm optimization problem from Eq.(3.32), Eq.(3.33) and Eq.(3.34), we have the following optimization problem:

$$\min_{X_k, Y_k, \Gamma} \sum_{i=1}^{p} \sum_{l=1}^{v} \sum_{m=1}^{s} \int_\Omega \Gamma_{i,l,m}(j\omega) d\omega \tag{4.9}$$

such that $\forall i \in \{1, \ldots, p\}$, $\forall l \in \{1, \ldots, v\}$, $\forall m \in \{1, \ldots, s\}$ and $\omega \in \Omega$:

$$\begin{bmatrix} \Gamma_{i,l,m} & (E_{r \to e,i} H_{d,l} + E_{u_v \to e,i} X_k) U_m \\ U_m^* (E_{r \to e,i} H_{d,l} + E_{u_v \to e,i} X_k)^* & Y_k^* Y_{k-1} + Y_{k-1}^* Y_k - Y_{k-1}^* Y_{k-1} \end{bmatrix} (j\omega) \geq 0 \tag{4.10}$$

$$\gamma^{-1} \left| W_f \left(E_{r \to e,i} H_{d,l} + E_{u_v \to e,i} X_k \right) \right| \leq Re\{Y_k\} \tag{4.11}$$

Here, the argument $(j\omega)$ is dropped for clarity in the equations. $X_{k-1}(j\omega)Y_{k-1}^{-1}(j\omega)$ is the controller from the previous iteration. Initially, we will use the controller from Eq.(4.8) as an initial stabilizing controller. $X_k(j\omega)$, $Y_k(j\omega)$ and $\Gamma(j\omega)$ are the optimizing variables. $\Gamma(j\omega)$ gives us the upper limit on the H_2 norm defined by Theorem 1.

The mixed H_2-H_∞ norm optimization problem can be iterated till the stopping condition is reached. A good example for a stopping condition is to have E_d within 5 percent of E. Assuming the mixed $H_2 - H_\infty$ norm optimization problem is iterated for n iterations, the feedforward controller for $K_{ff,VCM}(z)$ will be given by:

$$K_{ff,VCM}(z) = \frac{X_n(z)}{Y_n(z)} \tag{4.12}$$

The residual vibration coupling dynamics $G_{res,i,l}(j\omega)$ $\forall i \in \{1,\ldots,p\}$ and $\forall l \in \{1,\ldots,v\}$ will be given by:

$$G_{res,i,l}(j\omega) = E_{r\to e,i}(j\omega)H_{d,l}(j\omega) + E_{u_v\to e,i}(j\omega)K_{ff,VCM}(j\omega) \tag{4.13}$$

MA Feedforward Control Design

Now, the feedforward controller for the MA is designed to suppress the residual vibration given in Eq.(4.13). The controller factorization used to design feedforward controller for MA is given in Eq.(4.2).

Similar to the feedforward control design for VCM, first, the H_∞ norm feasibility problem is posed. Then, the H_2 objective function is introduced to iterate the mixed $H_2 - H_\infty$ norm optimization problem.

H_∞ Norm Feasibility Problem

The H_∞ norm feasibility problem to obtain stabilizing controller for MA is given by:

$\forall i \in \{1,\ldots,p\}$, $\forall l \in \{1,\ldots,v\}$ and $\forall \omega \in \Omega$ we have

$$\min_{X_{MA},Y_{MA}} 1 \tag{4.14}$$

$$\gamma^{-1}\left|W_{f_2}(j\omega)\left(G_{res,i,l}(j\omega) + E_{u_m\to e,i}(j\omega)X_{MA}(j\omega)\right)\right| \;\leq\; Re\{Y_{MA}(j\omega)\} \tag{4.15}$$

Here, $W_{f_2}(j\omega)$ is the weighting filter used to shape the frequency response. The frequency response of the stabilizing controller is given by:

$$K_{ff,MA}(j\omega) = X_{MA}(j\omega)Y_{MA}^{-1}(j\omega) \tag{4.16}$$

Mixed $H_2 - H_\infty$ Norm Optimization Problem

Using the MA controller from Eq.(4.16), according to Theorem 1 and Theorem 2 the mixed $H_2 - H_\infty$ norm optimization problem is given by:

$$\min_{X_k,Y_k,\Gamma} \sum_{i=1}^{p}\sum_{l=1}^{v}\sum_{m=1}^{s}\int_\Omega \Gamma_{i,l,m}(j\omega)d\omega \tag{4.17}$$

such that $\forall i \in \{1,\ldots,p\}$, $\forall l \in \{1,\ldots,v\}$, $\forall m \in \{1,\ldots,s\}$ and $\omega \in \Omega$:

$$\begin{bmatrix} \Gamma_{i,l,m} & (G_{res,i,l} + E_{u_m \to e,i} X_k) U_m \\ U_m^* (G_{res,i,l} + E_{u_m \to e,i} X_k)^* & Y_k^* Y_{k-1} + Y_{k-1}^* Y_k - Y_{k-1}^* Y_{k-1} \end{bmatrix} (j\omega) \geq 0 \tag{4.18}$$

$$\gamma^{-1} \left| W_{f_2} \left(G_{res,i,l} + E_{u_m \to e,i} X_k \right) \right| \leq Re\{Y_k\} \tag{4.19}$$

The argument $(j\omega)$ is dropped for compactness in the equations. $X_{k-1}(j\omega)Y_{k-1}^{-1}(j\omega)$ is the controller from the previous iteration. Initially, we use the controller from Eq.(4.16) as an initial stabilizing controller. $X_k(j\omega)$, $Y_k(j\omega)$ and $\Gamma(j\omega)$ are the optimizing variables. $\Gamma(j\omega)$ gives us the upper limit on the H_2 norm defined by Theorem 1.

Assuming the mixed $H_2 - H_\infty$ norm optimization problem is iterated for t iterations, the feedforward controller for MA will be given by:

$$K_{ff,MA}(z) = \frac{X_t(z)}{Y_t(z)} \tag{4.20}$$

Therefore, Eq.(4.12) and Eq.(4.20) give us the feedforward controllers for VCM and MA using the sequential SISO data driven control design methodology. The solver MOSEK [36] on MATLAB [34] is used to solve these locally convex iterative optimization problems.

SIMO Feedforward Control Design

A track following actuator arm has two actuators, VCM and MA, connected in series. The actuator arm has two inputs, one for each VCM and MA and has one output, the position of the read/write head. The actuator arm is a multi-input single-output (MISO) system. The ideal controller for a MISO system will be a SIMO controller.

In the SIMO feedforward control design methodology, the feedforward controllers for VCM and MA are designed simultaneously to suppress the vibration imparted by the coupling dynamics $H_d(j\omega)$ from Figure. 2.7.

In Figure 4.1, e is the ideal position error signal (PES) in absence of any vibration and feedforward action. e_d is the PES in presence of vibration and feedforward action. Let, $E(j\omega)$ be the frequency spectrum of PES e and $E_d(j\omega)$ be the frequency spectrum of PES e_d. Our objective is to design feedforward controllers such that the actual frequency spectrum $E_d(j\omega)$ approaches the ideal frequency spectrum $E(j\omega)$.

The control objectives are considered in terms of H_∞ norm constraints, Eq.(3.31) and an H_2 norm objective function, Eq.(3.20) and Eq.(3.21). The H_∞ norm constraints are necessary and sufficient convex constraints in the controller parameterization X, Eq.(4.1), and Y, Eq.(4.2). The convexity of the constraint ensures existence and uniqueness of the solution. The H_2 norm condition is only locally convex and requires an initial stabilizing controller to minimize the objective function.

The frequency spectrum $E(j\omega)$ is given by:

$$E(j\omega) = E_{r \to e}(j\omega) R(j\omega) \tag{4.21}$$

Here, $R(j\omega)$ is the frequency spectrum of the runout r. $E_{r\to e}(j\omega)$ is the closed loop transfer function from r to e. The frequency spectrum $E_d(j\omega)$ is given by:

$$\begin{aligned} E_d(j\omega) &= E_{r\to e}(j\omega)R(j\omega) + E_{r\to e}(j\omega)H_d(j\omega)U(j\omega) + \dots \\ &\quad \dots E_{u_v\to e}(j\omega)K_{ff,VCM}(j\omega)U(j\omega) + E_{u_m\to e}(j\omega)K_{ff,MA}(j\omega)U(j\omega) \end{aligned} \tag{4.22}$$

Here, $U(j\omega)$ is the frequency spectrum of the seeking input signals u_{seek}. $K_{ff,VCM}(j\omega)$ and $K_{ff,MA}(j\omega)$ are obtained by replacing z by $e^{j\omega}$ in Eq.(4.1) and Eq.(4.2). $E_{u_v\to e}(j\omega)$ is the closed loop transfer function from u_v to e as shown in Figure 4.1. $E_{u_m\to e}(j\omega)$ is the closed loop transfer function from u_m to e as shown in Figure 4.1. $H_d(j\omega)$ is the coupling transfer function between the seeking actuator and the track following actuator.

Our objective is to minimize the difference between E_d and E. H_2 norm objective function is used to minimize the difference between E_d and E. The H_2 norm minimization from Theorem 1 requires an initial stabilizing controller. Whereas, the H_∞ norm feasibility problem from Theorem 2 is a necessary and sufficient convex constraint. The convexity of the constraint ensures existence and uniqueness of the solution. Therefore, for the first iteration, only the H_∞ norm feasibility constraints are posed. Once a stabilizing controller is obtained from the H_∞ norm feasibility problem, H_2 norm objective function is introduced and iterated to minimize the difference between E_d and E.

A set of p frequency response measurements of VCM and MA are considered, where i denotes the i^{th} VCM and MA measurements. Also, a set of v frequency response measurements of the coupling dynamics $H_{d,l}(j\omega)$, where l denotes the l^{th} measurement data, and frequency response of s seeking input signals denoted by $U_m(j\omega)$, for the m^{th} frequency response of the seeking signal u_{seek}, are considered.

H_∞ Norm Feasibility Problem

From Theorem 2 the H_∞ norm feasibility problem is given by:

$\forall i \in \{1,\dots,p\}$, $\forall l \in \{1,\dots,v\}$ and $\forall \omega \in \Omega$ we have

$$\min_{X_{VCM},X_{MA},Y} 1 \tag{4.23}$$

$$\gamma^{-1}\left|W_f\left(E_{r\to e,i}H_{d,l} + E_{u_v\to e,i}X_{VCM} + E_{u_m\to e,i}X_{MA}\right)\right| \leq Re\{Y\} \tag{4.24}$$

The argument $(j\omega)$ is dropped for compactness. The controller factorization used for VCM and MA are chosen to have the same denominator $Y(z)$. The initial stabilizing controller for mixed $H_2 - H_\infty$ norm control optimization problem is obtained as the solution of the H_∞ norm feasibility problem.

$$K_{ff,VCM}(z) = \frac{X_{VCM}(z)}{Y(z)} \tag{4.25}$$

$$K_{ff,MA}(z) = \frac{X_{MA}(z)}{Y(z)} \tag{4.26}$$

Mixed $H_2 - H_\infty$ Norm Optimization Problem

Eq.(4.25) and Eq.(4.26) give us the initial stabilizing controllers for VCM and MA respectively. According to Eq.(3.32), Eq.(3.33) and Eq.(3.34), the mixed $H_2 - H_\infty$ norm optimization problem is given by:

$$\min_{X_{VCM,k}, X_{MA,k}, Y_k, \Gamma} \sum_{i=1}^{p} \sum_{l=1}^{v} \sum_{m=1}^{s} \int_{\Omega} \Gamma_{i,l,m}(j\omega) d\omega \tag{4.27}$$

such that $\forall i \in \{1, \ldots, p\}$, $\forall l \in \{1, \ldots, v\}$, $\forall m \in \{1, \ldots, s\}$ and $\omega \in \Omega$:

$$\begin{bmatrix} \Gamma_{i,l,m} & (R_{r\to e,i}H_{d,l} + E_{u_v\to e,i}X_{VCM,k} + E_{u_m\to e,i}X_{MA,k})U_m \\ U_m^*(E_{r\to e,i}H_{d,l} + E_{u_v\to e,i}X_{VCM,k} + E_{u_m\to e,i}X_{MA,k})^* & Y_k^*Y_{k-1} + Y_{k-1}^*Y_k - Y_{k-1}^*Y_{k-1} \end{bmatrix} \geq 0 \tag{4.28}$$

$$\gamma^{-1} \left| W_f \left(E_{r\to e,i}H_{d,l} + E_{u_v\to e,i}X_{VCM,k} + E_{u_m\to e,i}X_{MA,k} \right) \right| \leq Re\{Y_k\} \tag{4.29}$$

The argument $(j\omega)$ is dropped for compactness in the equations. The controllers from the previous iteration in the frequency domain are given by

$$K_{ff,VCM,k-1}(j\omega) = \frac{X_{VCM,k-1}(j\omega)}{Y_{k-1}(j\omega)} \tag{4.30}$$

$$K_{ff,MA,k-1}(j\omega) = \frac{X_{MA,k-1}(j\omega)}{Y_{k-1}(j\omega)} \tag{4.31}$$

The controllers from Eq.(4.25) and Eq.(4.26) are used to initial the optimization problem. Assuming the algorithm is run for n iterations, the final feedforward controllers for VCM and MA are given by:

$$K_{ff,VCM,n}(z) = \frac{X_{VCM,n}(z)}{Y_n(z)} \tag{4.32}$$

$$K_{ff,MA,n}(z) = \frac{X_{MA,n}(z)}{Y_n(z)} \tag{4.33}$$

Therefore, Eq.(4.32) and Eq.(4.33) are the feedforward controllers for VCM and MA designed to suppress the vibration imparted by the coupling dynamics $H_d(j\omega)$, as shown in Figure 2.7, in multi actuator drives. The solver MOSEK [36] on MATLAB [34] is used to solve these locally convex iterative optimization problems.

4.5 Design Results

The control block diagram of a multi actuator drive is as shown in Figure 4.1. In a multi actuator drive, we have two actuator arms functioning independently pivoted at the same point. This design configuration leads to vibration interaction between the two actuators

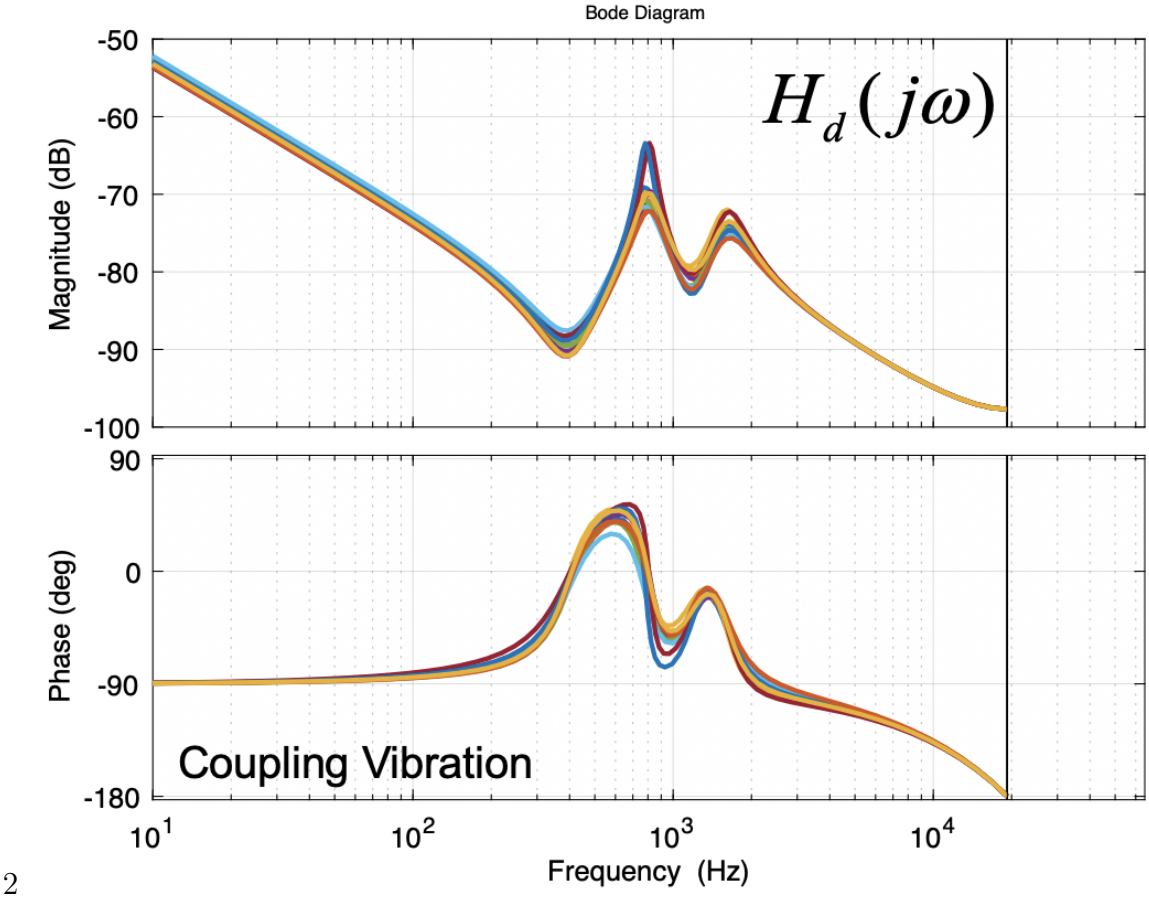

Figure 4.3: The frequency response measurements of the coupling dynamics imparting vibration are plotted. A set of five measurement data are considered for the design process. The frequency responses of the coupling dynamics were measured by our industry partners. The models plotted are representative of the true behavior of the interaction.

arms. The track seeking procedure in a hard disk drive generates considerable vibration to affect the functioning of the neighboring actuator arm.

Two data driven methodologies, sequential SISO design and SIMO design, used to design feedforward controllers for the track following actuator were presented in section 4.4. A track following actuator arm has two actuators, a voice coil motor (VCM) and a micro actuator (MA), connected in series. In the sequential SISO control design methodology, first, the VCM feedforward controller is designed to suppress the entire vibration. Then, the MA feedforward controller is designed to suppress any residual vibration. Whereas, in the SIMO control design methodology, VCM and MA feedforward controllers are simultaneously designed to suppress the vibration.

In the data driven algorithm, multiple sets of frequency response measurements of the

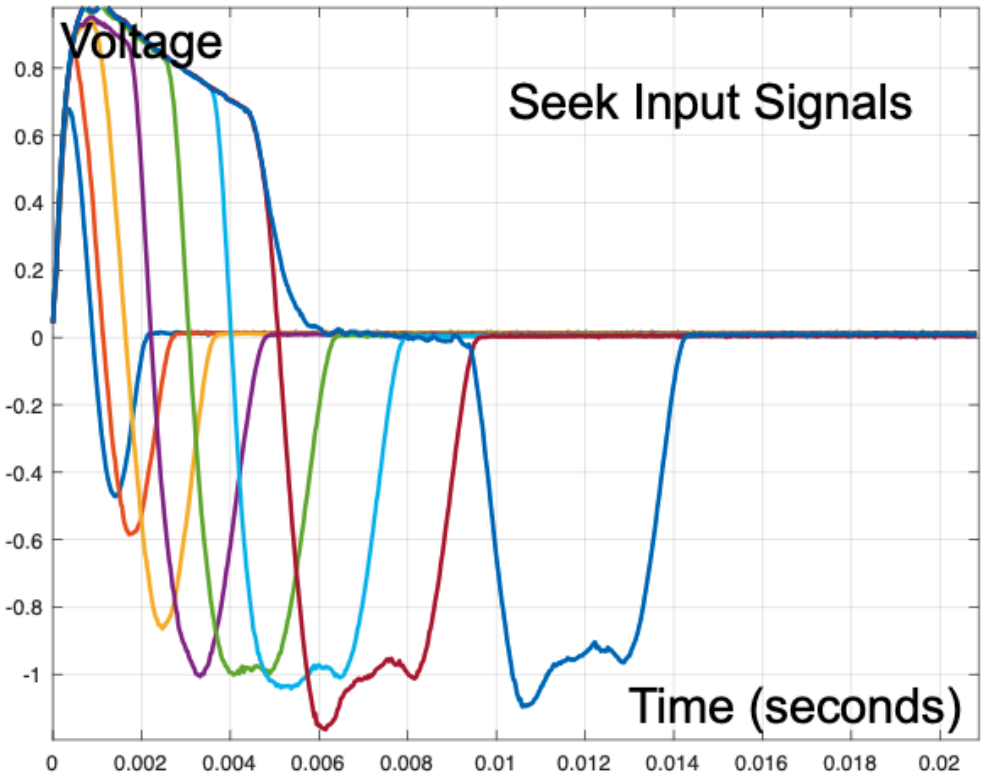

Figure 4.4: The seeking input signals $u_{seek}(k)$ used for the design process are plotted. All the seeking scenarios are considered simultaneously to obtain a robust controller. The seeking input signals are actual seeking input signals used in dual stage hard disk drives.

actuators VCM and MA are considered. In the design results presented in this section, two sets of VCM and MA data are considered. Multiple frequency response measurements of the vibration are also considered simultaneously in the design process. The frequency response measurements of the coupling dynamics imparting vibration considered are shown in Figure 4.3. The frequency responses of the coupling dynamics were measured by our industry partners. The models plotted in Figure 4.3 are representative of the true behavior of the interaction.

The control input signals of the seeking actuator arm generating the observed coupling dynamics in Figure 4.3 are available offline during the design process. The frequency spectrum of the control input signals are used for the design process. The excitation of the vibration depends on the seek lengths of the seeking actuator arm. A set of eight seeking scenarios are considered simultaneously ranging from short seeks to long seeks. The control input signals of these seeking scenarios are plotted in Figure 4.4. The control input signals are actual seeking input signals used in dual stage hard disk drives.

Our objective is to design feedforward controllers to suppress the imparted vibration by

the coupling dynamics in Figure 4.3, for the excitation signals in Figure 4.4. First, the results based on the sequential SISO control design methodology are presented. Then, the results based on the SIMO control design methodology are presented. A comparison between the two methodologies is also presented.

Frequency Domain

Sequential SISO Feedforward Control Design

In the sequential SISO feedforward control design, the VCM feedforward controller is first designed to suppress the imparted vibration Eq.(4.12), then, the MA feedforward controller is designed to suppress any residual vibration Eq.(4.20).

Figure 4.5 plots the frequency response of the PES obtained after designed the VCM feedforward controller. Here, e represents the ideal PES spectrum without any vibration or any feedforward action, shown in blue. e_{dist} represents the PES spectrum with vibration but no feedforward suppression. A number of vibration scenarios are plotted together. $e_{ff,VCM}$ represents the PES spectrum with vibration and feedforward action using the VCM actuator only. $e_{ff,VCM}$ is shown in red.

As shown in Figure 4.5, the VCM does a good job in the low frequency region in suppressing all the vibration disturbance. But, the VCM does not suppress the high frequency disturbance. This is due to the fact that the VCM servo has a low bandwidth.

Figure 4.6 plots the frequency response of the PES obtained after designing the VCM and MA feedforward controllers using the sequential SISO control design methodology. Here, e represents the ideal PES spectrum without any vibration or any feedforward action, shown in blue. e_{dist} represents the PES spectrum with vibration but no feedforward suppression. A number of vibration scenarios are plotted together. $e_{ff,VCM}$ represents the PES spectrum with vibration and feedforward action using the VCM actuator only. $e_{ff,VCM}$ is shown in red. $e_{ff,dual}$ represents the PES spectrum with vibration and feedforward action using both VCM and MA actuators. $e_{ff,dual}$ is shown in yellow.

The dual stage feedforward controllers suppress vibration in the low frequency as well as the high frequency region. The MA feedforward controller is designed to suppress the residual vibration after the VCM feedforward control design. The MA servo has a higher bandwidth and hence is capable of suppressing vibration in the high frequency region.

From Eq.(4.5), we define the closed loop coupling transfer function $G_{d,i,l}(j\omega)$ for i^{th} actuator measurement and l^{th} coupling vibration as follows:

$$G_{d,i,l}(j\omega) = E_{(r\to e),i}(j\omega)H_{d,l}(j\omega) \tag{4.34}$$

The closed loop feedforward controllers for i^{th} actuator measurement are defined as:

$$K_{cl,VCM,i}(j\omega) = E_{u_v\to e}(j\omega)K_{ff,VCM}(e^{j\omega}) \tag{4.35}$$

$$K_{cl,MA,i}(j\omega) = E_{u_m\to e}(j\omega)K_{ff,MA}(e^{j\omega}) \tag{4.36}$$

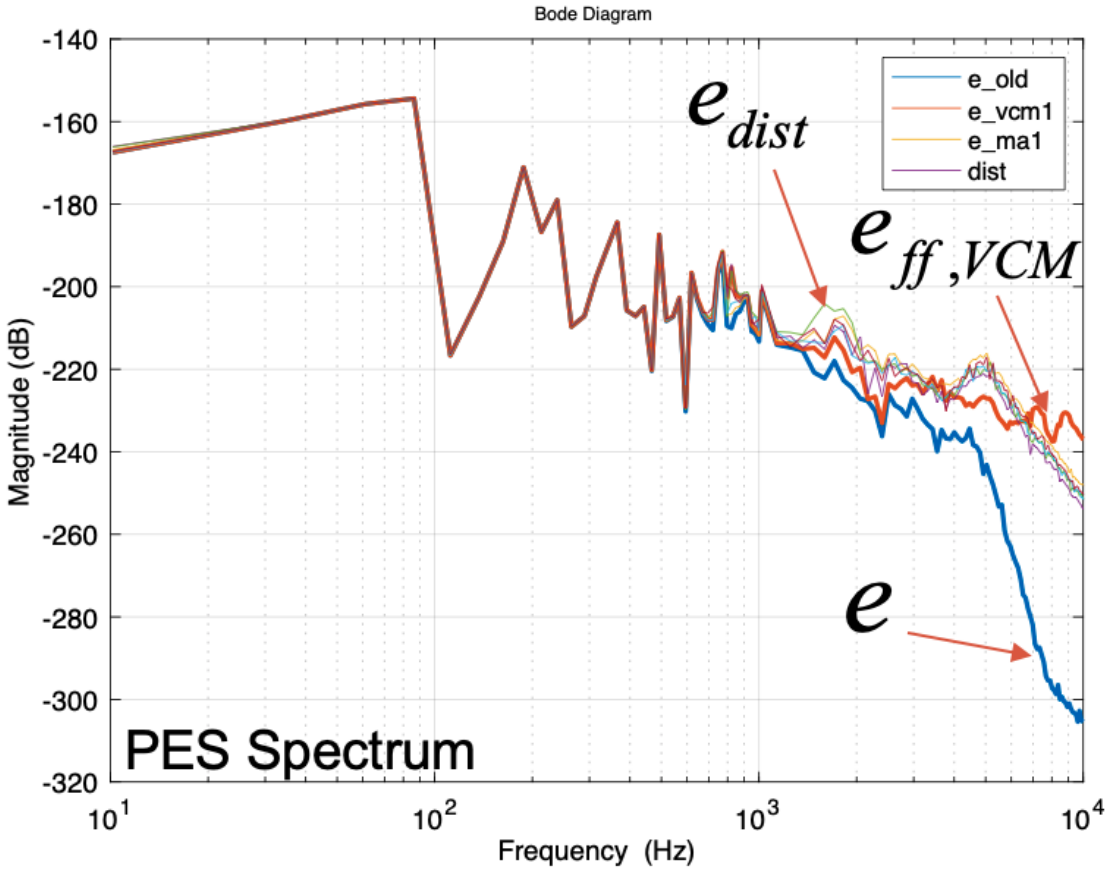

Figure 4.5: The frequency spectrum of the PES is plotted after designing VCM feedforward controller using the sequential SISO control design methodology. e, plotted in blue, represents the ideal PES spectrum without any vibration or any feedforward action. e_{dist} represents the PES spectrum with vibration but no feedforward suppression. A number of vibration scenarios are plotted together. $e_{ff,VCM}$, plotted in red, represents the PES spectrum with vibration and feedforward action using the VCM actuator only.

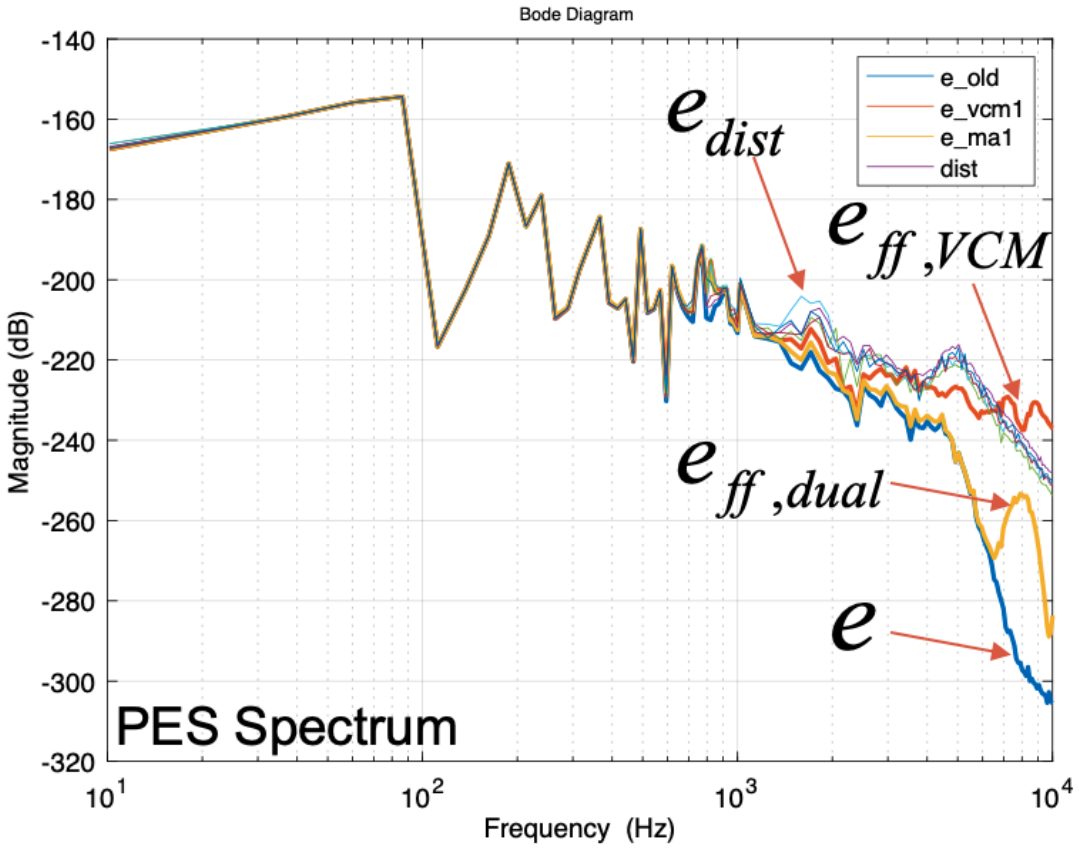

Figure 4.6: The frequency spectrum of the PES is plotted after obtaining the feedforward controllers for VCM and MA using the sequential SISO control design methodology. e, plotted in blue, represents the ideal PES spectrum without any vibration or any feedforward action. e_{dist} represents the PES spectrum with vibration but no feedforward suppression. A number of vibration scenarios are plotted together. $e_{ff,VCM}$, plotted in red, represents the PES spectrum with vibration and feedforward action using the VCM actuator only. $e_{ff,dual}$, plotted in yellow, represents the PES spectrum with vibration and feedforward action using both VCM and MA.

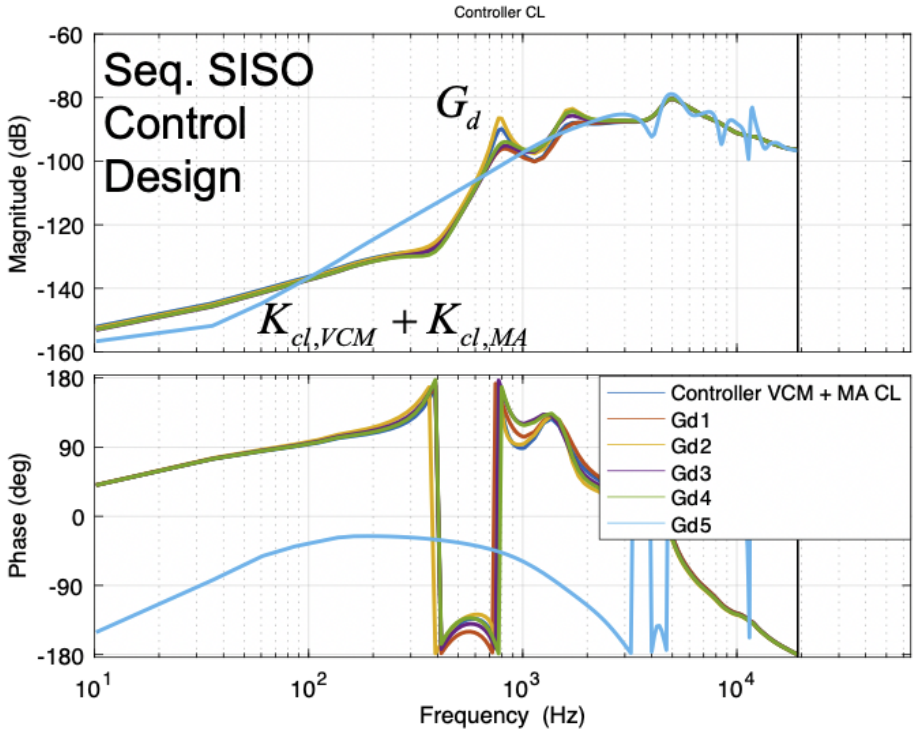

Figure 4.7: The objective of the feedforward control design is to match the closed loop coupling transfer function $G_{d,i,l}(j\omega)$ from Eq.(4.34) with the closed loop feedforward action given by Eq.(4.35) and Eq.(4.36). In this figure, we can observe that for one actuator plant data, the feedforward controllers are not able to closely match $G_d(j\omega)$ for five vibration scenarios. We can observe a small bias in the low frequency region and the mid frequency region is not matched.

The objective of the feedforward control design is to match the closed loop coupling transfer function $G_{d,i,l}(j\omega)$ from Eq.(4.34) with the closed loop feedforward action given by Eq.(4.35) and Eq.(4.36). The closed loop feedforward control transfer function and the closed loop coupling transfer function are plotted against each other in Figure 4.7. We can observe a small bias in the low frequency region and the mid frequency region is not matched.

SIMO Feedforward Control Design

In the SIMO feedforward control design, the VCM and MA feedforward controllers are designed simultaneously as given by Eq.(4.32) and Eq.(4.33).

Figure 4.8 plots the frequency response of the PES obtained after designing the VCM and MA feedforward controllers using the SIMO control design methodology. Here, e represents

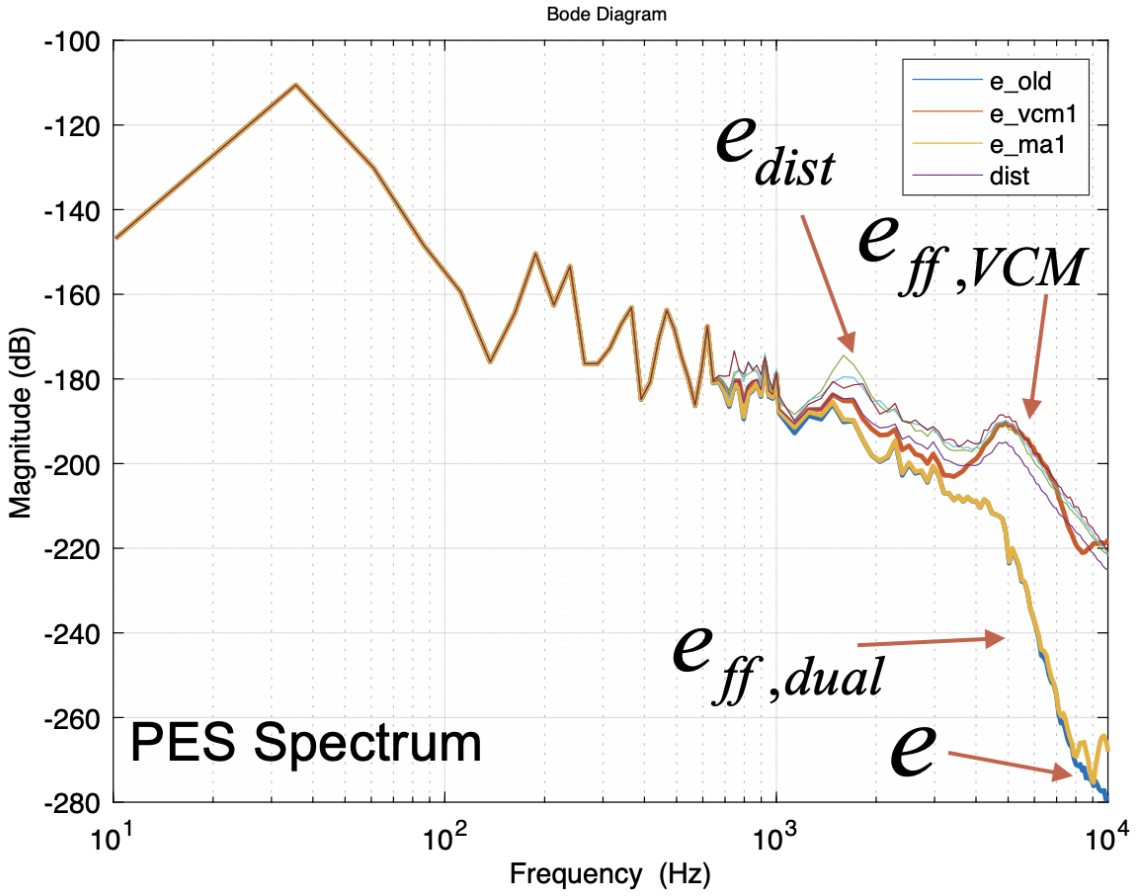

Figure 4.8: The frequency spectrum of the PES is plotted after obtaining the feedforward controllers for VCM and MA using the SIMO control design methodology. e, plotted in blue, represents the ideal PES spectrum without any vibration or any feedforward action. e_{dist} represents the PES spectrum with vibration but no feedforward suppression. A number of vibration scenarios are plotted together. $e_{ff,VCM}$, plotted in red, represents the PES spectrum with vibration and feedforward action using the VCM actuator only. $e_{ff,dual}$, plotted in yellow, represents the PES spectrum with vibration and feedforward action using both VCM and MA. The feedforward suppression obtained using the SIMO control design methodology does a better job at suppressing the imparted vibration than the sequential SISO control design methodology (Figure 4.6).

the ideal PES spectrum without any vibration or any feedforward action, shown in blue. e_{dist} represents the PES spectrum with vibration but no feedforward suppression. A number of vibration scenarios are plotted together. $e_{ff,VCM}$ represents the PES spectrum with vibration and feedforward action using the VCM actuator only. $e_{ff,VCM}$ is shown in red. $e_{ff,dual}$ represents the PES spectrum with vibration and feedforward action using both VCM and MA actuators. $e_{ff,dual}$ is shown in yellow.

The VCM and MA feedforward controllers obtained using the SIMO feedforward data driven control design methodology suppress the vibration more effectively than the feedforward controllers obtained using the sequential SISO feedforward data driven control design methodology. But, if the performance of the VCM feedforward controller is compared, the controller obtained using the sequential SISO control design methodology does a better job.

In the SIMO control design methodology, as the VCM and MA controllers are designed together, the two controllers are shaped such that VCM focuses on the low frequency region and the MA focuses on the high frequency region. Whereas, in the sequential SISO control design methodology, the VCM controller is designed to suppress both the low frequency and the high frequency region, leading to a less efficient design. In case of a MA failure, the VCM controller designed using the sequential SISO methodology does a better job at suppressing the vibration. The VCM controller obtained using the SIMO control design methodology is not designed to suppress the entire vibration spectrum.

The frequency spectrum of the PES obtained for five actuator measurements is compared with the frequency spectrum of the PES obtained for two actuator measurements in Figure 4.9. The feedforward controllers obtained for two actuator measurements perform better than the feedforward controllers obtained for five actuator measurements.

From Eq.(4.23), we define the closed loop coupling transfer function $G_{d,i,l}(j\omega)$ for i^{th} actuator measurement and l^{th} coupling vibration as follows:

$$G_{d,i,l}(j\omega) = E_{(r\to e),i}(j\omega)H_{d,l}(j\omega) \tag{4.37}$$

The closed loop feedforward controllers for i^{th} actuator measurement are defined as:

$$K_{cl,VCM,i}(j\omega) = E_{u_v\to e}(j\omega)K_{ff,VCM}(e^{j\omega}) \tag{4.38}$$

$$K_{cl,MA,i}(j\omega) = E_{u_m\to e}(j\omega)K_{ff,MA}(e^{j\omega}) \tag{4.39}$$

The objective of the feedforward control design is to match the closed loop coupling transfer function $G_{d,i,l}(j\omega)$ from Eq.(4.37) with the closed loop feedforward action given by Eq.(4.38) and Eq.(4.39). The closed loop feedforward control transfer function and the closed loop coupling transfer function are plotted against each other in Figure 4.10. We observe that the feedforward controllers obtained using the SIMO control design methodology match $G_d(j\omega)$ better than the feedback controllers obtained using the sequential SISO control design methodology.

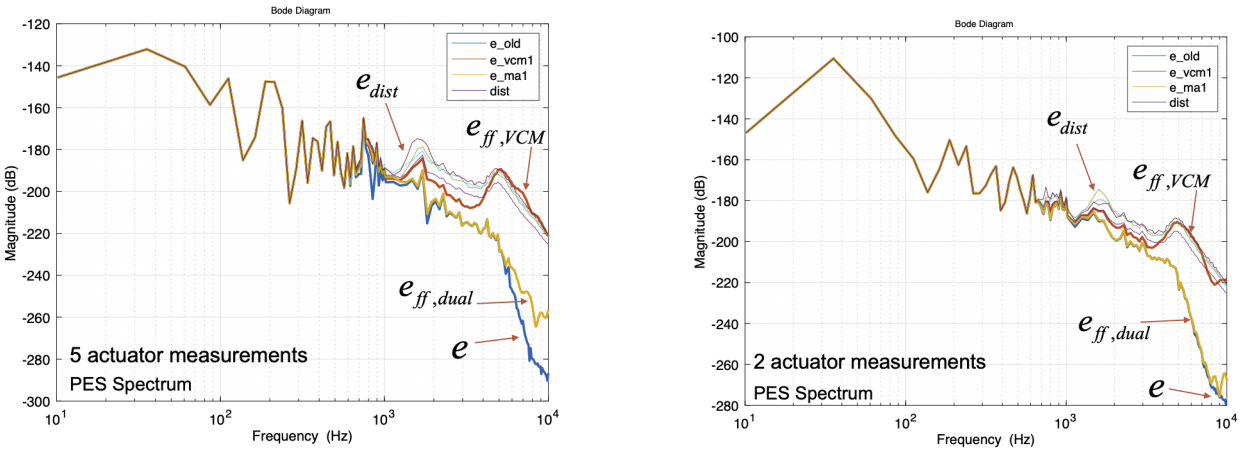

(a) Five actuator measurements

(b) Two actuator measurements

Figure 4.9: The frequency spectrum of the PES obtained for five actuator measurements is compared with the frequency spectrum of the PES obtained for two actuator plant measurements in this figure

Time Domain

Sequential SISO Feedforward Control Design

The effect of the disturbance signal u_d on the position error signal (PES) e is plotted in the time domain. The PES due to the runout r in Figure 4.1 is not plotted in these time domain plots to understand the performance of the feedforward controllers. The vibration disturbance signal is generated by passing the seeking input signals (Figure 4.4) through the coupling dynamics (Figure 4.3). The PES due to the disturbance signal is obtained by passing u_d through the closed loop transfer function $R_{r\to e}(z)$ as shown in Figure 4.1.

Figure 4.11 plots the PES in presence of vibration and no feedforward action and the PES in presence of vibration and feedforward action by the VCM and MA controllers obtained using the sequential SISO control design methodology. e_{dist} is the PES in presence of vibration and no feedforward action, shown in blue. $e_{dist+ff}$ is the PES in presence of vibration and, VCM and MA feedforward action, shown in red. Overall, a feedforward suppression of $2\times$ is observed.

SIMO Feedforward Control Design

The effect of the disturbance signal u_d on the position error signal (PES) e is plotted in the time domain. The PES due to the runout r in Figure 4.1 is not plotted in these time domain plots to understand the performance of the feedforward controllers. The vibration disturbance signal is generated by passing the seeking input signals (Figure 4.4) through

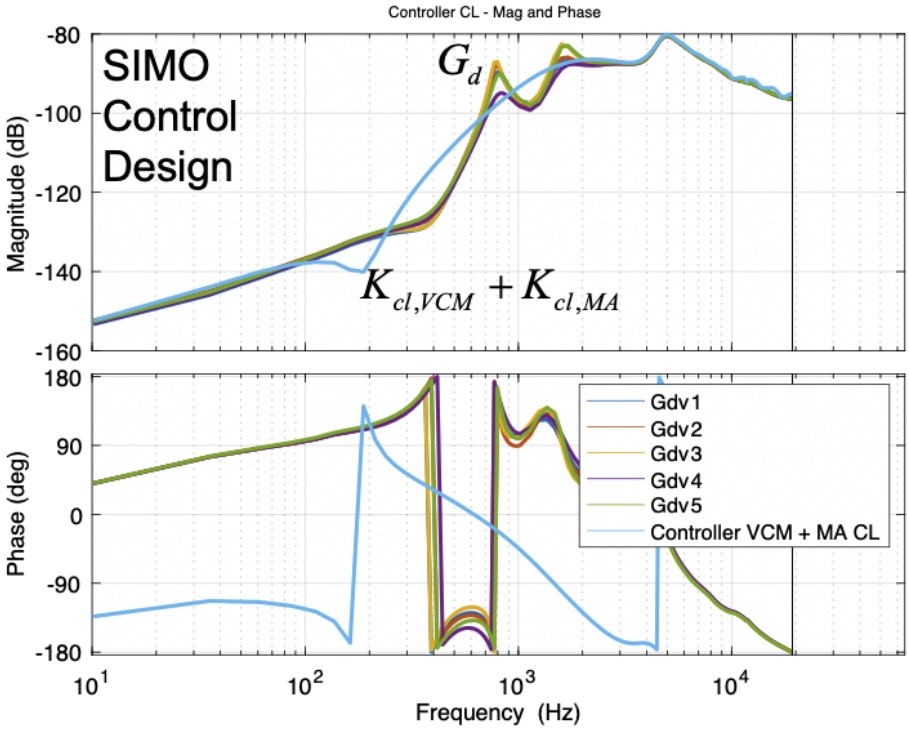

Figure 4.10: The objective of the feedforward control design is to match the closed loop coupling transfer function $G_{d,i,l}(j\omega)$ from Eq.(4.37) with the closed loop feedforward action given by Eq.(4.38) and Eq.(4.39). In this figure, we can observe that for one actuator plant data, the feedforward controllers are able to closely match $G_d(j\omega)$ for five vibration scenarios. The mid frequency region is not matched. The low frequency region and the high frequency region are matched properly.

the coupling dynamics (Figure 4.3). The PES due to the disturbance signal is obtained by passing u_d through the closed loop transfer function $R_{r\to e}(z)$ as shown in Figure 4.1.

Figure 4.12 plots the PES in presence of vibration and no feedforward action and the PES in presence of vibration and feedforward action by the VCM and MA controllers obtained using the SIMO control design methodology. e_{dist} is the PES in presence of vibration and no feedforward action, shown in blue. $e_{dist+ff}$ is the PES in presence of vibration and, VCM and MA feedforward action, shown in red. Overall, a feedforward suppression of 3× is observed.

The SIMO feedforward controllers achieve 3× suppression but, the sequential SISO controllers achieve only 2× suppression. The SIMO control design methodology optimizes the controllers further than the sequential SISO control design methodology. The main advantage in the design process is that both VCM and MA controllers are shaped together in the SIMO design process. But, in the sequential SISO design process, the VCM controller stays fixed while designing the MA controller resulting in some mutual fighting between the two

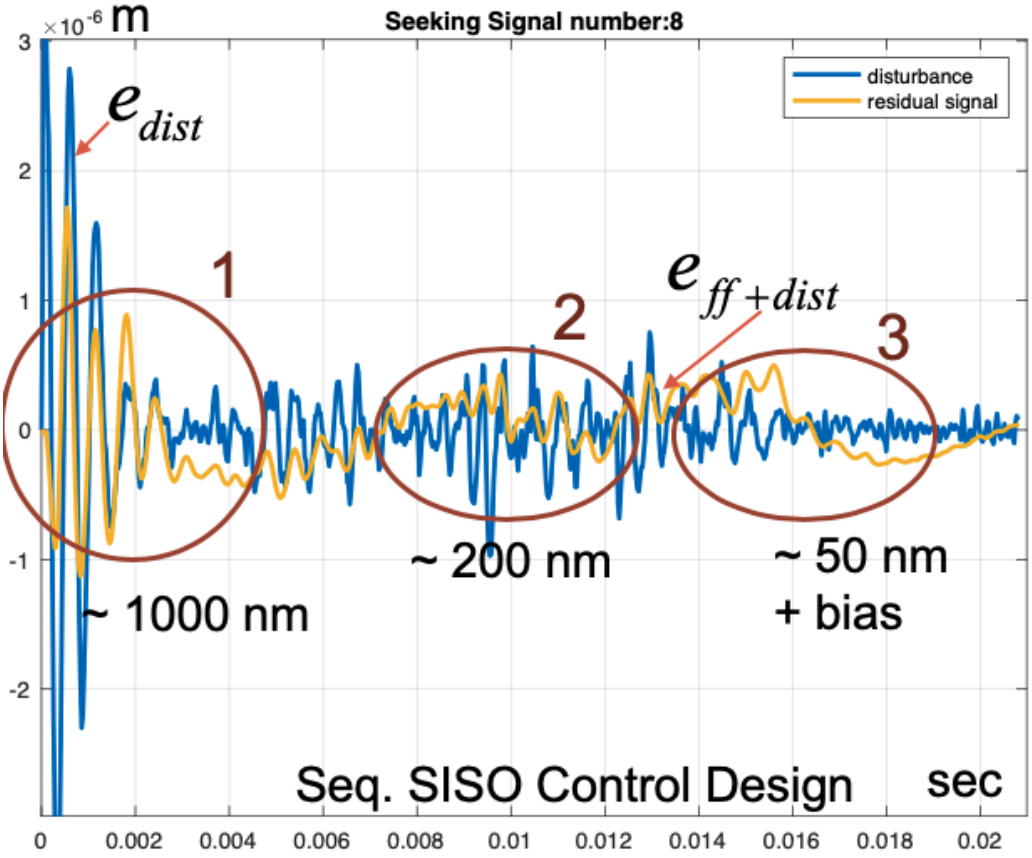

Figure 4.11: PES in time domain obtained after VCM and MA feedforward control design using the sequential SISO methodology is plotted. e_{dist} is the PES in the presence of vibration but no feedforward action. $e_{dist+ff}$ is the resultant PES in the presence of vibration and, VCM and MA feedforward action. A feedforward suppression of 2× is observed throughout the seeking process.

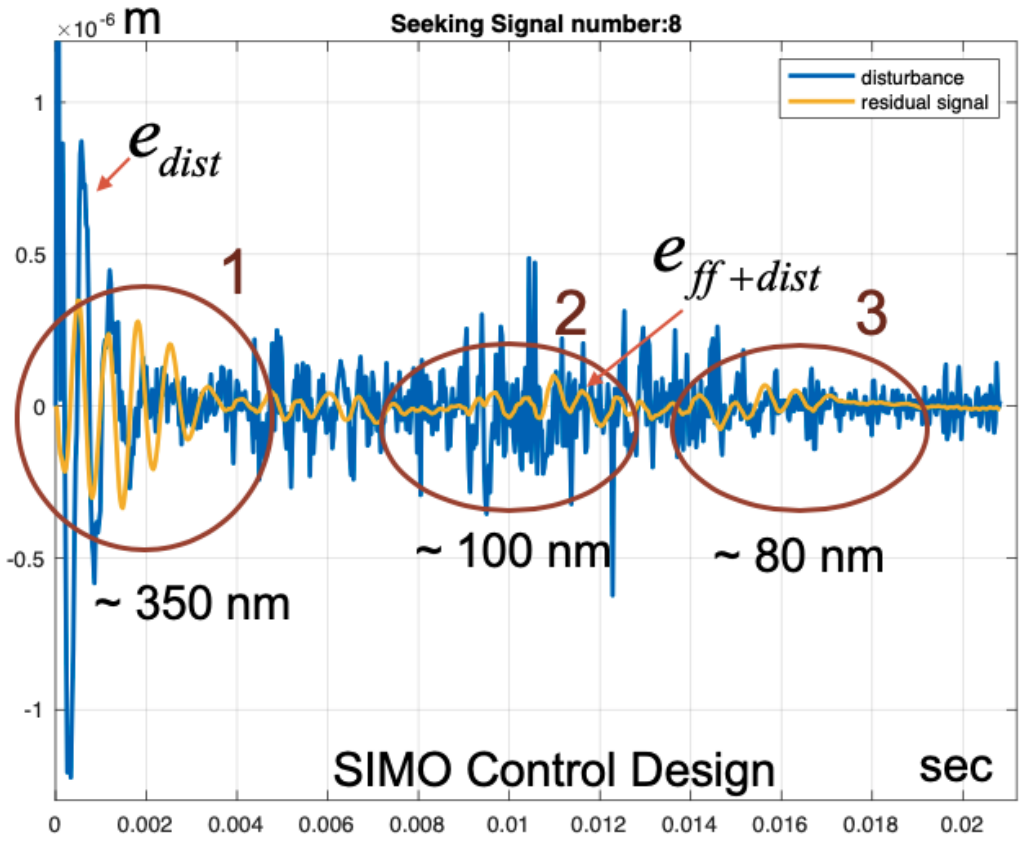

Figure 4.12: PES in time domain obtained after VCM and MA feedforward control design using the sequential SISO methodology is plotted. e_{dist} is the PES in the presence of vibration but no feedforward action. $e_{dist+ff}$ is the resultant PES in the presence of vibration and, VCM and MA feedforward action. A feedforward suppression of 3× is observed throughout the seeking process.

actuators.

The design objective set by our industry partners require a feedforward suppression upto 2×. This design objective is met for both the sequential SISO control design approach as well as the SIMO control design approach. In the time domain plots, based on the residual vibration, track following process cannot begin until phase 2 is reached in Figure 4.11 and in Figure 4.12.

Chapter 5

Joint Feedback Feedforward Data Driven Control Design

5.1 Introduction

In chapter 3, the data driven feedforward control design methodologies were presented. The feedback controllers were assumed to be pre-designed. In this chapter, joint feedback and feedforward data driven control design methodologies are proposed based on frequency response measurements.

Traditionally, control design methods fit a model to the frequency response data and design controllers based on the model. Whereas, the data driven control design approach designs controllers directly based on the frequency response measurements. In chapter 3, the feedback controller is pre-designed and does not account for the imparted vibration. A joint feedback - feedforward control design will optimize the feedback and feedforward controllers further to provide a more robust control design.

H_∞ norm and H_2 norm conditions are used as control objectives to design the feedback and feedforward controllers. An H_∞ norm data driven design methodology for SISO systems was presented in [28]. The design methodology was extended for MISO in [8, 7]. A mixed $H_2 - H_\infty$ norm control design methodology for feedback systems was presented in [27, 8]. A data driven control design methodology for feedforward systems was presented in [46].

In section 5.2 the preliminaries and the control block diagram used to formulate the problem are discussed. The controller factorization used for the design process are discussed in section 5.3. The joint data driven feedback feedforward control design methodologies are discussed in section 5.4. Two data driven methodologies are presented to obtain the feedback and feedforward control design. An alternating iterative data driven control design approach and a simultaneous feedback - feedforward data driven control design approach.

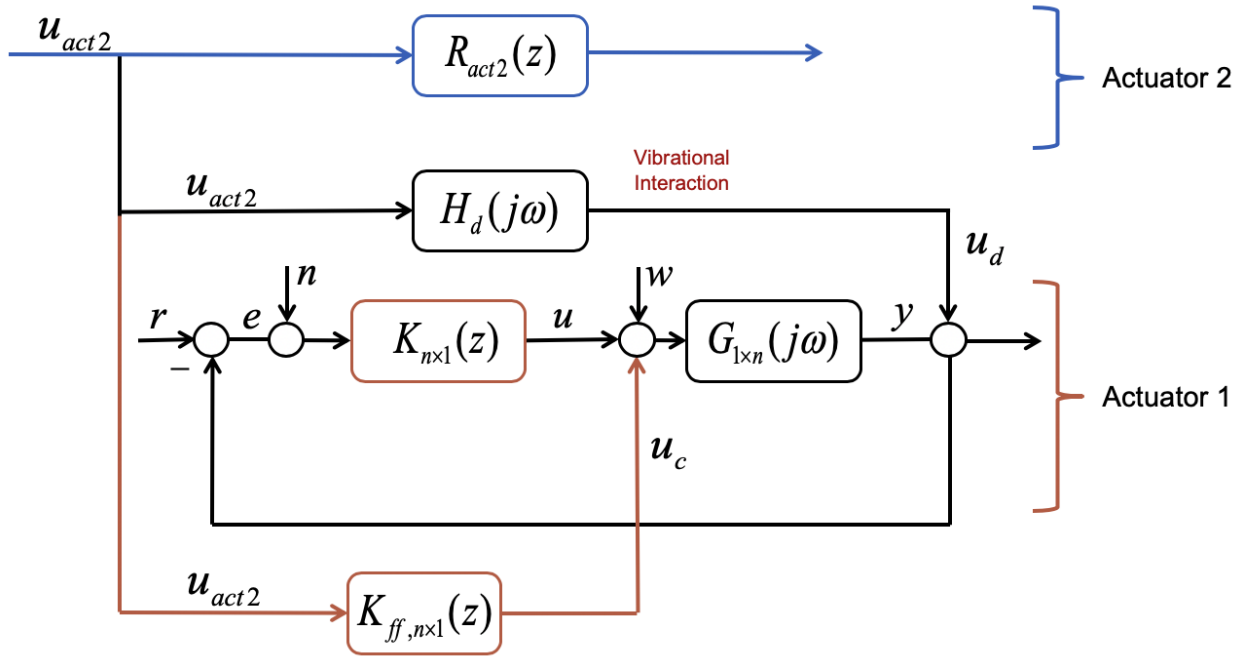

Figure 5.1: The control block diagram used to obtain the joint feedback-feedforward data driven control design methodologies for a two-actuator setup is shown. This figure is similar to Figure 3.1, but, both the feedback and feedforward controllers will be designed in this chapter.

5.2 Preliminaries

In this section, the control block diagram used to obtain the feedback and feedforward controllers for the two actuator setup is discussed.

In Figure 5.1, the control block diagram used to develop the joint feedback-feedforward data driven control design methodologies for a two-actuator setup is shown. This figure is similar to Figure 3.1, but, both the feedback and feedforward controllers are designed in this chapter.

In Figure 5.1, $R_{act2}(z)$ is the closed loop transfer function of actuator 2. u_{act2} is its control input signal. This control input signal is available offline and is used to design the feedforward controller.

$G_{1\times n}(j\omega)$ is the frequency response measurement of the open loop actuator 1. Multiple sets of frequency response measurements $G_{1\times n}(j\omega)$ can be considered simultaneously in the data driven control design methodologies. The open loop actuator has n inputs and one output. $K_{n\times1}(z)$ is the feedback controller to be designed for the actuator $G_{1\times n}(j\omega)$. e is the error signal, u is the feedback control input and y is the output of the actuator 1. r and w are noises entering the system. n is the measurement noise of the sensing device. In

most industrial actuation, only the error signal e is accessible online. The objective of the feedback control design is to stabilize the closed loop system and minimize the error signal e.

$H_d(j\omega)$ is the frequency response measurement of the coupling dynamics between actuator 2 to actuator 1. Multiple sets of measurement response data of the coupling dynamics are available during the design process. The data driven control design methodologies consider multiple sets of frequency response measurements $H_d(j\omega)$ simultaneously during the design process. Considering multiple sets of data ensures robustness of the control design. It helps to approximate non linear behavior of the actuator. In some cases the controller can be designed for multiple actuators simultaneously. u_d is the vibration disturbance imparted by actuator 2 onto actuator 1.

$K_{ff,n\times1}(z)$ is a $n \times 1$ dimensional feedforward controller to be designed to suppress the vibration imparted by the coupling dynamics $H_d(j\omega)$.

The joint feedback-feedforward data driven control design approach will use the frequency response measurements of $H_d(j\omega)$, the open loop actuator $G_{1\times n}(j\omega)$ and the control input signals u_{act2} of actuator 2.

5.3 Plant and Controller Factorization

The controller factorization for the feedback and the feedforward control design are defined in this section. The open loop transfer function of actuator 1 is also factorized for feedback control design.

Controller Factorization for Feedforward Control Design

The feedforward controller factorization used for the joint feedback-feedforward control design is similar to Eq.(3.1) from chapter 3.

The stable factorization from [56] are used for the feedforward controller $K_{ff,n\times1}(z)$ in Figure 3.1.

$$K_{ff,n\times1}(z) = X_{ff,n\times1}(z)Y^{-1}_{ff,1\times1}(z) \tag{5.1}$$

where $X_{n\times1} \in \mathbb{RH}^{n\times1}_\infty$, $Y_{1\times1} \in \mathbb{RH}^{1\times1}_\infty$ are asymptotically stable rational proper transfer functions. The factorization are for frequency domain and the z domain. The stable factorization can be transformed to frequency domain simply by substituting z by $e^{j\omega}$. We will factorize the controller $K_{ff,n\times1}(z)$ using finite impulse response filters (FIRs), with all poles at the origin.

$$\begin{aligned} X_{ff,n\times1}(z) &= \frac{1}{z^p}\begin{bmatrix} x_{1,p}z^p + x_{1,p-1}z^{p-1} + \cdots + x_{1,1}z + x_{1,0} \\ \vdots \\ x_{n,p}z^p + x_{n,p-1}z^{p-1} + \cdots + x_{n,1}z + x_{n,0} \end{bmatrix} \\ Y_{ff,1\times1}(z) &= \frac{z^p + y_{p-1}z^{p-1} + \cdots + y_1 z + y_o}{z^p} \end{aligned} \tag{5.2}$$

where p is the controller order and the controller parameters $\{y_{p-1}, \cdots, y_o\} \in \mathbb{R}^{1\times1}$ and $\{x_{i,p}, \cdots, x_{i,0}\} \in \mathbb{R}^{1\times1} \forall i \in \{1 \dots n\}$ are to be determined.

For simplicity the poles of the stable factorization are chosen to be at the origin, but they can be placed anywhere inside the unit circle. The stable factorization can be written in terms of the controller coefficients and filter terms

$$X_{ff,n\times1}(z) = \rho_{x,ff} F_{x,ff}(z) \tag{5.3}$$
$$Y_{ff,1\times1}(z) = \rho_{y,ff} F_{y,ff}(z) \tag{5.4}$$

where $\rho_{x,ff}$ and $\rho_{y,ff}$ are given by:

$$\rho_{x,ff} = \begin{bmatrix} x_{1,p}, & \dots, & x_{1,1}, & x_{1,0} \\ & & \vdots & \\ x_{n,p}, & \dots, & x_{n,1}, & x_{n,0} \end{bmatrix} \tag{5.5}$$
$$\rho_{y,ff} = \begin{bmatrix} y_{1,p}, & \dots, & y_{1,1}, & y_{1,0} \end{bmatrix} \tag{5.6}$$

and the filter terms $F_{x,ff}(z)$ and $F_{y,ff}(z)$ are given by:

$$F_{x,ff}(z) = \frac{1}{z^p} \begin{bmatrix} z^p & \dots & z^1 & z^0 \end{bmatrix}^\top \tag{5.7}$$
$$F_{y,ff}(z) = \frac{1}{z^p} \begin{bmatrix} z^p & \dots & z^1 & z^0 \end{bmatrix}^\top \tag{5.8}$$

Plant and Controller Factorization for Feedback Control Design

The open loop controllable MISO system $G_{1\times n}(j\omega)$ in Figure 5.1 accepts n control inputs and has only one sensor measurement as an output. The controller $K_{n\times1}(z)$ uses this single measurement to generate n control inputs. This controller is a SIMO system. The dimension notation used as a subscript may be eliminated in few places for the purpose of simplifying the notations.

The plant and controller factorization used for the feedback control design were presented earlier in [7, 8]. The plant and controller are factorized using the stable factorization [56] are given as:

$$G_{1\times n}(j\omega) = \tilde{M}^{-1}_{1\times1}(j\omega)\ \tilde{N}_{1\times n}(j\omega) \tag{5.9}$$
$$K_{n\times1}(z) = X_{n\times1}(z)\ Y^{-1}_{1\times1}(z) \tag{5.10}$$

where, $\tilde{M}_{1\times1} \in \mathbb{RH}^{1\times1}_\infty$, $\tilde{N}_{1\times n} \in \mathbb{RH}^{1\times n}_\infty$, $X_{n\times1} \in \mathbb{RH}^{n\times1}_\infty$ and $Y_{1\times1} \in \mathbb{RH}^{1\times1}_\infty$. The stable factorization can be obtained in the frequency domain as well as the z domain. The stable factorization in the z domain can be converted to the frequency domain by replacing z by $e^{j\omega}$.

Obtaining stable factorization for the plant $G_{1\times n}(j\omega)$ can be challenging. The stability of a frequency response measurement cannot be evaluated directly. Three different scenarios for stable factorization for the plant $G_{1\times n}$ are considered.

- *Stable* $G_{1\times n}(j\omega)$: For stable plant, the factorization of $G_{1\times n}(j\omega)$ are given by:

$$\tilde{N}_{1\times n}(j\omega) = G_{1\times n}(j\omega) \quad (5.11)$$
$$\tilde{M}_{1\times 1}(j\omega) = 1 \quad (5.12)$$

- *Unstable* $G_{1\times n}(j\omega)$: A stabilizing controller $K^0_{n\times 1}(z)$ is used to obtain the stable factorization:

$$\tilde{N}_{1\times n}(j\omega) = \frac{G_{1\times n}(j\omega)}{1+G_{1\times n}(j\omega)K^0_{n\times 1}(e^{j\omega})} \quad (5.13)$$
$$\tilde{N}_{1\times n}(j\omega) = \frac{1}{1+G_{1\times n}(j\omega)K^0_{n\times 1}(e^{j\omega})} \quad (5.14)$$

  Eq.(5.13) and Eq.(5.14) give the stable factorization $\tilde{N}_{1\times n}(j\omega)$ and $\tilde{M}_{1\times 1}(j\omega)$. Here, The frequency response $\tilde{N}$ and $\tilde{M}$ are stabilized using the controller $K^0_{n\times 1}(z)$.

- *Known marginally stable poles times a stable* $G^0_{1\times n}(j\omega)$: In case of known marginally stable poles, the poles can be considered as zeros in $\tilde{M}_{1\times 1}(j\omega)$. For example, consider the following $G_{1\times n}(j\omega)$

$$G_{1\times n}(j\omega) = \frac{e^{j\omega}}{e^{j\omega}-1}G^0_{1\times n}(j\omega) \quad (5.15)$$

  The stable factorization can be derived as:

$$\tilde{N}_{1\times n}(j\omega) = G^0_{1\times n}(j\omega) \quad (5.16)$$
$$\tilde{M}_{1\times 1}(j\omega) = \frac{e^{j\omega-1}}{e^{j\omega}} \quad (5.17)$$

  here, $\tilde{N}_{1\times n}(j\omega)$ and $\tilde{M}_{1\times 1}(j\omega)$ are stable factorization of $G_{1\times n}(j\omega)$ in the frequency domain.

The controller $K_{n\times 1}(z)$ is implemented in the z domain. The factorization for the controller $K_{n\times 1}(z)$ are obtained in the z domain as well. The poles of the factorization are stable if and only if the poles lie within the unit circle. The controller is given by:

$$K_{n\times 1}(z) = \frac{1}{y_m z^m + \cdots + y_1 z + y_0}\begin{bmatrix} x_{1,m}z^m + \cdots + x_{1,1}z + x_{1,0} \\ \vdots \\ x_{n,m}z^m + \cdots + x_{n,1}z + x_{n,0}\end{bmatrix} \quad (5.18)$$

A simple set of stable factorization with be the finite impulse response, FIR, filter with all poles at the origin.

$$X_{n\times 1}(z) = \frac{1}{z^m}\begin{bmatrix} x_{1,m}z^m + \cdots + x_{1,1}z + x_{1,0} \\ \vdots \\ x_{n,m}z^m + \cdots + x_{n,1}z + x_{n,0}\end{bmatrix}, \quad (5.19)$$
$$Y_{1\times 1}(z) = \frac{y_m z^m + \cdots + y_1 z + y_0}{z^m} \quad (5.20)$$

For simplicity the poles of the stable factorization are chosen to be at the origin, but they can be placed anywhere inside the unit circle. The stable factorization can be written in terms of the controller coefficients and filter terms

$$X_{n\times 1}(z) = \rho_x F_x(z) \tag{5.21}$$
$$Y_{1\times 1}(z) = \rho_y F_y(z) \tag{5.22}$$

where ρ_x and ρ_y are given by:

$$\rho_x = \begin{bmatrix} x_{1,m}, & \dots, & x_{1,1}, & x_{1,0} \\ & & \vdots & \\ x_{n,m}, & \dots, & x_{n,1}, & x_{n,0} \end{bmatrix} \tag{5.23}$$
$$\rho_y = \begin{bmatrix} y_{1,m}, & \dots, & y_{1,1}, & y_{1,0} \end{bmatrix} \tag{5.24}$$

and the filter terms $F_x(z)$ and $F_y(z)$ are given by:

$$F_x(z) = \frac{1}{z^m}\begin{bmatrix} z^m & \dots & z^1 & z^0 \end{bmatrix}^\top \tag{5.25}$$
$$F_y(z) = \frac{1}{z^m}\begin{bmatrix} z^m & \dots & z^1 & z^0 \end{bmatrix}^\top \tag{5.26}$$

Fixed Controller Factorization

A fixed structure can be considered inside the feedback or the feedforward controller while deriving the stable factorization for the controller. For example, if the design requires the first element of the controller to include an integrator with the following structure

$$K_{fixed,1}(z) = \frac{z}{z-1} \tag{5.27}$$

The stable factorization are modified to include the integrator in the structure

$$X_{n\times 1}(z) = \frac{1}{(z-\alpha)z^{m-1}} \begin{bmatrix} z(x_{1,m-1}z^{m-1} + \dots + x_{1,1}z + x_{1,0}) \\ (z-1)(x_{2,m-1}z^{m-1} + \dots + x_{2,1}z + x_{2,0}) \\ \vdots \\ (z-1)(x_{n,m-1}z^{m-1} + \dots + x_{n,1}z + x_{n,0}) \end{bmatrix}, \tag{5.28}$$
$$Y_{1\times 1}(z) = \frac{z-1}{z-\alpha}\frac{y_{m-1}z^{m-1} + \dots + y_1 z + y_0}{z^{m-1}} \tag{5.29}$$

Here $|\alpha| < 1$ is a pole inside the unit circle. These controller factorization can also be written in terms of the controller coefficients for example using Eq.(5.21) and Eq.(5.22) for the feedback controller.

Closed Loop Transfer Functions

In Figure 5.1, the lower case letters represent discrete time sequences loosely referred to as signals. The uppercase letters represent transfer functions either in the z domain or the frequency domain.

Expressions for the closed loop transfer functions will be obtained, which will be denoted by an uppercase letter and a subscript that represents its input to output causality in terms of the controller and plant factorization. As the plant $G_{j\omega}$ in Figure 5.1 is in the form of frequency response data, the closed loop transfer functions obtained will also be in the frequency domain. The closed loop transfer functions from the external signals (r, n and w) to the error signal e, control input signal u and the output y are

$$\begin{bmatrix} E_{r\to e} & E_{n\to e} & E_{w\to e} \\ U_{r\to u} & U_{n\to u} & U_{w\to u} \\ Y_{r\to y} & Y_{n\to y} & Y_{w\to y} \end{bmatrix} = \frac{1}{\tilde{N}X + \tilde{M}Y} \begin{bmatrix} \tilde{M}Y & -\tilde{M}Y & -\tilde{N}Y \\ \tilde{M}X & \tilde{M}X & -X\tilde{N} \\ \tilde{N}X & \tilde{N}X & \tilde{N}Y \end{bmatrix} \tag{5.30}$$

For compactness of the notations, the frequency domain arguments are dropped. Eq.(5.30) gives us the closed loop transfer functions of actuator 1. Here, X and Y are feedback controller factorization from Eq.(5.10) and, $\tilde{M}$ and $\tilde{N}$ are the plant factorization from Eq.(5.9).

5.4 Joint Feedback - Feedforward Data Driven Control Design

In this section, two data driven control design methodologies are presented to design feedback and feedforward controllers simultaneously. The objective of the feedback control design is to stabilize the closed loop of the system and minimize the error signal e in Figure 5.1. The objective of the feedforward controller is to suppress the vibration imparted by the neighboring actuator. The control design is developed in the frequency domain. The data driven approach obtains controllers directly based on the frequency response measurements. Traditionally, a model is fit to the frequency response measurement and the controller is designed based on the transfer function of the model. This approach introduces model mismatch in the design process. Whereas, the data driven approach avoids the model mismatch altogether.

Two joint feedback - feedforward data driven control design methodologies are presented. First, an alternating iterative data driven approach. This procedure alternately iterates between the feedback control design optimization and the feedforward control design optimization problem. Second, a simultaneous joint data driven approach. This procedure obtains one optimization problem for both the feedback and feedforward control design. The controllers are simultaneously optimized. H_2 norm and H_∞ norm control objectives are used to obtain the optimization problem.

Multiple Frequency Response Measurements

The data driven control design methodologies consider multiple frequency response measurements simultaneously in the design process. Multiple measurements of the system $G_{1\times n}(j\omega)$ are considered simultaneously. Also, multiple measurements of the imparted vibration are considered simultaneously. Considering multiple measurements simultaneously ensures robustness of the design. The non linear behavior of the system that cannot be captured by a single measurement can be considered in multiple measurements. The ability to consider multiple measurements let's one design controllers for multiple actuators simultaneously. Multiple control input signals u_{act2} (Figure 5.1) exciting the imparted vibration are also considered simultaneously for the feedforward control design.

The frequency response measurements are considered for $\omega \in \Omega$, except for the finite frequencies that correspond to the poles of $G_{1\times n}(j\omega)$ and the coupling dynamics $H_d(j\omega)$.

$$\Omega = \left\{\omega \middle| -\frac{\pi}{T_s} \leq \omega \leq \frac{\pi}{Ts}\right\} \tag{5.31}$$

where, T_s is the sampling time of the frequency response measurements.

Alternating Iterative Data Driven Control Design

As the name suggests, this data driven methodology alternates between feedback control design and the feedforward control design as shown in Figure 5.2. H_2 norm and H_∞ norm conditions are used as control objectives. The data driven feedforward control design methodology used is from chapter 3. The data driven feedback control design methodology was earlier presented in [7, 8].

An optimization problem is obtained using the H_2 norm and H_∞ norm conditions for both feedback and feedforward control design. The feedforward control design optimization problem is locally convex in the feedforward controller coefficients $\rho_{x,ff}$, (Eq.5.5), and $\rho_{y,ff}$, Eq.(5.6). Whereas, the feedback control design optimization problem is locally convex in the feedback controller coefficients ρ_x, Eq.(5.23), and ρ_y Eq.(5.24). But, the two problems cannot be directly combined into one locally convex optimization problem in ρ_x, ρ_y, $\rho_{x,ff}$ and $\rho_{y,ff}$. The combination of the two problems results in cross multiplication of these controller coefficients resulting in non convexity of the problem.

One approach to counter this complexity is by alternately iterating between the feedback control design problem and the feedforward control design problem. First, the control objectives used for the feedback control design problem are presented. Then, the control objectives used for the feedforward control design problem are stated. The two optimization problems will be combined together using the algorithm shown in Figure 5.2.

Feedback Control Design

The data driven feedback control design methodology was presented earlier in [7] and [8]. The objective of the feedback control design is to stabilize the closed loop of the system and

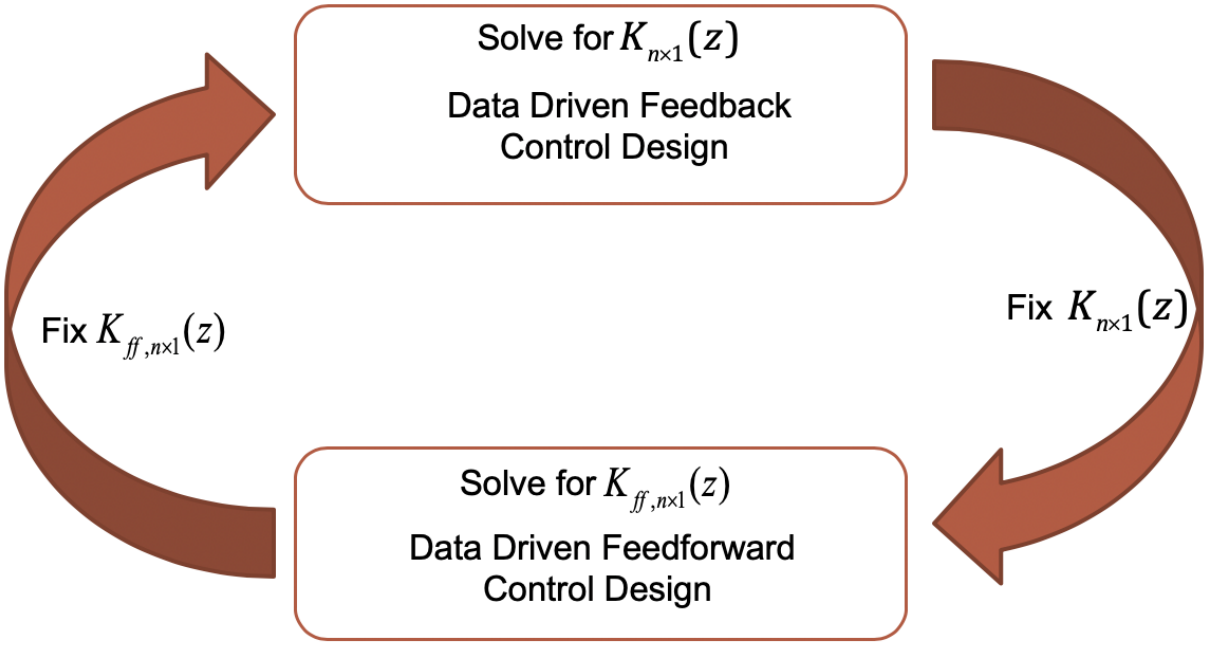

Figure 5.2: The basic structure used to obtain feedback and feedforward controllers for the data driven Alternating Iterative approach is shown in this figure.

minimize the variance of the error signal. H_∞ norm conditions are used to stabilize the closed loop of the system. The variance of the error signal is minimized using an H_2 norm objective function. These norms are used to design constraints in the frequency domain to achieve desired stability and performance levels. Consider p frequency response measurements of the plant, $G_i(j\omega) = \tilde{M}_i^{-1}(j\omega)\tilde{N}_i(j\omega)$, available to the designer, where i represents the i^{th} frequency response measurement.

H_∞ Norm

For a stable SISO system, the H_∞ norm is defined as the peak gain, the largest value of the frequency response magnitude. Whereas, for a MIMO system, the H_∞ norm is defined as the largest singular value across the frequency range Ω, Eq.(5.31).

The H_∞ norm can be used to shape the closed loop transfer function in the frequency domain. Consider the following transfer function:

$$U_{(r\to e),i} = \frac{\tilde{M}_i X}{\tilde{N}_i X + \tilde{M}_i Y} \tag{5.32}$$

Here, X and Y are the controller factorization from Eq.(5.10). The argument for the dimensions are dropped for clarity. H_∞ norm condition for transfer function $U_{(r\to e),i}$ is given

by:

$$||W_{U_{r\to e}} U_{(r\to e),i}||_\infty \triangleq \bar{\sigma}(W_{U_{r\to e}} U_{(r\to e),i}) \leq \gamma \tag{5.33}$$

$\forall i \in \{1 \ \dots \ p\}$. Where, $W_{U_{r\to e}}$ is a weighting filter designed as per requirements of the designer and γ is a positive constant. $\bar{\sigma}(.)$ is the maximum singular value function. Eq.(5.33) is not convex in X and Y.

The H_∞ norm condition in Eq.(5.33) can be transformed into a convex constraint in X and Y as developed for SISO systems in [28] and extended to MISO systems in [7]. The theorem from [7] is stated below:

Theorem 3 *Assume that the i^{th} frequency response measurement of the plant $G_i(j\omega)$ is given over the frequency region Ω and is factorized according to Eq.(5.9). Given a positive scalar γ, the following two statements are equivalent:*

I Controller $K(z)$ stabilizes the plant $G_i(j\omega)$ and the following H_∞ norm condition is met:

$$||W_{U_{r\to e}} U_{(r\to e),i}||_\infty \leq \gamma \tag{5.34}$$

II There exist a stable controller factorization $X_{n\times 1}(z)|_{e^{j\omega}}$ and $Y_{1\times 1}(z)|_{e^{j\omega}}$ according to Eq.(5.10), such that the following convex inequality holds,

$$\gamma^{-1}\bar{\sigma}\big(w_{U_{r\to e}}(j\omega)X(e^{j\omega})\tilde{N}_i(j\omega)\big) \leq Re\big\{\tilde{N}_i(j\omega)X(e^{j\omega}) + \tilde{M}_i(j\omega)Y(e^{j\omega})\big\} \tag{5.35}$$

where, $Re\{r\}$ represents the real part of r.

The inequality constraint in Eq.(5.35) is convex in the control coefficients ρ_x and ρ_y from Eq.(5.23) and Eq.(5.24). In practice the convex constraint is evaluated at a finite set of frequencies $\omega \in \Omega$ as given in Eq.(5.31).

This H_∞ norm convex constraint is considered for all plants p, that is, $\forall\ i \ \in \{1 \ \dots \ p\}$. Similar convex constraints can be obtained for the other closed loop transfer functions. The weighting function $W_{U_{r\to e}}$ is selected by the designer as per the requirements.

Necessary and sufficient convex constraints are obtained using Theorem 3. The solution is not iterative and does not depend on the controller from the previous iteration.

H_2 Norm

H_2 norm of a $m \times n$ MIMO system with a frequency response $H(j\omega)$ is defined as:

$$||H(j\omega)||_2^2 \triangleq \frac{1}{2\pi}\int_\Omega \mathrm{Tr}[H(j\omega)^* H(j\omega)]d\omega \tag{5.36}$$

where $H^*(j\omega) = \bar{H}^*(j\omega)$ is the complex conjugate transpose and Tr(H) is the trace of the matrix H.

H_2 norm is an estimate of the energy of a system. Here, H_2 norm of $H_{m\times n}$ provides us a measure of the energy stored in the system $H_{m\times n}$. According to Parseval's theorem [52],

energy of a system evaluated in the time domain and the frequency domain should be the same. The variance of a time signal provides an estimate of the energy stored in the time domain. Therefore, H_2 norm of a transfer function can be used to constrain the variance of the output of the transfer function in the time domain.

The variance of the error signal e_i, for the i^{th} frequency response measurement of the system $G_i(j\omega)$, in absence of any vibration from the coupling dynamics $H_d(j\omega)$ and feedforward control action is given by:

$$||e_i||_2^2 = ||E_{(r\to e),i}R(j\omega)||_2^2 + ||E_{(w\to e),i}W(j\omega)||_2^2 + ||E_{(n\to e),i}N(j\omega)||_2^2 \tag{5.37}$$

where, $R(j\omega)$, $W(j\omega)$ and $N(j\omega)$ are open loop frequency responses generating the external signals r, w and n in Figure 5.1. Consider v frequency response measurements of the coupling dynamics $H_{d,l}(j\omega)$ are available for design, where l represents the l^{th} frequency response measurement of the coupling dynamics. Also, consider s control input signals of actuator 2 $u_{act2,m}$ are available for design, where m represents the m^{th} control input signal. The frequency response of the m^{th} control input signal $u_{act2,m}$ on Fast Fourier Transform is given by $U_m(j\omega)$. The argument $(j\omega)$ is dropped hence forth for compactness.

The error signal $e_{i,l,m}$, for the i^{th} measurement of the system, l^{th} measurement of the coupling dynamics and m^{th} measurement of the excitation signal u_{act2} is given by:

$$||e_{i,l,m}||_2^2 = ||E_{(r\to e),i}(R + H_{d,l}U_m)||_2^2 + ||E_{(w\to e),i}(W + K_{ff}U_m)||_2^2 + ||E_{(n\to e),i}N||_2^2 \tag{5.38}$$

The Parseval's theorem [52] can be used to constrain the variance of time signals, for example, the variance of the output $y_{i,l,m}$, where the i^{th} measurement of the system, l^{th} measurement of the coupling dynamics and m^{th} measurement of the excitation signal u_{act2} is considered, will be given by:

$$||y_{i,l,m}||_2^2 = ||Y_{(r\to y),i}(R + H_{d,l}U_m)||_2^2 + ||Y_{(w\to y),i}(W + K_{ff}U_m)||_2^2 + ||Y_{(n\to y),i}N||_2^2 \leq \beta \tag{5.39}$$

$\forall\ i\ \in \{1,\ \ldots,\ p\}, \forall\ l\ \in \{1,\ \ldots,\ v\}$ and $\forall\ m\ \in \{1,\ \ldots,\ s\}$.

Similarly, the variance of the error signal across all p systems, v coupling dynamics and m excitation signals can be minimized with respect to the controller coefficients as shown below:

$$\begin{aligned}\frac{1}{p}\frac{1}{v}\frac{1}{s}\sum_{i=1}^{p}\sum_{l=1}^{v}\sum_{m=1}^{s}||e_{i,l,m}||_2^2 \;=\; & \frac{1}{p}\frac{1}{v}\frac{1}{s}\min_{X,Y}\sum_{i=1}^{p}\sum_{l=1}^{v}\sum_{m=1}^{s}||E_{(r\to e),i}(R + H_{d,l}U_m)||_2^2 \\ & + ||E_{(w\to e),i}(W + K_{ff}U_m)||_2^2 + ||E_{(n\to e),i}N||_2^2 \end{aligned} \tag{5.40}$$

Eq.(5.39) and Eq.(5.40) are not convex in X and Y. The theorem from [27] is used to determine the upper bound of the H_2 norms. For the feedback control design in presence of vibration and feedforward action we have the following theorem,

Theorem 4 *Over the frequency region Ω, p factorized frequency response measurements of the system are given, where the i^{th} measurement is given by $G_i(j\omega) = \tilde{M}_i^{-1}(j\omega)\tilde{N}_i(j\omega)$, v frequency response measurements of the coupling dynamics $H_{d,l}(j\omega)$ are given, where l represents the l^{th} measurement, Fourier Transform of s excitation signals, denoted by U_m are given, where m represents the m^{th} measurement and the feedforward controller $K_{ff}(z)$ is given. Also, an initial factorized stabilizing feedback controller $K_{k-1}(z) = X_{k-1}(z)Y_{k-1}^{-1}(z)$ is given. The upper bound of the average variance of the error signal defined in Eq.(5.40) can be computed as follows:*

$$\min_{X_k,Y_k} \frac{1}{p}\frac{1}{v}\frac{1}{s}\sum_{i=1}^{p}\sum_{l=1}^{v}\sum_{m=1}^{s}||e_{i,l,m}||_2^2 \leq \tag{5.41}$$

$$\min_{X_k,Y_k} \frac{1}{2\pi pvs}\sum_{i=1}^{p}\sum_{l=1}^{v}\sum_{m=1}^{s}\int_{\Omega}\Big[\mathrm{Tr}(\Gamma_{E_{r\to e},i,l,m}(j\omega)) + \mathrm{Tr}(\Gamma_{E_{w\to e},i,l,m}(j\omega)) + \mathrm{Tr}(\Gamma_{E_{n\to e},i,l,m}(j\omega))\Big]d\omega$$

$\forall\ i\ \in \{1,\ \ldots,\ p\}, \forall\ l\ \in \{1,\ \ldots,\ v\}, \forall\ m\ \in \{1,\ \ldots,\ s\}$ *and* $\forall\ \omega\ \in\ \Omega$*:*

$$\begin{bmatrix} \Gamma_{E_{r\to e},i,l,m} & Y_k\tilde{M}_i(R + H_{d,l}U_m) \\ (R + H_{d,l}U_m)^*\tilde{M}_i^*Y_k^* & P_{k-1,i}^*P_{k,i} + P_{k,i}^*P_{k-1,i} - P_{k-1,i}^*P_{k-1,i} \end{bmatrix}(j\omega) \succeq 0 \tag{5.42}$$

$$\begin{bmatrix} \Gamma_{E_{w\to e},i,l,m} & \tilde{N}_iY_k(W + K_{ff}U_m) \\ (W + K_{ff}U_m)^*Y_k^*\tilde{N}_i^* & P_{k-1,i}^*P_{k,i} + P_{k,i}^*P_{k-1,i} - P_{k-1,i}^*P_{k-1,i} \end{bmatrix}(j\omega) \succeq 0 \tag{5.43}$$

$$\begin{bmatrix} \Gamma_{E_{r\to e},i,l,m} & Y_k\tilde{M}_iN \\ N^*\tilde{M}_i^*Y_k^* & P_{k-1,i}^*P_{k,i} + P_{k,i}^*P_{k-1,i} - P_{k-1,i}^*P_{k-1,i} \end{bmatrix}(j\omega) \succeq 0 \tag{5.44}$$

$$P_{k,i} = \tilde{N}_iX_k + \tilde{M}_iY_k\,, \qquad P_{k-1,i} = \tilde{N}_iX_{k-1} + \tilde{M}_iY_{k-1} \tag{5.45}$$

Eqs (5.42) - (5.44) are Linear Matrix Inequalities (LMIs). Hence, these equations are convex in X_k, Y_k, $\Gamma_{E_{r\to e},i,l,m}(j\omega)$, $\Gamma_{E_{w\to e},i,l,m}(j\omega)$ and $\Gamma_{E_{n\to e},i,l,m}(j\omega)$ $\forall\omega\ \in \Omega, \forall\ i\ \in \{1,\ \ldots,\ p\}$, $\forall\ l\ \in \{1,\ \ldots,\ v\}$ and $\forall\ m\ \in \{1,\ \ldots,\ s\}$. Theorem 4 provides an iterative solution to minimize the variance of the error signal e. k is the iteration number. The solution of iteration k depends on the controller from iteration $k-1$.

Theorem 4 does not guarantee the closed loop stability, but, coupled with the H_∞ norm constraints a stable controller is guaranteed.

Mixed $H_2 - H_\infty$ norm

The mixed $H_2 - H_\infty$ norm control optimization problem is characterized by H_∞ norm constraints, minimization of an H_2 norm objective function and/or H_2 constraints.

The locally convex H_2 norm conditions from Eq. (5.42) - (5.45) and convex H_∞ norm condition from Eq. (5.35) are combined together to obtain a mixed $H_2 - H_\infty$ norm locally

convex optimization problem:

H_2 **Norm Objective Function:**

$$\min_{X_k,Y_k} \frac{1}{p}\frac{1}{v}\frac{1}{s}\sum_{i=1}^{p}\sum_{l=1}^{v}\sum_{m=1}^{s}||e_{i,l,m}||_2^2 \leq \tag{5.46}$$

$$\min_{X_k,Y_k} \frac{1}{2\pi pvs}\sum_{i=1}^{p}\sum_{l=1}^{v}\sum_{m=1}^{s}\int_{\Omega}\Big[\mathrm{Tr}(\Gamma_{E_{r\to e},i,l,m}(j\omega)) + \mathrm{Tr}(\Gamma_{E_{w\to e},i,l,m}(j\omega)) + \mathrm{Tr}(\Gamma_{E_{n\to e},i,l,m}(j\omega))\Big]d\omega$$

$\forall\ i\ \in \{1,\ \ldots,\ p\}, \forall\ l\ \in \{1,\ \ldots,\ v\}, \forall\ m\ \in \{1,\ \ldots,\ s\}$ and $\forall\ \omega\ \in\ \Omega$:

H_2 **Norm Constraints:**

$$\begin{bmatrix} \Gamma_{E_{r\to e},i,l,m} & Y_k\tilde{M}_i(R + H_{d,l}U_m) \\ (R + H_{d,l}U_m)^*\tilde{M}_i^*Y_k^* & P_{k-1,i}^*P_{k,i} + P_{k,i}^*P_{k-1,i} - P_{k-1,i}^*P_{k-1,i} \end{bmatrix}(j\omega) \succeq 0 \tag{5.47}$$

$$\begin{bmatrix} \Gamma_{E_{w\to e},i,l,m} & \tilde{N}_iY_k(W + K_{ff}U_m) \\ (W + K_{ff}U_m)^*Y_k^*\tilde{N}_i^* & P_{k-1,i}^*P_{k,i} + P_{k,i}^*P_{k-1,i} - P_{k-1,i}^*P_{k-1,i} \end{bmatrix}(j\omega) \succeq 0 \tag{5.48}$$

$$\begin{bmatrix} \Gamma_{E_{r\to e},i,l,m} & Y_k\tilde{M}_iN \\ N^*\tilde{M}_i^*Y_k^* & P_{k-1,i}^*P_{k,i} + P_{k,i}^*P_{k-1,i} - P_{k-1,i}^*P_{k-1,i} \end{bmatrix}(j\omega) \succeq 0 \tag{5.49}$$

$$P_{k,i} = \tilde{N}_iX_k + \tilde{M}_iY_k\,, \qquad P_{k-1,i} = \tilde{N}_iX_{k-1} + \tilde{M}_iY_{k-1} \tag{5.50}$$

H_∞ **Norm Constraints:**

$$\gamma^{-1}\bar{\sigma}\big(w_{U_{r\to e}}(j\omega)X(e^{j\omega})\tilde{N}_i(j\omega)\big) \leq Re\big\{\tilde{N}_i(j\omega)X(e^{j\omega}) + \tilde{M}_i(j\omega)Y(e^{j\omega})\big\} \tag{5.51}$$

Feedforward Control Design

The feedforward control design methodology used for the alternating iterative control design approach is given by Theorem 2 and Theorem 1 from chapter 3. Eqs. (3.32) - (3.34) give us the mixed optimization problem for the data driven feedforward control design.

Algorithm

The algorithm used to obtain feedback and feedforward controllers using the alternating iterative approach is shown in Figure 5.3 To initiate the alternating iterative approach initial stabilizing controllers are obtained for both feedback and feedforward controllers independently using their respective H_∞ norm constraints.

Once the initial stabilizing controllers are obtained, the algorithm for the alternating iterative approach can be followed from *Step 1* to *Step 4*. The controllers obtained become the new initial stabilizing controllers for the respective feedback and feedforward problems. The solver MOSEK [36] on MATLAB [34] is used to solve these locally convex iterative optimization problems.

Stopping condition for this algorithm is chosen by the designer. A good stopping condition would be a limit constraint on the variance of the error signal for the feedback design.

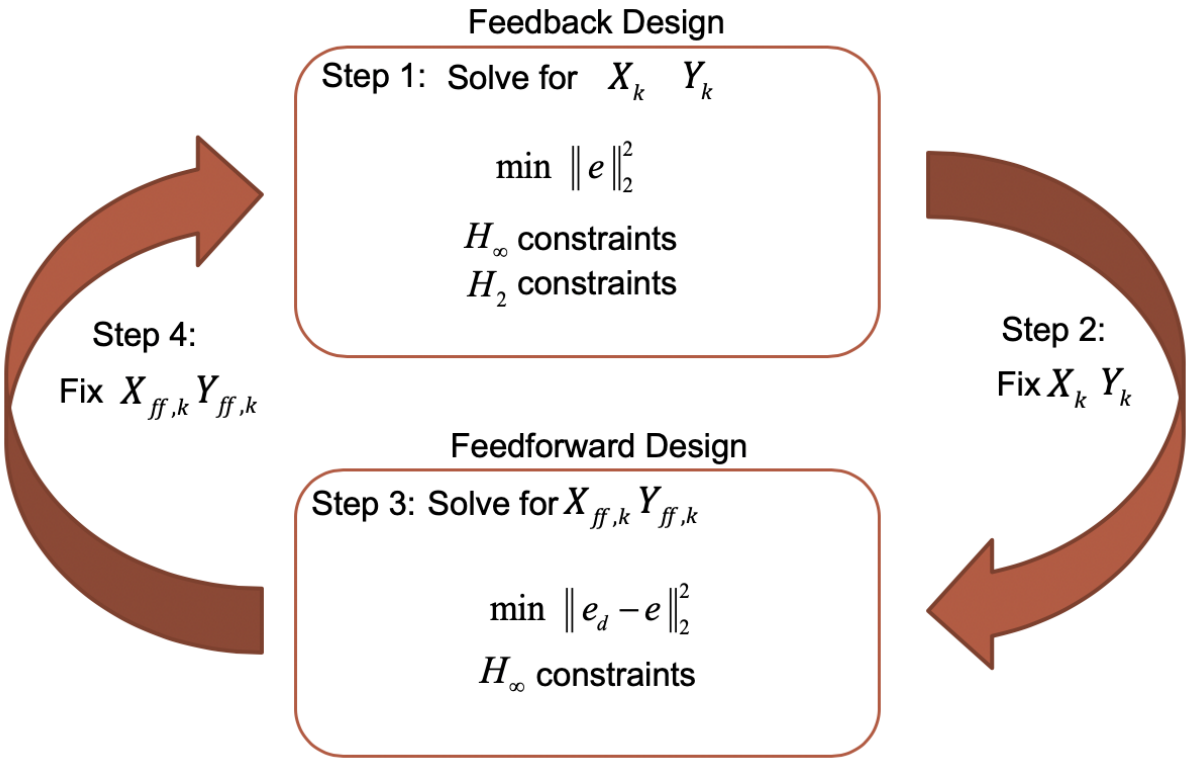

Figure 5.3: The algorithm used to obtain the feedback and feedforward controllers using the data driven Alternating Iterative approach is shown in this figure.

Simultaneous Joint Data Driven Control Design

In the previous section, an alternating iterative data driven control design methodology was presented. The algorithm optimized the feedback control objectives and the feedforward control objectives alternately. In this section, a simultaneous feedback - feedforward data driven control design methodology is presented. The feedback control design and the feedforward control design are unified into one locally convex optimization problem. The H_∞ norm conditions for feedback control and feedforward control are independent and can be directly stacked up into one problem. But, the H_2 norm objective function involve cross terms of the feedforward control coefficients and feedback control coefficients.

Convex - Concave Constraint

Classical control problems can be transformed to constraints on the spectral norm of the system and in general are reformulated as:

$$F^*F - P^*P \leq \gamma I \tag{5.52}$$

where, $F \in \mathbb{C}^{n\times n}$ and $P \in \mathbb{C}^{n\times n}$ are linear in the optimization variables. $(.)^*$ denotes the complex conjugate transpose. Eq.(5.52) is a convex - concave constraint. Convex - concave constraints can be convexified using the Taylor expansion of the non-linear product P^*P around P_c an arbitrary known matrix [15].:

$$P^*P \approx P_c^*P_c + (P - P_c)^*P_c + P_c^*(P - P_c) \tag{5.53}$$

It can be shown that the left hand side is greater than equal to the right and side, that is:

$$P^*P \geq P^*P_c + P_c^*P - P_c^*P_c \tag{5.54}$$

The above equation can be obtained by expansion of the inequality $(P - P_c)^*(P - P_c) \geq 0$. Eq.(5.54) is used to convexify the cross coupling terms of the feedback and feedforward control coefficients in the design of the H_2 norm control objective.

H_2 Norm

According to Parseval's Theorem, the variance of the error signal of the system in Figure 5.1, for the i^{th} measurement of the system, l^{th} measurement of the coupling dynamics and the m^{th} measurement of the excitation signal u_{act2} is approximately given by:

$$\begin{aligned} ||e_{i,l,m}||_2^2 \approx\ & ||E_{(r\to e),i}R||_2^2 + ||E_{(w\to e),i}W||_2^2 + ||E_{(n\to e),i}N||_2^2 \\ & + ||E_{(r\to e),i}H_{d,l}U_m + E_{(w\to e),i}K_{ff}U_m||_2^2 \end{aligned} \tag{5.55}$$

In Eq.(5.55), the first three terms pertain to the feedback control design of the system. The last term pertains to the feedforward control design of the system. There are no cross coupling terms in the feedback control design part. But, $E_{w\to e}K_{ff}$ leads to cross coupling terms of the controller coefficients. The convex concave constraint obtained on expanding the H_2 norm condition is convexified using the Taylor expansion as shown in Eq.(5.54).

The feedback controller is factorized using the stable factorization from Eq.(5.10) and the feedforward controllers are factorized using the stable factorization from Eq.(5.1), that is:

$$K_{n\times 1}(z) = X_{n\times 1}(z)\ Y_{1\times 1}^{-1}(z) \tag{5.56}$$

$$K_{ff,n\times 1}(z) = X_{ff,n\times 1}(z)\ Y_{ff,1\times 1}^{-1}(z) \tag{5.57}$$

The subscript pertaining to the dimensions will be dropped for clarity. The initial stabilizing feedback and feedforward controllers are given:

$$K_{k-1}(z) = X_{k-1}(z)\ Y_{k-1}^{-1}(z) \tag{5.58}$$

$$K_{ff,k-1}(z) = X_{ff,k-1}(z)\ Y_{ff,k-1}^{-1}(z) \tag{5.59}$$

Here, $k-1$ denotes the previous iteration. k is the current iteration of the problem. The following non linear products for iteration k are convexified for Theorem 5 using the initial

stabilizing feedback and feedforward controllers from iteration $k-1$ given in Eq.(5.58) and Eq.(5.59):

$$X_{ff,k}Y_k \approx X_{ff,k-1}Y_k + X_{ff,k}Y_{k-1} - X_{ff,k-1}Y_{k-1} \tag{5.60}$$
$$X_kY_{ff,k} \approx X_kY_{ff,k-1} + X_{k-1}Y_{ff,k} - X_{k-1}Y_{ff,k-1} \tag{5.61}$$
$$Y_kY_{ff,k} \approx Y_kY_{ff,k-1} + Y_{k-1}Y_{ff,k} - Y_{k-1}Y_{ff,k-1} \tag{5.62}$$
$$\tag{5.63}$$

Theorem 5 *Over the frequency region Ω, p factorized frequency response measurements of the system are given, where the i^{th} measurement is given by $G_i(j\omega) = \tilde{M}_i^{-1}(j\omega)\tilde{N}_i(j\omega)$, v frequency response measurements of the coupling dynamics $H_{d,l}(j\omega)$ are given, where l represents the l^{th} measurement and the Fourier Transform of s excitation signals, denoted by U_m are given, where m represents the m^{th} measurement is given. Also, an initial factorized stabilizing feedback controller $K_{k-1}(z) = X_{k-1}(z)Y_{k-1}^{-1}(z)$ and an initial factorized stabilizing feedforward controller $K_{ff,k-1}(z) = X_{ff,k-1}(z)Y_{ff,k-1}^{-1}(z)$ are given. Using Eqs. (5.60) - (5.62), the upper bound on the average variance of the error signal defined in Eq.(5.55) can be computed as follows:*

$$\min_{X_k,Y_k,X_{ff,k},Y_{ff,k}} \frac{1}{p}\frac{1}{v}\frac{1}{s}\sum_{i=1}^{p}\sum_{l=1}^{v}\sum_{m=1}^{s}||e_{i,l,m}||_2^2 \leq$$

$$\min_{X_k,Y_k,X_{ff,k},Y_{ff,k}} \frac{1}{2\pi pvs}\sum_{i=1}^{p}\sum_{l=1}^{v}\sum_{m=1}^{s}\int_\Omega \Big[\mathrm{Tr}(\Gamma_{E_{r\to e},i,l,m}) + \mathrm{Tr}(\Gamma_{E_{w\to e},i,l,m}) + \mathrm{Tr}(\Gamma_{E_{n\to e},i,l,m}) + \mathrm{Tr}(\Gamma_{ff,i,l,m})\Big](j\omega)d\omega \tag{5.64}$$

$\forall\ i \in \{1,\ \ldots,\ p\}, \forall\ l \in \{1,\ \ldots,\ v\}, \forall\ m \in \{1,\ \ldots,\ s\}$ *and* $\forall\ \omega \in \Omega$*:*

Feedback Control Constraints:

$$\begin{bmatrix}\Gamma_{E_{r\to e},i,l,m} & Y_k\tilde{M}_iR \\ R^*\tilde{M}_i^*Y_k^* & P_{k-1,i}^*P_{k,i} + P_{k,i}^*P_{k-1,i} - P_{k-1,i}^*P_{k-1,i}\end{bmatrix}(j\omega) \succeq 0 \tag{5.65}$$

$$\begin{bmatrix}\Gamma_{E_{w\to e},i,l,m} & \tilde{N}_iY_kW \\ W^*Y_k^*\tilde{N}_i^* & P_{k-1,i}^*P_{k,i} + P_{k,i}^*P_{k-1,i} - P_{k-1,i}^*P_{k-1,i}\end{bmatrix}(j\omega) \succeq 0 \tag{5.66}$$

$$\begin{bmatrix}\Gamma_{E_{r\to e},i,l,m} & Y_k\tilde{M}_iN \\ N^*\tilde{M}_i^*Y_k^* & P_{k-1,i}^*P_{k,i} + P_{k,i}^*P_{k-1,i} - P_{k-1,i}^*P_{k-1,i}\end{bmatrix}(j\omega) \succeq 0 \tag{5.67}$$

$$P_{k,i} = \tilde{N}_iX_k + \tilde{M}_iY_k\,, \qquad P_{k-1,i} = \tilde{N}_iX_{k-1} + \tilde{M}_iY_{k-1} \tag{5.68}$$

Feedforward Control Constraints:

$$\begin{bmatrix}\Gamma_{ff,i,l,m} & (Y_kY_{ff,k}\tilde{M}_iH_{d,l} - X_{ff,k}Y_k\tilde{N}_i)U_m \\ U_m^*(Y_kY_{ff,k}\tilde{M}_iH_{d,l} - X_{ff,k}Y_k\tilde{N}_i)^* & Q_{k-1,i}^*Q_{k,i} + Q_{k,i}^*Q_{k-1,i} - Q_{k-1,i}^*Q_{k-1,i}\end{bmatrix}(j\omega) \succeq 0 \tag{5.69}$$

$$Q_{k,i} = (\tilde{N}_iX_k + \tilde{M}_iY_k)Y_{ff,k}\,, \qquad Q_{k-1,i} = (\tilde{N}_iX_{k-1} + \tilde{M}_iY_{k-1})Y_{ff,k-1} \tag{5.70}$$

The non-convex terms in these equations are convexified using Eqs. (5.60) - (5.62). Eqs. (5.65) - (5.67) and Eq.(5.69) are linear matrix inequalities in X_k, Y_k, $X_{ff,k}$, $Y_{ff,k}$, $\Gamma_{E_{r\to e},i,l,m}(j\omega)$, $\Gamma_{E_{w\to e},i,l,m}(j\omega)$, $\Gamma_{E_{n\to e},i,l,m}(j\omega)$ and $\Gamma_{ff,i,l,m}(j\omega)$ $\forall\ \omega \in \Omega$, $\forall\ i\ \in \{1,\ \ldots,\ p\}$, $\forall\ l\ \in \{1,\ \ldots,\ v\}$ and $\forall\ m\ \in \{1,\ \ldots,\ s\}$.. The variance of the error signal is minimized by minimizing the upper bounds defined in Eq.(5.64). The linear matrix inequalities are obtained using the Schur complement lemma. Theorem 5 provides an iterative solution to simultaneously obtain the feedback controller and the feedforward controller using a data driven control design strategy.

The H_∞ norm constraints for the feedback loop (Theorem 3) and the H_∞ norm constraints for the feedforward loop (Theorem 2) can be directly added to the above equations to obtain the mixed $H_2 - H_\infty$ norm locally convex optimization problem to design feedback and feedforward controllers using a data driven approach.

Algorithm

The algorithm used to implement the Simultaneous feedback - feedforward data driven control design approach is shown in Figure 5.4.The simultaneous feedback - feedforward data driven control design approach is implemented in two steps. First, the initial stabilizing controllers for the feedback and the feedforward design are obtained independently using H_∞ norm conditions (Theorem 2) and Theorem 3. Then, the joint feedback - feedforward control design is implemented for $n-1$ iterations with the H_∞ norm constraints and the H_2 norm objective from Theorem 5.

Stopping condition for this algorithm is chosen by the designer. A good stopping condition would be a limit constraint on the variance of the error signal e. The solver MOSEK [36] on MATLAB [34] is used to solve these locally convex iterative optimization problems.

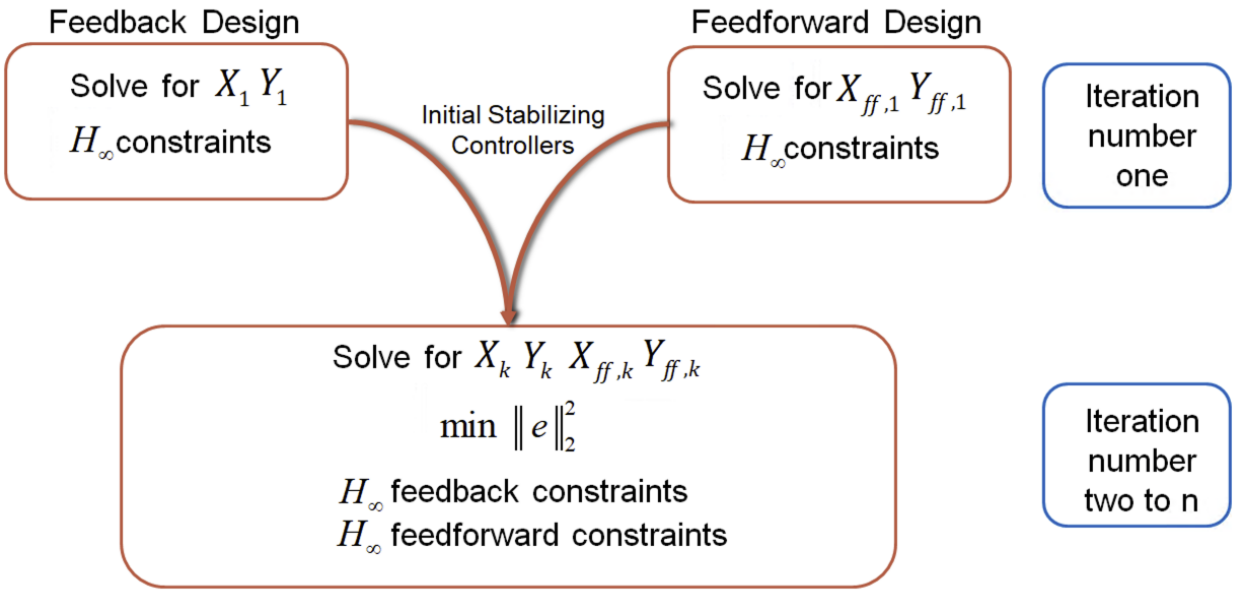

Figure 5.4: The simultaneous feedback - feedforward data driven control design approach is implemented in two steps. First, the initial stabilizing controllers for the feedback and the feedforward design are obtained independently using H_∞ norm conditions (Theorem 2) and Theorem 3. Then, the joint feedback - feedforward control design is implemented for $n-1$ iterations with the H_∞ norm constraints and the H_2 norm objective from Theorem 5.

Chapter 6

Application of Joint Feedback Feedforward Data Driven Control Design to Multi Actuator Drives

6.1 Introduction

In the previous chapter, two joint feedback - feedforward data driven control design methodologies were presented. This allows both the controllers to be designed simultaneously. The advantage being that the feedback control design also takes into account the vibration data available during the design process.

In this chapter, feedback and feedforward controllers are designed for a multi actuator hard disk drive (Figure 2.9). The alternating iterative approach and the simultaneous control design approach will be implemented. In section 6.2, the control block diagram of the multi actuator drive used to design the feedback and feedforward controllers is discussed in detail. The controller factorization used for the alternating iterative approach and the simultaneous control design approach are discussed in section 6.3. The constraints and the objective function used for the feedback design and the feedforward design are discussed in section 6.4. The control optimization problems for the alternating iterative approach is discussed in section 6.5 and the simultaneous control design approach is discussed in section 6.6. Finally, the design results for both the approaches are shown in section 6.7.

6.2 Control Block Diagram - Multi Actuator Drive

A multi actuator hard disk drive has two actuator arms operating on the same pivot timber. Multi actuator drives were introduced by Seagate in December, 2017 [44] to meet the high standards of the access speed demands. A multi actuator drive is equivalent to operation of two drives but at a lower cost of energy.

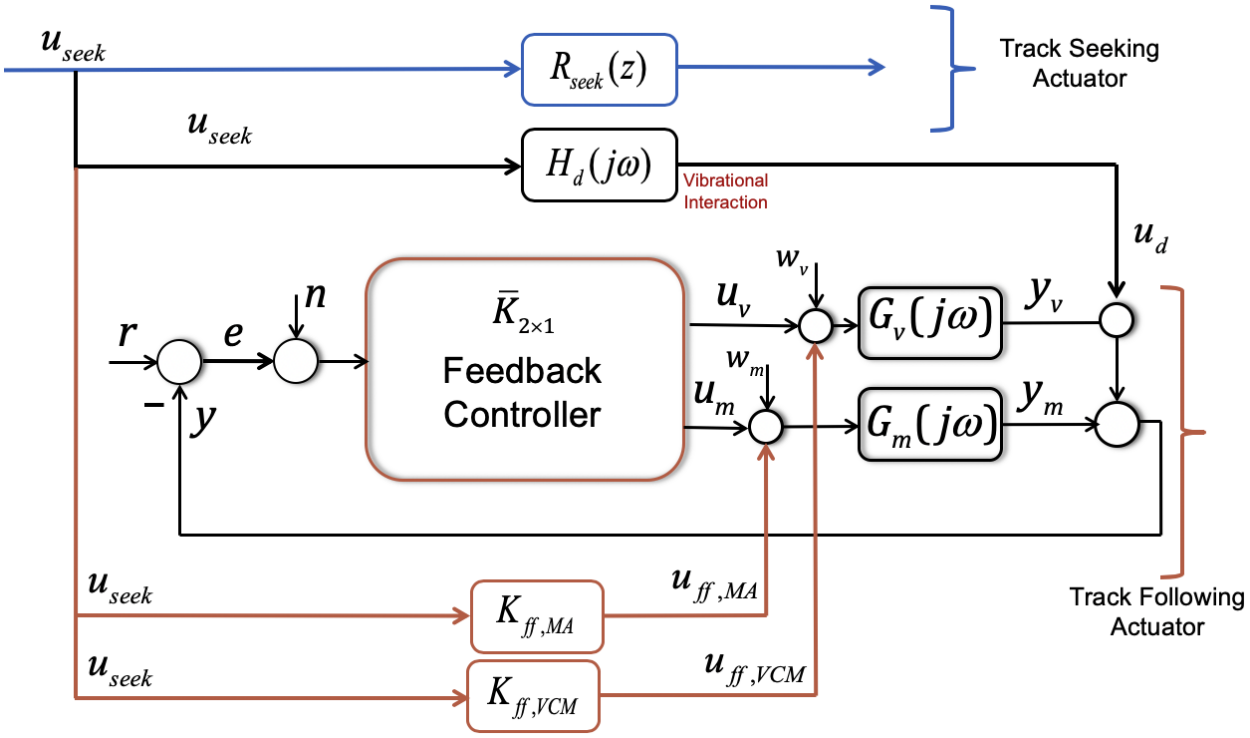

Figure 6.1: The control block diagram of a multi actuator drive is shown.

This new technology introduces new control challenges in the hard disk drive industry. The two actuator arms operating independently can impart vibration to one another. The imparted vibration adversely affects the functioning of the actuator arms. An actuator arm operates in two specific modes. First - track following mode - the head of the actuator arm follows a data track on the disk while performing read / write functionalities. Second - track seeking mode - the actuator arm sweeps through data tracks to settle onto a new desired track to start track following. The track seeking mode generally generates a lot of vibration, adversely affecting the performance of the neighboring actuator arm.

In this chapter, we design feedback and feedforward controllers for the track following actuator to stabilize the closed loop of the system, to minimize the position error signal of the head for smooth track following and suppress the vibration imparted by the neighboring track seeking actuator arm.

Figure 6.1 shows the control block diagram of a multi actuator drive. Here, $R_{seek}(z)$ is the closed loop of the track seeking actuator arm. u_{seek} is it's control input signal. Knowledge of u_{seek} signals during the design process is used in the data driven methodology to design feedforward controllers to suppress the imparted vibration. Eight different u_{seek} signals are used for the data driven control design to generate one feedforward controller for different classes of excitation signals as shown in Figure 6.2.

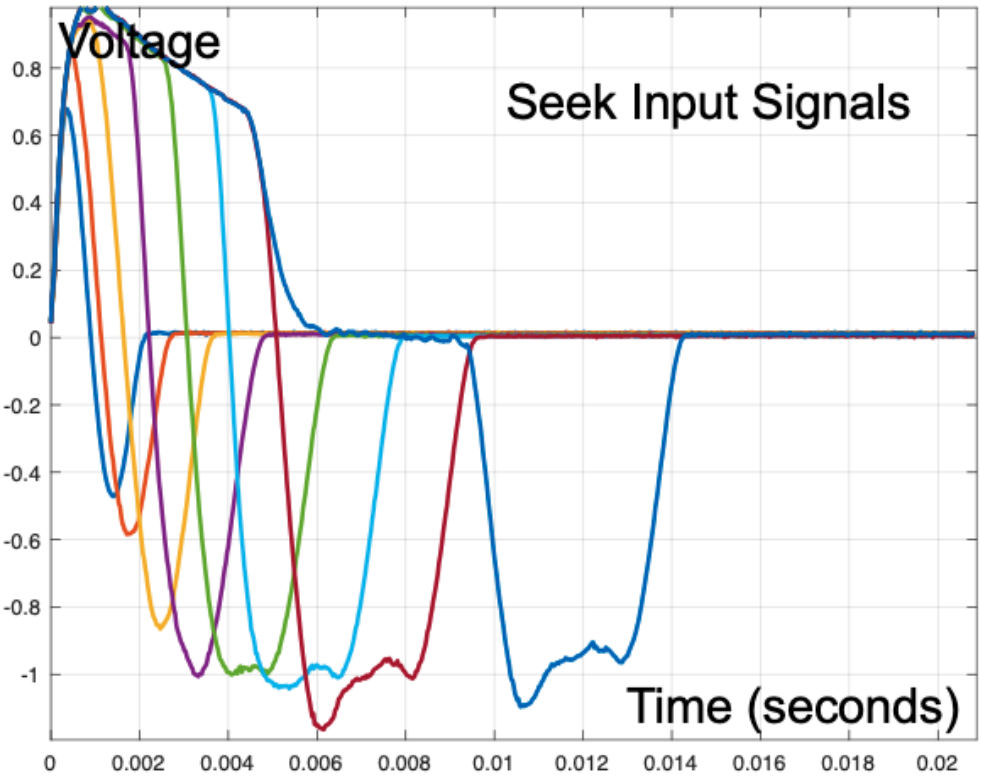

Figure 6.2: The control input signals of the track seeking actuator arm are shown. These control input signals excite the coupling transfer function $H_d(j\omega)$, imparting disturbances to the track following actuator.

$G_v(j\omega)$ is the input - output frequency response measurement of the voice coil motor (VCM) of the track following actuator arm. Similarly, $G_m(j\omega)$ is the input - output frequency response measurement of the micro actuator (MA). Multiple frequency response measurements of VCM and MA will be considered simultaneously in the data driven design process. u_v and u_m are the respective feedback control inputs of VCM and MA, y_v and y_m are the corresponding outputs. e is the position error signal (PES) of the read/write head. e is the only output of the sensing unit. Therefore, a track following actuator arm is a multi input, single output (MISO) system. A single input, multi output (SIMO) feedback controller $K_{2\times1}(z)$ is designed to stabilize the closed loop system and minimize the variance of the PES e. A set of two frequency response measurements of VCM and MA are used, for the design process, as shown in Figure 6.3.

r is the runout, radial noise generated by the spindle motor, a limiting factor for the performance of a hard disk drive. n is the measurement noise of the sensing device and, w_v and w_m are windage, noise generated by the rotating air in the hard disk drive. Nowadays, Helium is used instead of air in the hard disk drive [31], reducing this noise to a great extent.

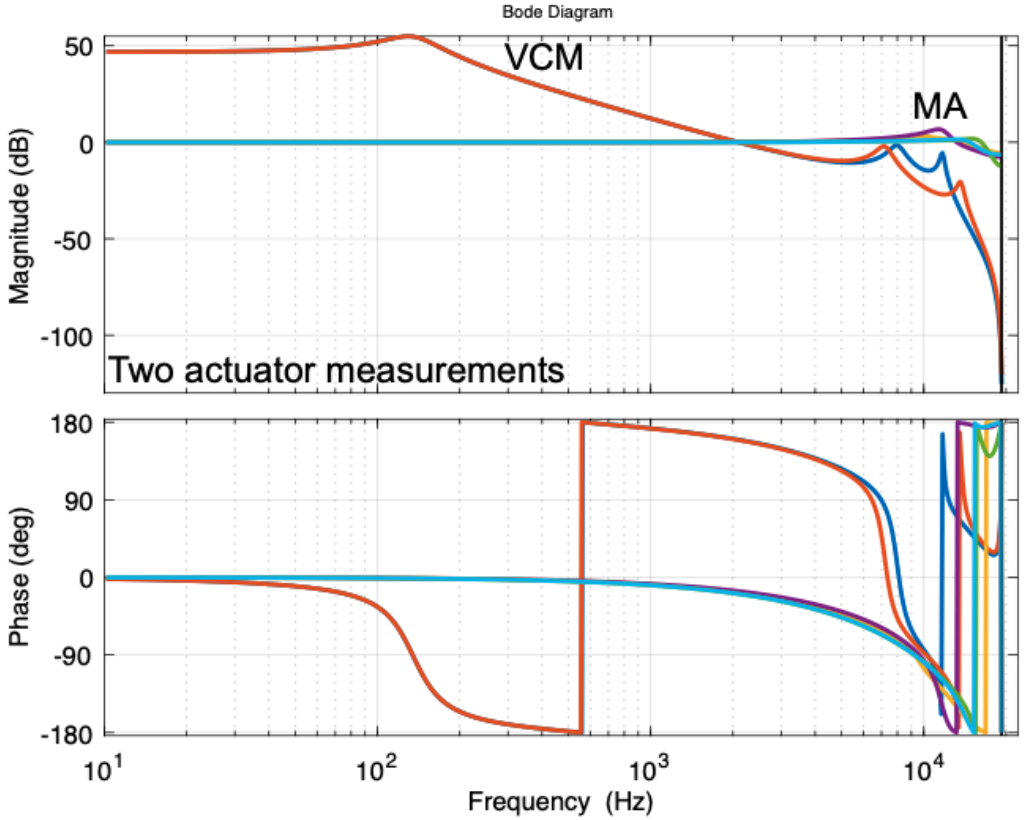

Figure 6.3: Frequency Response Measurements of VCM and MA used for the design process are shown. A set of five measurements are considered simultaneously to ensure robustness of the design process.

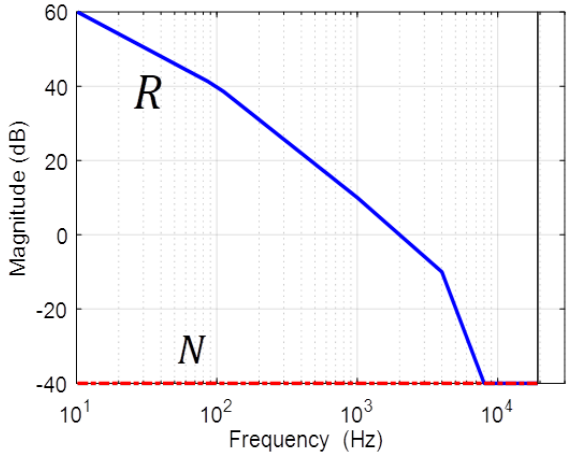

Figure 6.4: Spectrum of the runout r and measurement noise n is shown.

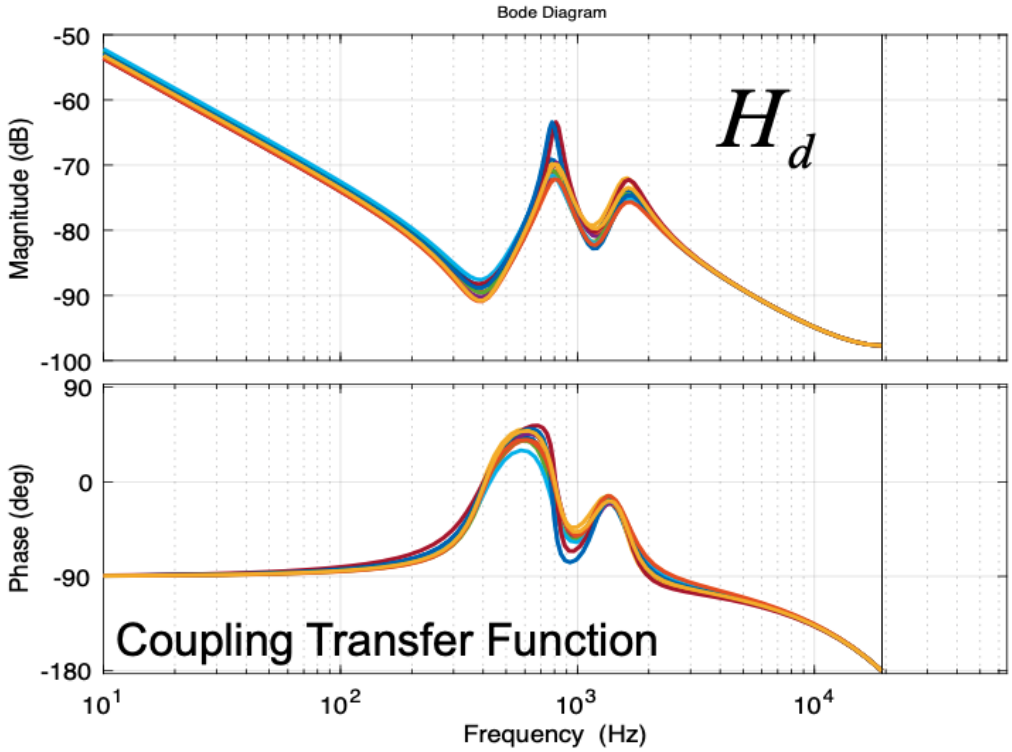

Figure 6.5: Frequency response measurements of the coupling transfer function $H_d(j\omega)$ is shown in this figure. The coupling transfer functions are measured by our industry partners, the models plotted in this figure are only representative of the behavior observed but not informative of the true data.

We shall assume windage to be lumped into the runout r and measurement noise n. The runout and measurement noise used for the design process is as shown in Figure 6.4.

$H_d(j\omega)$ represents the coupling transfer function between the track seeking actuator and the track following actuator. A vibration disturbance u_d is imparted to the track following actuator. Multiple frequency response measurements of the coupling transfer function will be considered simultaneously for the data driven control design. Figure 6.5 shows five frequency response measurements of $H_d(j\omega)$ used for feedback and feedforward control design. $K_{ff,VCM}(z)$ and $K_{ff,MA}(z)$ are VCM and MA feedforward controllers to be designed to suppress the vibration imparted by the track seeking actuator. $u_{ff,VCM}$ and $u_{ff,MA}$ are the feedforward compensating signals generated by VCM and MA feedforward controllers.

6.3 Controller and Actuator Factorization

Feedforward Control Design

The stable factorization from [56] are used for the feedforward controllers $K_{ff,VCM}(z)$ and $K_{ff,MA}(z)$ of Figure 6.1. The controller factorization used are according to the $H_2 - H_\infty$ norm data driven methodology presented in chapter 5, Eq.(5.1). We will consider the same order of the controller for both VCM and MA with the same denominator $Y(z)$.

$$K_{ff,VCM}(z) = X_{VCM}(z)Y_{VCM}^{-1}(z) \tag{6.1}$$
$$K_{ff,MA}(z) = X_{MA}(z)Y_{MA}^{-1}(z) \tag{6.2}$$

where $X_{VCM} \in \mathbb{RH}_\infty^{1\times1}$, $Y_{VCM} \in \mathbb{RH}_\infty^{1\times1}$, $X_{MA} \in \mathbb{RH}_\infty^{1\times1}$ and $Y_{MA} \in \mathbb{RH}_\infty^{1\times1}$ are all asymptotically stable rational proper transfer functions. The factorization are for frequency domain and the z-domain. The stable factorization can be transformed to frequency domain simply by substituting z by $e^{j\omega}$. In this chapter, we will factorize the controller $K_{ff,VCM}(z)$ and $K_{ff,MA}(z)$ using finite impulse response filters (FIRs), with all poles at the origin.

$$\begin{aligned} X(z) &= X_p z^p + X_{p-1}z^{p-1} + \cdots + X_o \\ Y(z) &= z^p + Y_{p-1}z^{p-1} + \cdots + Y_o \end{aligned} \tag{6.3}$$

where p is the controller order and the controller parameters $\{Y_{p-1}, \cdots, Y_o\} \in \mathbb{R}^{1\times1}$ and $\{X_p, \cdots, X_o\} \in \mathbb{R}^{1\times1}$ are to be determined. A controller order of 15 is selected for the feedforward controllers for both VCM and MA.

Feedback Control Design

The stable factorization from [56] are used for the feedforward controllers $K_{2\times1}(z)$ of Figure 6.1. The controller factorization used are according to the $H_2 - H_\infty$ norm data driven methodology presented in chapter 5, Eq.(5.10).

$$K_{2\times1}(z) = X_{2\times1}(z)Y_{1\times1}^{-1}(z) \tag{6.4}$$

where $X_{2\times1} \in \mathbb{RH}_\infty^{2\times1}$ and $Y_{1\times1} \in \mathbb{RH}_\infty^{1\times1}$ are asymptotically stable rational proper transfer functions. The factorization are for frequency domain and the z-domain. The stable factorization can be transformed to frequency domain simply by substituting z by $e^{j\omega}$.

An integrator will be included in the first element according to Eq.(5.28) and Eq.(5.29). For the Alternating Iterative approach, the controller order of 20 is selected for $K_{2\times1}(z)$. The subscript for the dimensions will be dropped for clarity hence forth.

Actuator Factorization

The actuator frequency response measurements $G_v(j\omega)$ and $G_m(j\omega)$ are stable in Figure 6.3. Together they will be combined as $G_{1\times2}(j\omega)$. Stable factorization from Eq.(5.11) and Eq.(5.11) will be used to factorize the actuator frequency response data.

$$\tilde{N}_{1\times2}(j\omega) = G_{1\times2}(j\omega) \tag{6.5}$$
$$\tilde{M}_{1\times1}(j\omega) = 1 \tag{6.6}$$

6.4 Data Driven Control Design

In chapter 5, two data driven control design approaches are presented to obtain feedback and feedforward controllers in the frequency domain. In this section, the constraints and objective functions used for designing the controllers for a multi actuator drive are discussed.

p frequency response measurements of the open loop actuators $G_{v,i}(j\omega)$ and $G_{m,i}(j\omega)$ are considered, where i represents the i^{th} measurement data. v frequency response measurements of the coupling transfer function $H_{d,l}(j\omega)$ are also considered, where l represents the l^{th} measurement data. s seeking input signals u_{seek} are considered. The frequency response of the seeking input signals is represented by $U_m(j\omega)$ where, m represents the m^{th} seeking input signal considered. The closed loop transfer function are defined as shown in Eq.(5.30).

H_∞ Norm

The major objectives of the feedback control design are to stabilize the closed loop of the system and minimize the variance of the PES e. H_∞ norm for both the dual-stage (VCM and MA together) and the single-stage (VCM only) will be constrained. According to Theorem 3, the H_∞ norm constraints guarantee the stability of the closed loop system. In case the MA fails, the single-stage H_∞ norm constraints guarantee the stability of the VCM. The HDD can still function without the MA.

$\forall i \in \{1, \ldots, p\}$, the following dual-stage H_∞ norm constraints are considered:

$$||W_{E_{r\to e}} E_{r\to e,i}||_\infty \leq 1, \; ||W_{U_{r\to u}} U_{r\to u,i}||_\infty \leq 1 \tag{6.7}$$
$$||W_{E_{w\to e}} E_{w\to e,i}||_\infty \leq 1, \; ||W_{U_{w\to u}} U_{w\to u,i}||_\infty \leq 1 \tag{6.8}$$

Here, $W_{E_{r\to e}}$ is the weighting filter used to shape the transfer function $E_{r\to e}$. The weighting filters are to be chosen by the designers to shape the closed loop transfer functions as required. The weighting filter for each transfer function is designed independently.

Similarly, the H_∞ norm constraints for the single-stage are given by, $\forall i \in \{1, \ldots, p\}$:

$$||W_{E^s_{r\to e}} E^s_{r\to e,i}||_\infty \leq 1, \; ||W_{U^s_{r\to u}} U^s_{r\to u_v,i}||_\infty \leq 1 \tag{6.9}$$
$$||W_{E^s_{w\to e}} E^s_{w_v\to e,i}||_\infty \leq 1, \; ||W_{U^s_{w\to u}} U^s_{w_v\to u_v,i}||_\infty \leq 1 \tag{6.10}$$

The superscript s denotes the single-stage transfer functions are used.

H_∞ norm feasibility constraint is posed for the feedforward control design problem, $\forall i \in \{1, \ldots, p\}$ and $\forall l \in \{1, \ldots, v\}$, we have

$$||W_{ff}(E_{(r\to e),i}H_{d,l} + E_{(w_v\to e),i}K_{ff,VCM} + E_{(w_m\to e),i}K_{ff,MA})||_\infty \leq 1 \tag{6.11}$$

Theorem 2 is used to transform Eq.(6.11) to a necessary and sufficient convex constraint. The H_∞ norm constraints are used to obtain initial stabilizing controllers for the Alternating Iterative Approach as well as the Simultaneous Control Design Approach.

H_2 Norm

The H_2 norm condition will be used to minimize the variance of the PES e. The H_2 norm constraint is transformed into a locally convex optimization problem using the Theorem 4. The variance of the PES e is given according to Eq.(5.38). $\forall i \in \{1, \ldots, p\}$, $\forall l \in \{1, \ldots, v\}$ and $\forall m \in \{1, \ldots, s\}$ we have:

$$||e_{i,l,m}||_2^2 \approx ||E_{(r\to e),i}(R + H_{d,l}U_m)||_2^2 + ||E_{(w\to e),i}(K_{ff}(e^{j\omega})U_m)||_2^2 + ||E_{(n\to e),i}N||_2^2 \tag{6.12}$$

Here, R, N are runout and measurement noise spectrum as shown in Figure 6.4. $K_{ff}(e^{j\omega})$ is the feedforward controller for VCM and MA stacked together as shown below:

$$K_{ff}(e^{j\omega}) = \begin{bmatrix} K_{ff,VCM}(e^{j\omega}) \\ K_{ff,MA}(e^{j\omega}) \end{bmatrix} \tag{6.13}$$

For the alternating iterative approach, the feedforward controller is fixed during the feedback design stage. Hence, Eq.(6.12) is transformed to a locally convex optimization problem in the controller coefficients of the feedback controller $K(z)$.

$\forall i \in \{1, \ldots, p\}$, $\forall l \in \{1, \ldots, v\}$ and $\forall m \in \{1, \ldots, s\}$ the variance of the PES e is also given by:

$$\begin{aligned} ||e_{i,l,m}||_2^2 \;\approx\; & ||E_{(r\to e),i}R||_2^2 + ||E_{(n\to e),i}N||_2^2 \\ & + ||(E_{(r\to e),i}H_{d,l} + E_{(w_v\to e),i}K_{ff,VCM} + E_{(w_m\to e),i}K_{ff,MA})U_m||_2^2 \end{aligned} \tag{6.14}$$

The right hand side of Eq.(6.14) separates the feedback control design part of the problem from the feedforward control design part of the problem. Eq.(6.14) is transformed into a locally convex optimization problem using the Theorem 5 to optimize the feedback controller and the feedforward controller simultaneously.

Eq.(6.12) and Eq.(6.14) give the variance of the PES for i^{th} measurement of the actuators, l^{th} coupling dynamics and m^{th} seeking input excitation. The optimization problem is formulated for the average variance of the PES e, given by:

$$\begin{aligned} \min_{K,K_{ff}} \frac{1}{pvs}\sum_{i=1}^{p}\sum_{l=1}^{v}\sum_{m=1}^{s}||e_{i,l,m}||_2^2 \;=\; & \min_{K,K_{ff}} \frac{1}{pvs}\sum_{i=1}^{p}\sum_{l=1}^{v}\sum_{m=1}^{s}||E_{(r\to e),i}R||_2^2 + ||E_{(n\to e),i}N||_2^2 \\ & + ||(E_{(r\to e),i}H_{d,l} + E_{(w_v\to e),i}K_{ff,VCM} + E_{(w_m\to e),i}K_{ff,MA})U_m||_2^2 \end{aligned} \tag{6.15}$$

The PES e without any vibration or feedforward action is given by:

$$||e_i||_2^2 \approx ||E_{(r\to e),i}R||_2^2 + ||E_{(n\to e),i}N||_2^2 \tag{6.16}$$

For a data driven feedforward control design problem, the difference between the PES e with vibration and feedforward action, Eq.(6.14) and the PES e without and vibration, Eq.(6.16) is minimized:

$$\min_{K_{ff}} \frac{1}{pvs}\sum_{i=1}^{p}\sum_{l=1}^{v}\sum_{m=1}^{s} ||(E_{(r\to e),i}H_{d,l} + E_{(w_v\to e),i}K_{ff,VCM} + E_{(w_m\to e),i}K_{ff,MA})U_m||_2^2 \tag{6.17}$$

H_2 norm condition can also be posed as constraints on the output of MA. The micro actuator has a fixed stroke (β_{y_m}) and can fracture if the output exceeds the stroke of MA.

$$\begin{aligned}\frac{1}{pvs}\sum_{i=1}^{p}\sum_{l=1}^{v}\sum_{m=1}^{s} ||y_{i,l,m}||_2^2 \;=\; &\frac{1}{pvs}\sum_{i=1}^{p}\sum_{l=1}^{v}\sum_{m=1}^{s} ||Y_{(r\to y_m),i}(R + H_{d,l}U_m)||_2^2 \\ &+||Y_{(w\to y_m),i}(K_{ff}(e^{j\omega})U_m)||_2^2 + ||Y_{(n\to y_m),i}N||_2^2 \le \beta_{y_m}\end{aligned} \tag{6.18}$$

H_2 norm constraint is also posed on the control input signal of VCM to constrain the energy usage of the track following actuator. Theorem 4 is used to obtain locally convex constraints of Eq.(6.18) and Eq.(6.19).

$$\begin{aligned}\frac{1}{pvs}\sum_{i=1}^{p}\sum_{l=1}^{v}\sum_{m=1}^{s} ||u_{vcm,i,l,m}||_2^2 \;=\; &\frac{1}{pvs}\sum_{i=1}^{p}\sum_{l=1}^{v}\sum_{m=1}^{s} ||U_{(r\to u_{vcm}),i}(R + H_{d,l}U_m)||_2^2 \\ &+||U_{(w\to u_{vcm}),i}(K_{ff}(e^{j\omega})U_m)||_2^2 + ||U_{(n\to u_{vcm}),i}N||_2^2 \le \beta_{u_{vcm}}\end{aligned} \tag{6.19}$$

6.5 Alternating Iterative Control Design Approach

In the alternating iterative control design approach, the feedback control design problem and the feedforward control design problem are optimized alternately. The H_2 norm conditions are iterative locally convex constraints and require initial stabilizing controllers. The H_∞ norm constraints are necessary and sufficient convex constraints. H_∞ norm constraints stabilize the closed loop system and are used to synthesize initial stabilizing controllers for the H_2 norm problem.

The alternating iterative approach is implemented as shown in Figure 5.3. The controller factorization used are as given in Eq.(6.4), Eq.(6.1) and Eq.(6.2). The actuator factorization used are given in Eq.(6.5) and Eq.(6.6). The initial stabilizing controllers are obtained by solving an H_∞ norm feasibility problem for feedback control design as well as the feedforward control design.

The control design uses frequency response measurements of the actuators VCM $G_v(j\omega)$ and MA $G_m(j\omega)$, frequency response measurements of the coupling transfer function $H_d(j\omega)$ and the frequency response of the seeking input signals u_{seek}.

Feedback Control Design

Feedback control design is characterized by minimizing the variance of the PES e and stabilizing the closed loop system. The objective function is to minimize the PES e. The dual stage closed loop system is stabilized using H_∞ norm constraints. The VCM only single-stage system is also stabilized using H_∞ norm constraints. H_2 norm constraints are used to bound the output of MA and the input of VCM.
The feedback control design is formulated as the following problem:

$$\min ||e||_2^2 \quad Eq.\ (6.12) \tag{6.20}$$
$$H_\infty \textit{ norm constraints} \quad Eqs.\ (6.7),\ (6.8),\ (6.9) \textit{ and } (6.10) \tag{6.21}$$
$$H_2 \textit{ norm constraints} \quad Eqs.\ (6.18) \textit{ and } (6.19) \tag{6.22}$$

Feedforward Control Design

Feedforward control design is characterized by minimizing the error between the PES with vibration and feedforward action and the PES without any vibration. H_∞ norm constraints are used to obtain initial stabilizing controllers. H_2 norm of the difference between the PES with vibration and PES without vibration is minimized.
The feedforward control design is formulated as the following problem:

$$\min ||e||_2^2 \quad Eq.\ (6.17) \tag{6.23}$$
$$H_\infty \textit{ norm constraints} \quad Eqs.\ (6.11) \tag{6.24}$$

The feedback control design problem and the feedforward control design problem are iterated alternately till the stopping condition is reached.

6.6 Simultaneous Control Design Approach

In the simultaneous control design approach, the feedback control design problem and the feedforward control design problem are optimized simultaneously using Theorem 5. The H_2 norm of the PES e is minimized to reduce the position error of the read / write head and to suppress the imparted vibration simultaneously. The H_∞ norm constraints are used to stabilize the closed loop of the system and to synthesize initial stabilizing controllers for the H_2 norm objective function.

The simultaneous control design problem is implemented as shown in Figure 5.4. The controller factorization used are as given in Eq.(6.4), Eq.(6.1) and Eq.(6.2). The actuator factorization used are given in Eq.(6.5) and Eq.(6.6).

The control design uses frequency response measurements of the actuators VCM $G_v(j\omega)$ and MA $G_m(j\omega)$, frequency response measurements of the coupling transfer function $H_d(j\omega)$ and the frequency response of the seeking input signals u_{seek}.

Joint Feedback - Feedforward Control Design

The joint data driven control design problem is characterized by H_2 norm objective function to minimize the PES e and suppress the imparted vibration simultaneously. H_∞ norm constraints are used to obtain initial stabilizing controllers. H_∞ norm constraints also stabilize the closed loop of the system. H_2 norm constraints are used to constrain the output of MA and the input of VCM.
The joint feedback - feedforward control design is formulated as the following problem:

$$\min ||e||_2^2 \quad Eq.\ (6.14) \tag{6.25}$$

$$H_\infty \textit{ norm constraints} \quad Eqs.\ (6.7),\ (6.8),\ (6.9) \textit{ and } (6.10),\ (6.11) \tag{6.26}$$

$$H_2 \textit{ norm constraints} \quad Eqs.\ (6.18) \textit{ and } (6.19) \tag{6.27}$$

The feedback and the feedforward controllers are obtained simultaneously.

6.7 Design Results

In this section, the control design results of the alternating iterative data driven approach and the simultaneous data driven approach are discussed. The frequency domain results and the time domain results are discussed for both the approaches.

The objective is to design a feedback controller for a track following actuator to stabilize the closed loop system and minimize the variance of the error signal e and, to suppress the vibration imparted by the neighboring seeking actuator. Two frequency response measurements of the track following actuators VCM G_v and MA G_m are considered as shown in Figure 6.3. The frequency response measurements of the coupling transfer function $H_d j\omega$ considered are shown in Figure 6.5. Five measurements of the coupling transfer function are considered. Also, eight seeking control signals u_{seek} are considered for the control design.

Alternating Iterative Control Design Approach

In the alternating iterative data driven control design approach, the feedback control design problem and the feedforward control design problem are iterated alternately, as shown in section 6.5. The results shown here are obtained after ten iterations.

Feedback Control Design

The feedback control design is characterized by minimization of the variance of the error signal e and stabilization of the closed loop system. H_∞ norm conditions are used to shape the closed loop transfer functions and stabilize the closed loop system, as given by Eqs. (6.7) - (6.10).

Figure 6.6 plots the closed loop transfer function $E_{r\to e}(j\omega)$ along with its weighting filter W_s in the frequency domain. The evolution of the closed loop transfer function with each

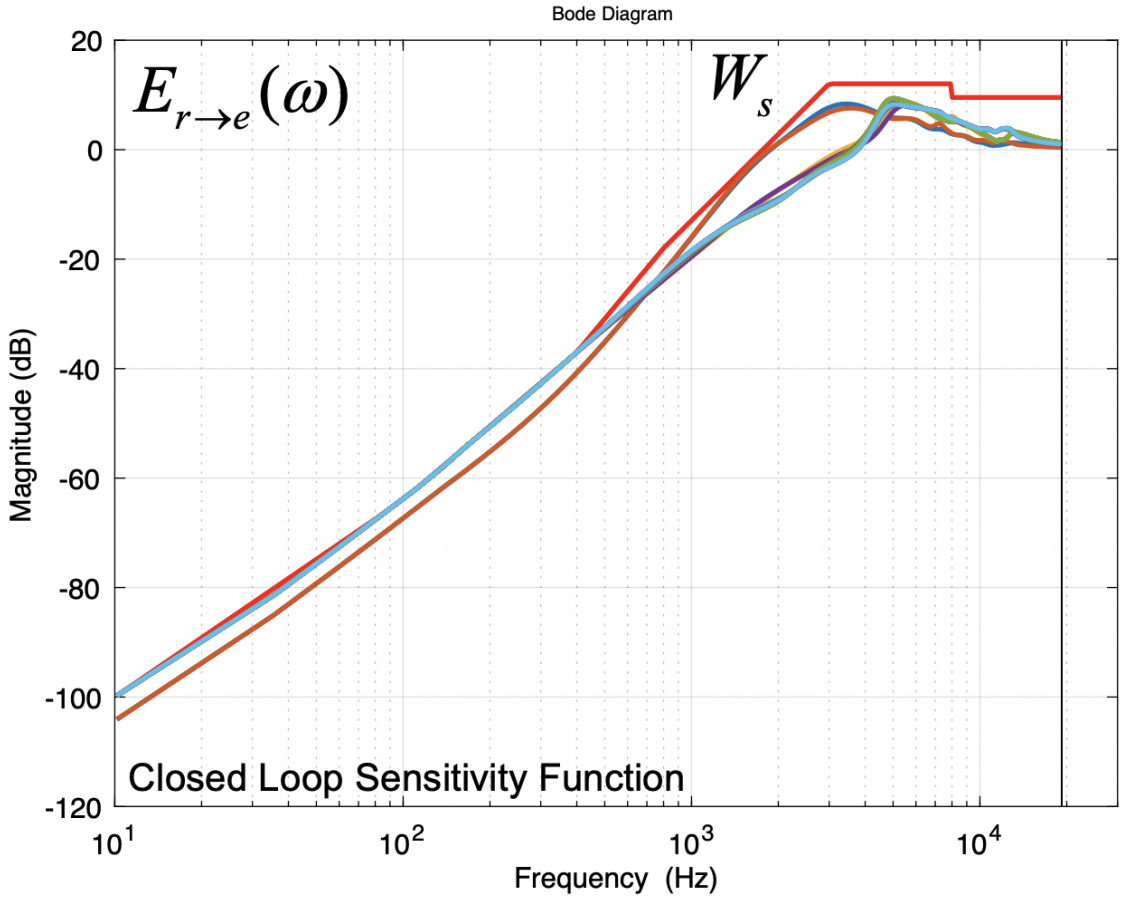

Figure 6.6: The overall closed loop sensitivity transfer function $E_{r\to e}(j\omega)$ is shown in this figure. W_s is the weighting filter used to shape the closed loop transfer function $E_{r\to e}(j\omega)$. As the closed loop transfer function lies under the weighting filter, the H_∞ norm constraint is satisfied. Evolution of $E_{r\to e}(j\omega)$ with each iteration is plotted in this figure.

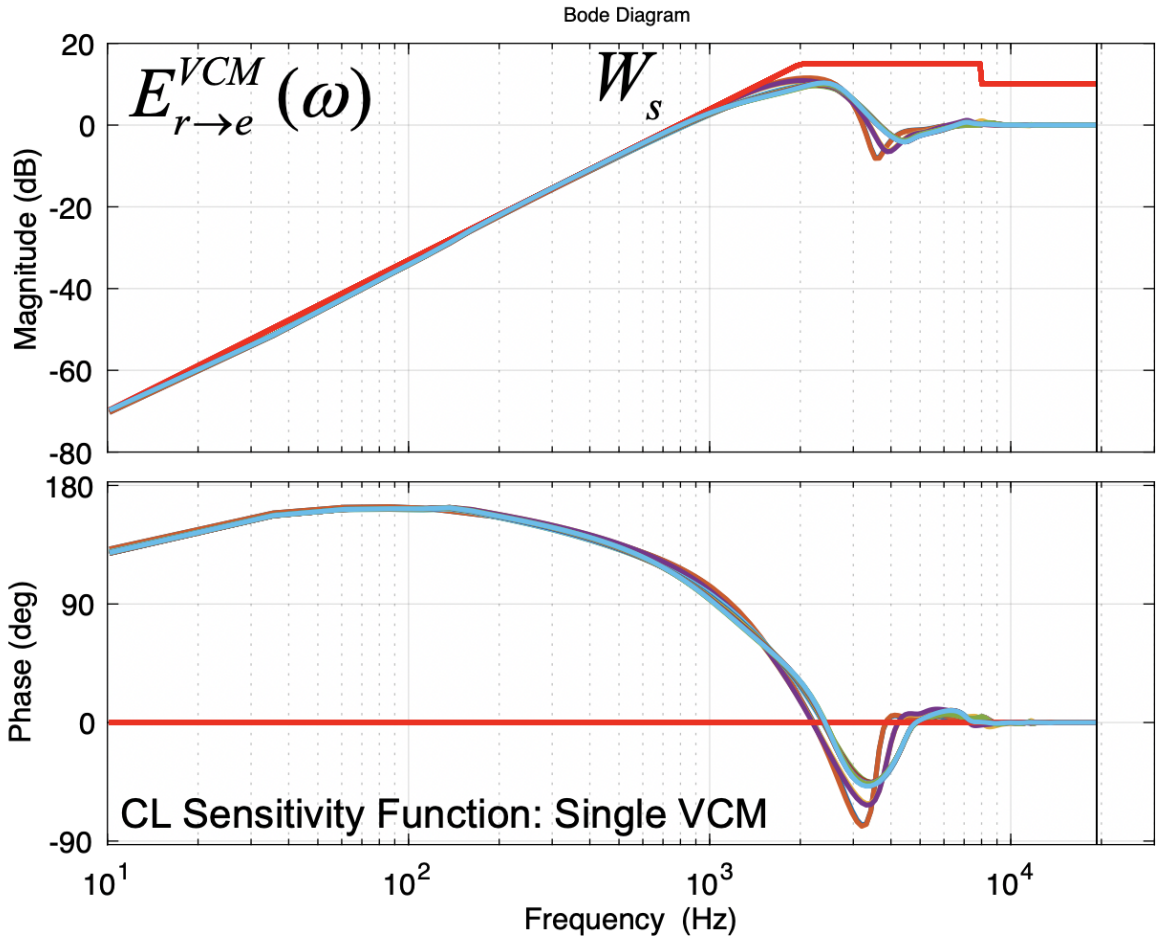

Figure 6.7: The single-stage VCM closed loop sensitivity transfer function $E_{r\to e}^{VCM}(j\omega)$ is shown in this figure. W_s is the weighting filter used to shape the closed loop transfer function $E_{r\to e}^{VCM}(j\omega)$. As the closed loop transfer function lies under the weighting filter, the H_∞ norm constraint is satisfied. Evolution of $E_{r\to e}^{VCM}(j\omega)$ with each iteration is plotted in this figure.

iteration can be observed in this figure. The H_∞ norm constraint reshapes $E_{r\to e}(j\omega)$ to meet the constraint set by the weighting filter W_s.

Similarly, the frequency domain plot of the single stage VCM closed loop sensitivity transfer function $E_{r\to e}^{VCM}(j\omega)$ is shown in Figure 6.7. W_s denotes the weighting filter used to shape the closed loop transfer function. As the transfer function lies under the weighting filter W_s, the H_∞ norm constraint is met.

The H_2 norm objective function is used to minimize the average position error signal of the read / write head of the track following actuator. The average variance of the PES e versus iteration number is plotted in Figure 6.8 for all the actuator data considered in the

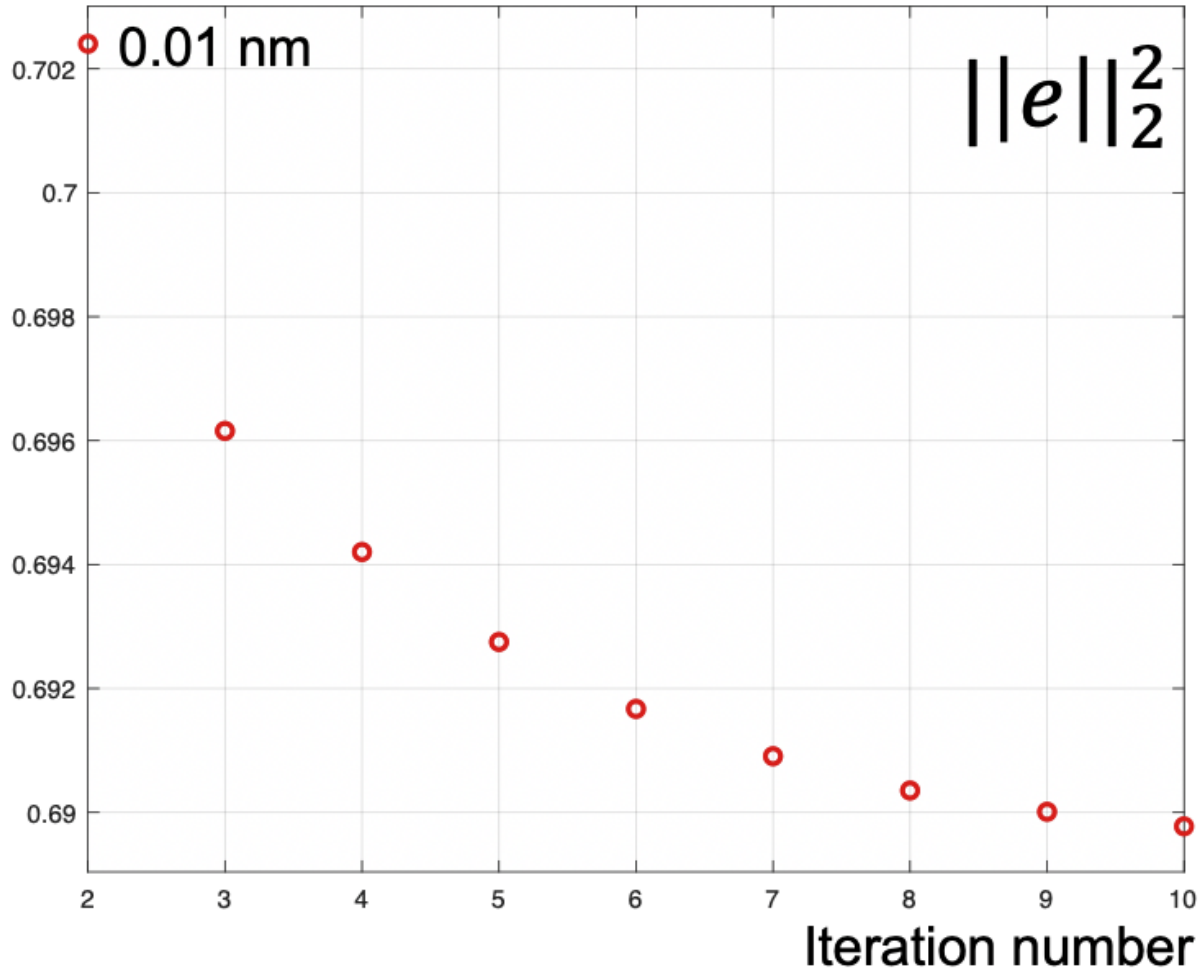

Figure 6.8: The variance of the position error signal $||e||_2^2$ is plotted versus the iteration number in this figure. The variance of the error signal is minimized with each iteration until it converges to a constant value.

design process. It can be observed that the variance of the position error signal is minimized with each iteration until it converges to a constant value for all actuator measurements.

Feedforward Control Design

The objective of the feedforward control design is to suppress the imparted vibration by the track seeking actuator. A set of five coupling transfer functions $H_d(j\omega)$ and a set of eight seeking input signals u_{seek} were considered in the design process. The shortest seek

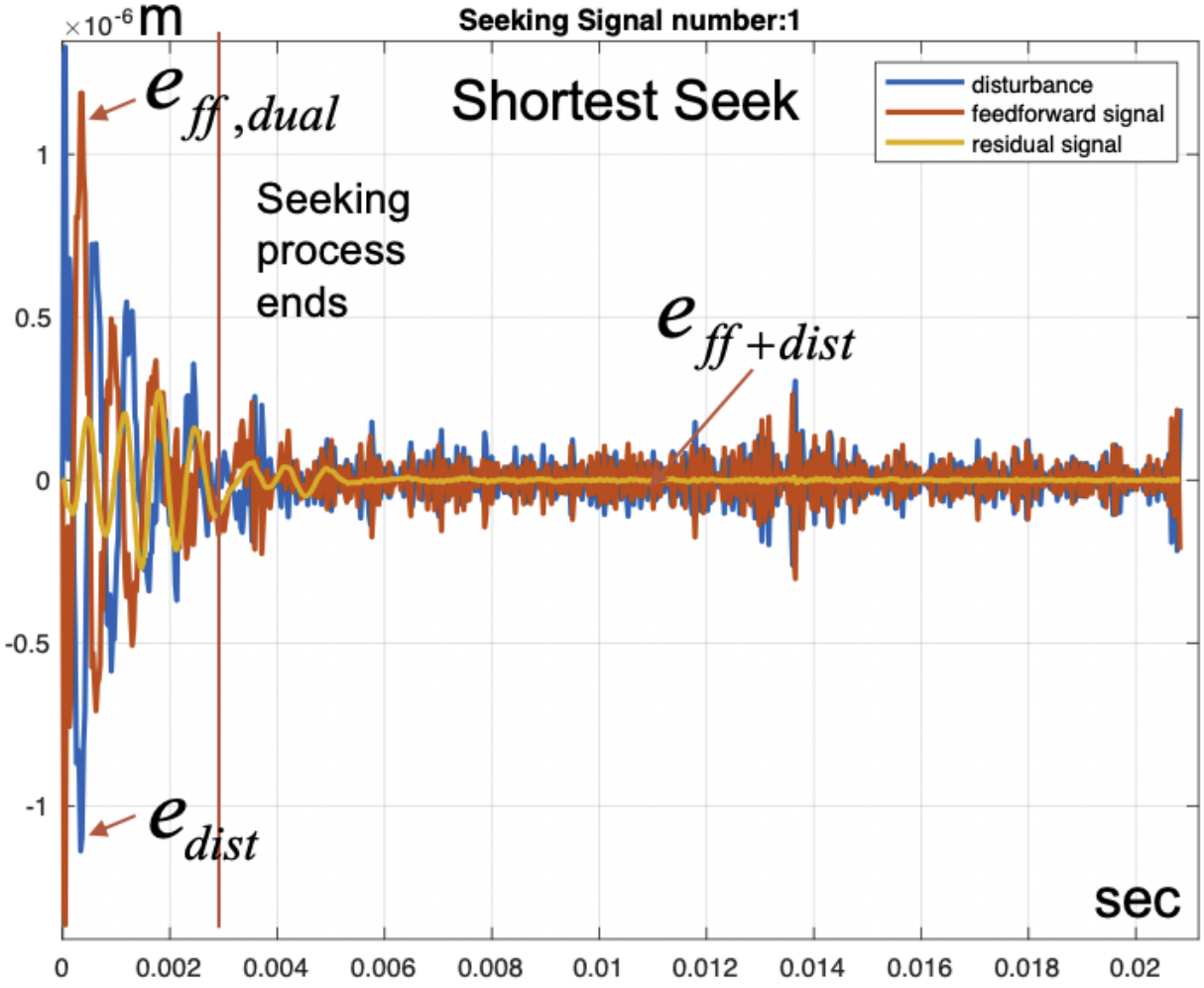

Figure 6.9: The vibration disturbance e_{dist}, the dual actuator feedforward suppression signal $e_{ff,dual}$ and the residual signal after feedforward suppression $e_{ff+dist}$ for the shortest seek is plotted in the time domain. A feedforward suppression upto 3× initially and 8× later is observed. The feedforward signal matches the gain of the vibration disturbance signal to a large extent with negative phase.

is completed in 0.002 seconds, whereas, the longest seek requires around 0.014 seconds, as shown in Figure 6.2.

Figure 6.9 plots the vibration disturbance e_{dist}, the dual actuator feedforward suppression signal $e_{ff,dual}$ and the residual signal after feedforward suppression $e_{ff+dist}$ for the shortest seek in the time domain. A feedforward suppression upto 3× initially and 8× later is observed. The feedforward signal matches the gain of the vibration disturbance signal to a large extent with negative phase.

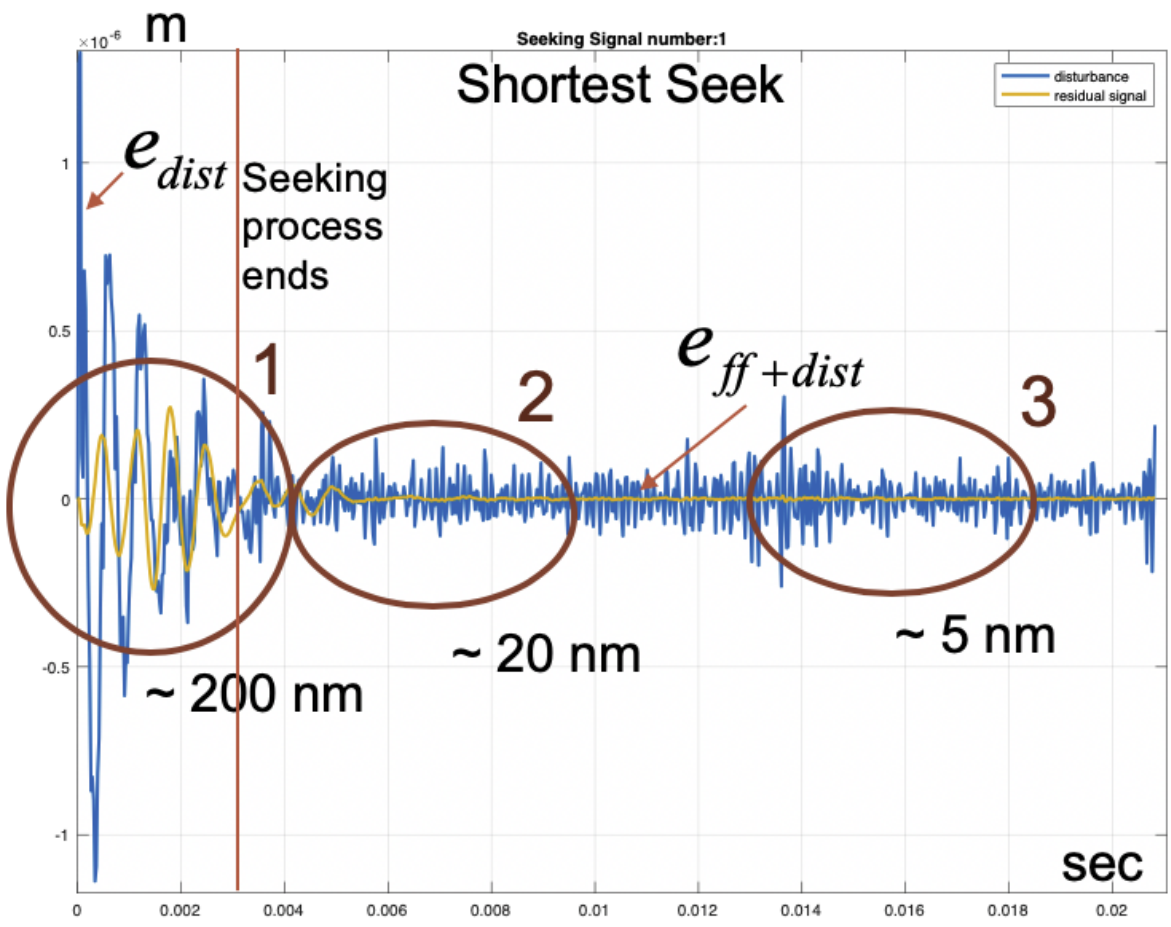

Figure 6.10: The vibration disturbance e_{dist} and the residual signal after feedforward compensation $e_{ff+dist}$ for the shortest seek is plotted, in this figure, in time domain. A feedforward suppression upto 3× initially and 8× later is observed. The seeking process ends around 0.003 seconds, denoted by the vertical red line.

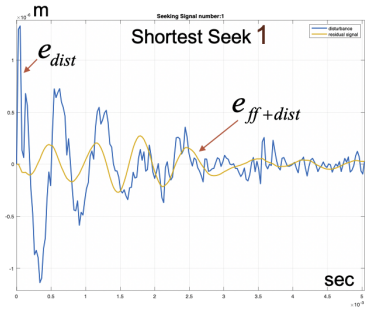

(a) Part 1

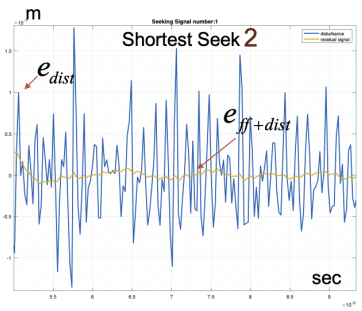

(b) Part 2

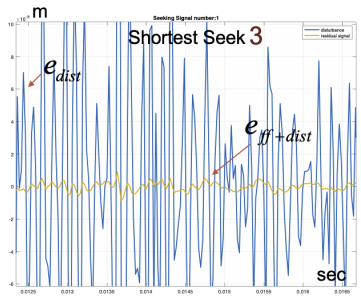

(c) Part 3

Figure 6.11: The vibration disturbance e_{dist} and residual signal $e_{ff+dist}$ from Figure 6.10 is divided into three parts as shown in Figure 6.11. Part 1, as shown in Figure 6.11a, is the first part of the seeking process. The imparted vibration starts with a jerk and the feedforward controller is able to suppress it to a good extent. The residual signal of ≈ 200 nano-meters is obtained. In part 2, as shown in Figure 6.11b, the seeking process had ended but vibration from the initial jerk has not entirely died down. The residual signal on feedforward suppression is ≈ 20 nano-meters. In part 3, as shown in Figure 6.11c, the seeking process has ended and the residual signal obtained on feedforward suppression is ≈ 5 nano-meters.

Figure 6.10 plots the vibration disturbance e_{dist} and the residual signal after feedforward suppression $e_{ff+dist}$ in the time domain for the shortest seek scenario. A feedforward suppression upto $8\times$ is observed after the initial jerk dies down. The vibration disturbance e_{dist} and residual signal $e_{ff+dist}$ from Figure 6.10 is divided into three parts as shown in Figure 6.11. Part 1, as shown in Figure 6.11a, is the first part of the seeking process. The imparted vibration starts with a jerk and the feedforward controller is able to suppress it to a good extent. The residual signal of ≈ 200 nano-meters is obtained. In part 2, as shown in Figure 6.11b, the seeking process had ended but vibration from the initial jerk has not entirely died down. The residual signal on feedforward suppression is ≈ 20 nano-meters. In part 3, as shown in Figure 6.11c, the seeking process has ended and the residual signal obtained on feedforward suppression is ≈ 5 nano-meters.

Figure 6.12 plots the vibration disturbance e_{dist} and the residual signal after feedforward suppression $e_{ff+dist}$ in the time domain for the longest seek scenario. A feedforward suppression upto $5\times$ is observed. The vibration disturbance e_{dist} and residual signal $e_{ff+dist}$ from Figure 6.12 is divided into three parts as shown in Figure 6.13. Part 1, as shown in Figure 6.13a, is the first part of the seeking process. The imparted vibration starts with a jerk and the feedforward controller is able to suppress it to a good extent. The residual signal of ≈ 200 nano-meters is obtained. In part 2, as shown in Figure 6.13b, the seeking process continues but vibration from the initial jerk has died down. The residual signal on feedforward suppression is ≈ 50 nano-meters. In part 3, as shown in Figure 6.13c, the seek-

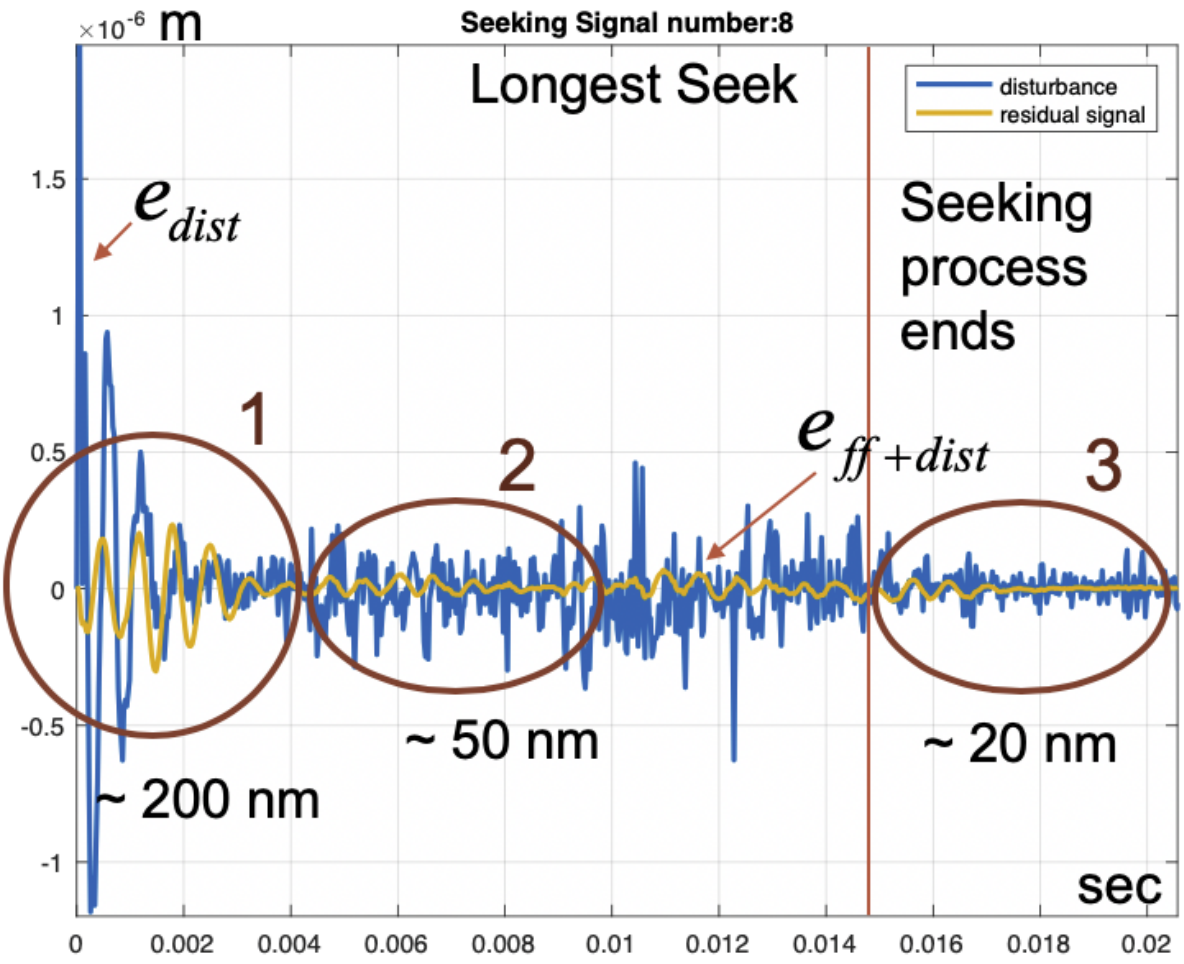

Figure 6.12: The vibration disturbance e_{dist} and the residual signal after feedforward compensation $e_{ff+dist}$ for the longest seek is plotted, in this figure, in time domain. A feedforward suppression of up to 5× is observed. The seeking process ends around 0.015 seconds, denoted by the vertical red line.

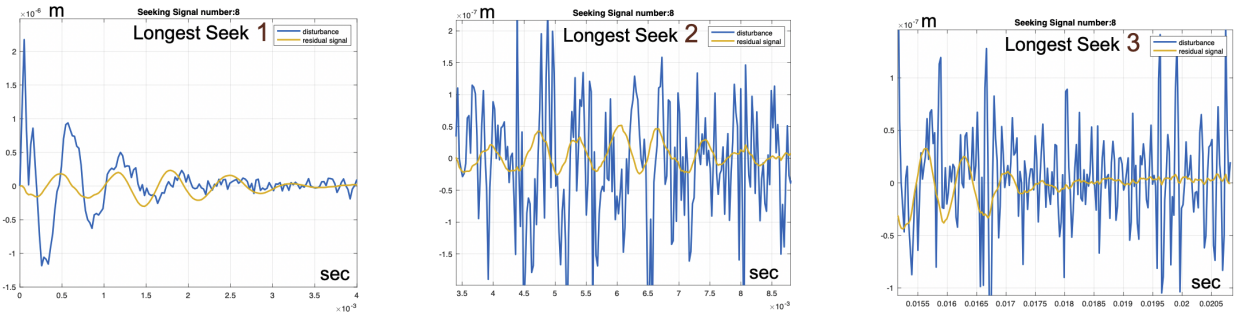

(a) Part 1 (b) Part 2 (c) Part 3

Figure 6.13: The vibration disturbance and residual signal from Figure 6.12 is divided into three parts. Part 1, as shown in Figure 6.13a, is the first part of the seeking process. The imparted vibration starts with a jerk and the feedforward controller is able to suppress it to a good extent. The residual signal of ≈ 200 nano-meters is obtained. In part 2, as shown in Figure 6.13b, the seeking process continues but vibration from the initial jerk has died down. The residual signal on feedforward suppression is ≈ 50 nano-meters. In part 3, as shown in Figure 6.13c, the seeking process has ended and the residual signal obtained on feedforward suppression is ≈ 20 nano-meters.

ing process has ended and the residual signal obtained on feedforward suppression is ≈ 20 nano-meters.

From Eq.(6.17), we define the closed loop coupling transfer function $G_{d,i,l}(j\omega)$ for i^{th} actuator measurement and l^{th} coupling dynamics as follows:

$$G_{d,i,l}(j\omega) = E_{(r\to e),i}(j\omega)H_{d,l}(j\omega) \tag{6.28}$$

The closed loop feedforward controllers for i^{th} actuator measurement are defined as:

$$K_{cl,VCM,i}(j\omega) = E_{w_v\to e}(j\omega)K_{ff,VCM}(e^{j\omega}) \tag{6.29}$$
$$K_{cl,MA,i}(j\omega) = E_{w_m\to e}(j\omega)K_{ff,MA}(e^{j\omega}) \tag{6.30}$$

The objective of the feedforward control design is to match the closed loop coupling transfer function $G_{d,i,l}(j\omega)$ from Eq.(6.28) with the closed loop feedforward action given by Eq.(6.29) and Eq.(6.30). The closed loop feedforward control transfer function and the closed loop coupling transfer function are plotted against each other in Figure 6.14.

Simultaneous Control Design Approach

In the simultaneous control design approach, the feedback controller and the feedforward controller for the track following actuator are designed simultaneously, as shown in section 6.6. The feedback control design and the feedforward control design obtained are similar

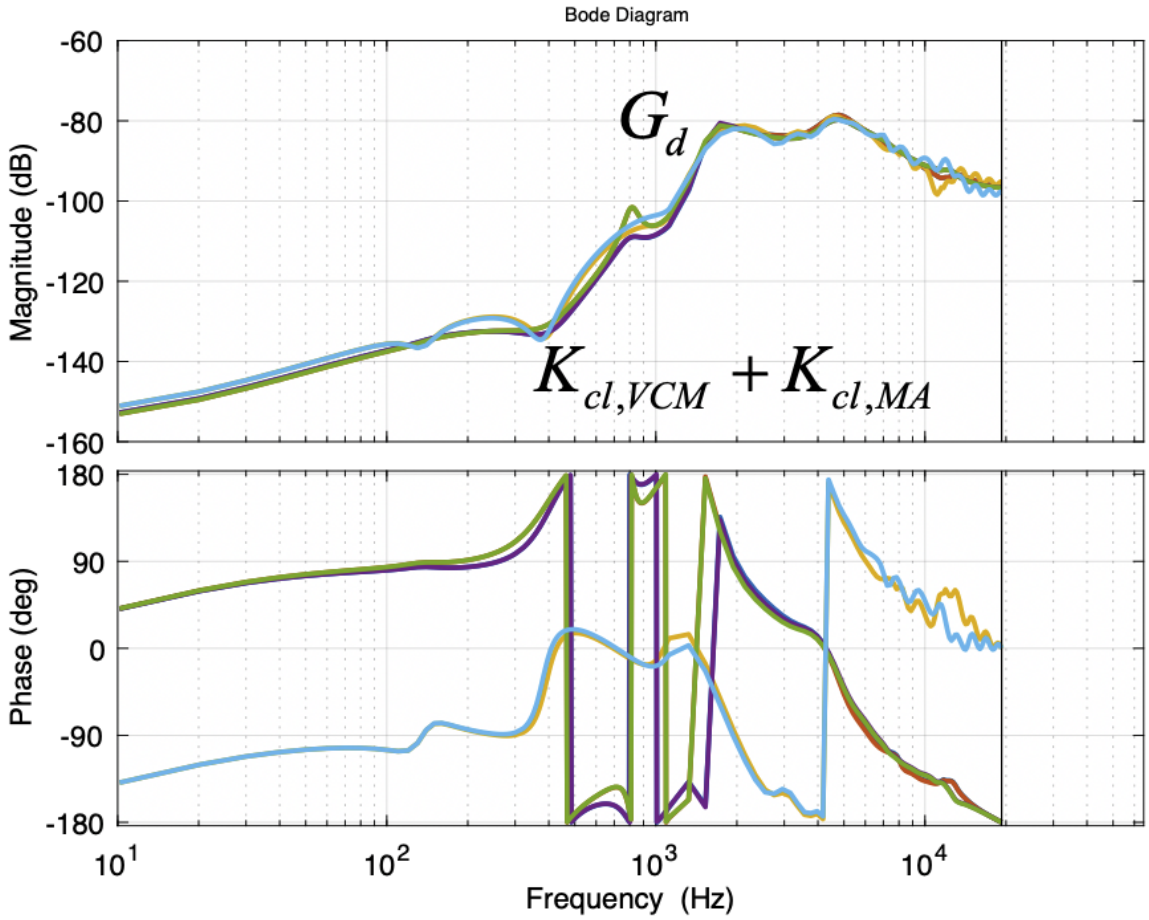

Figure 6.14: The objective of the feedforward control design is to match the closed loop coupling transfer function $G_{d,i,l}(j\omega)$ from Eq.(6.28) with the closed loop feedforward action given by Eq.(6.29) and Eq.(6.30). In this figure, we can observe that for one actuator plant data, the feedforward controllers are able to closely match $G_d(j\omega)$ for five coupling scenarios.

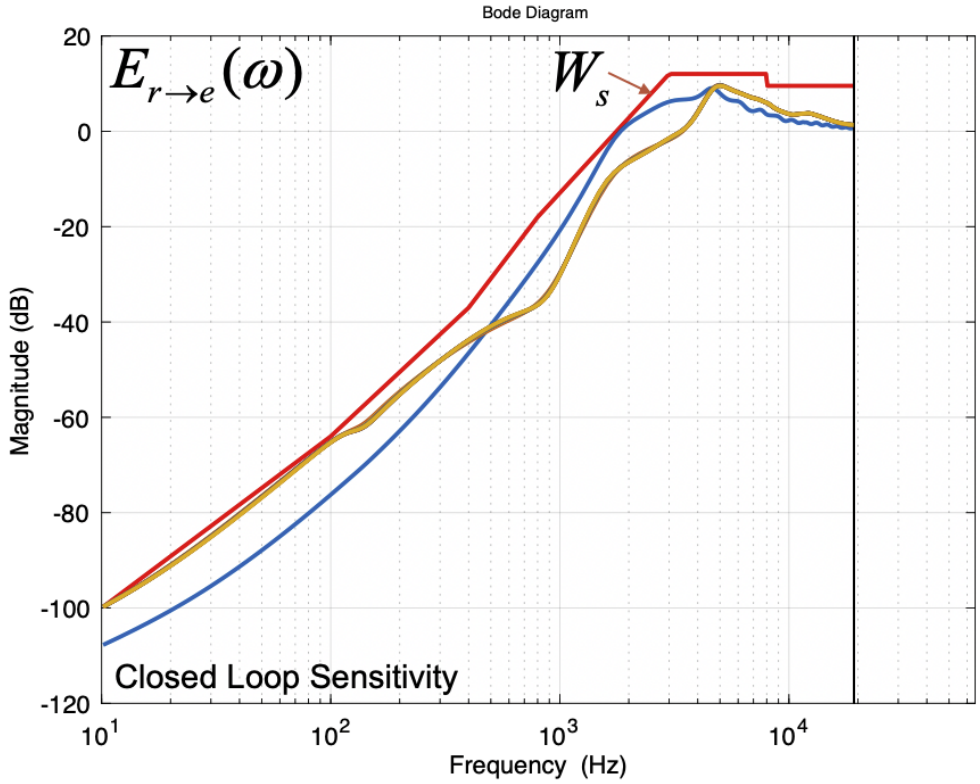

Figure 6.15: The overall closed loop sensitivity transfer function $E_{r\to e}(j\omega)$ is shown in this figure. W_s is the weighting filter used to shape the closed loop transfer function $E_{r\to e}(j\omega)$. As the closed loop transfer function lies under the weighting filter, the H_∞ norm constraint is satisfied. Evolution of $E_{r\to e}(j\omega)$ with each iteration is plotted in this figure.

to the results shown for the alternating iterative control design approach. A brief overview of the results for the simultaneous control design approach is shown in this section. The comparison of the two approaches is conducted in the next section.

Feedback Control Design

The feedback control design is characterized by minimization of the variance of the error signal e and stabilization of the closed loop system. H_∞ norm conditions are used to shape the closed loop transfer functions and stabilize the closed loop system, as given by Eqs. (6.7) - (6.10). Figure 6.15 plots the evolution of the closed loop sensitivity transfer function $E_{r\to e}(j\omega)$ with each iteration. Here, W_s is the weighting filter used to shape the closed loop transfer function $E_{r\to e}(j\omega)$.

The open loop feedback controller $K_{2\times1}(z)$ is plotted in Figure 6.16. The first element of the controller (in blue) has an integrator as a fixed part of the controller. The stable

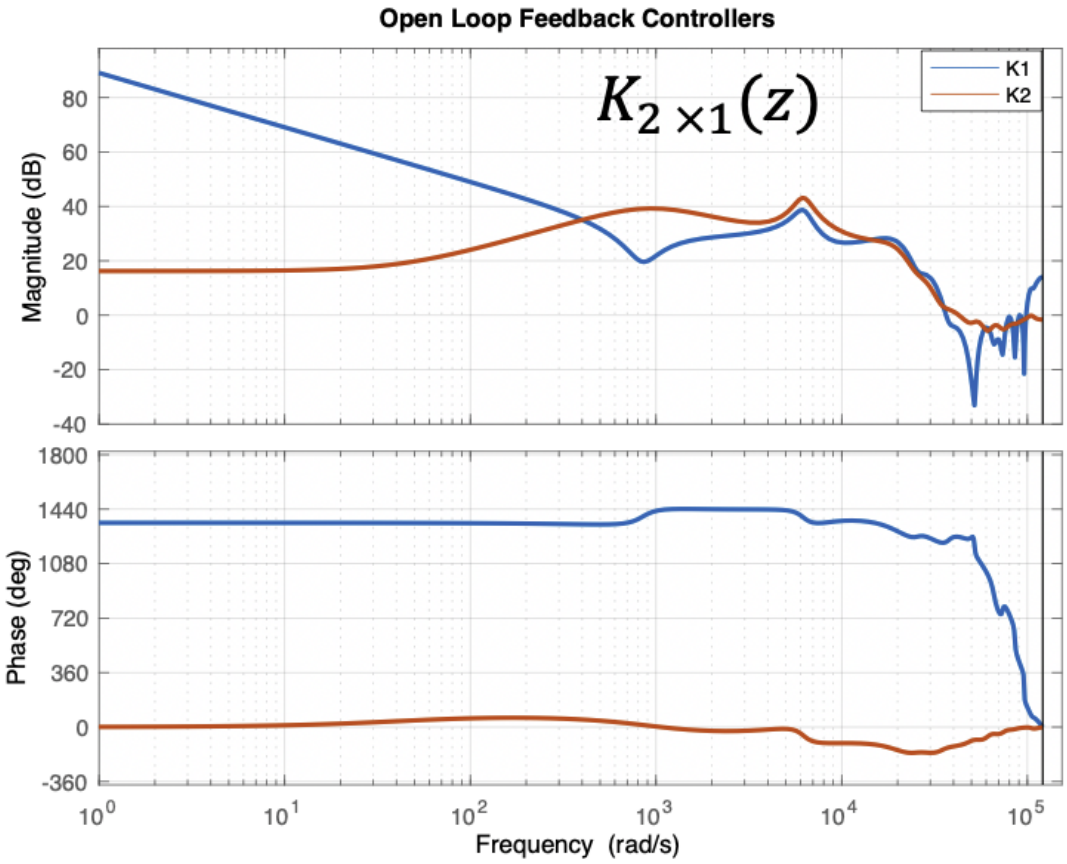

Figure 6.16: The open loop feedback controller $K_{2\times1}(z)$ is plotted in this figure. The first element of the controller, which corresponds to the VCM controller, is plotted in blue and the second element of the controller, which corrresponds to the MA controller, is plotted in red. The first element of the controller has an integrator as the fixed part, this is evident by a slope of -20 dB in the low frequency region.

factorization with a fixed part are obtained using Eq.(5.28) and Eq.(5.29).

The H_2 norm objective function is used to minimize the average position error signal of the read / write head of the track following actuator. The average variance of the PES e versus iteration number is plotted in Figure 6.17 for all the actuator data considered in the design process. It can be observed that the average variance of the position error signal is minimized with each iteration until it converges to a constant value.

Feedforward Control Design

The objective of the feedforward control design is to suppress the imparted vibration by the track seeking actuator. A set of five coupling transfer functions $H_d(j\omega)$ and a set of

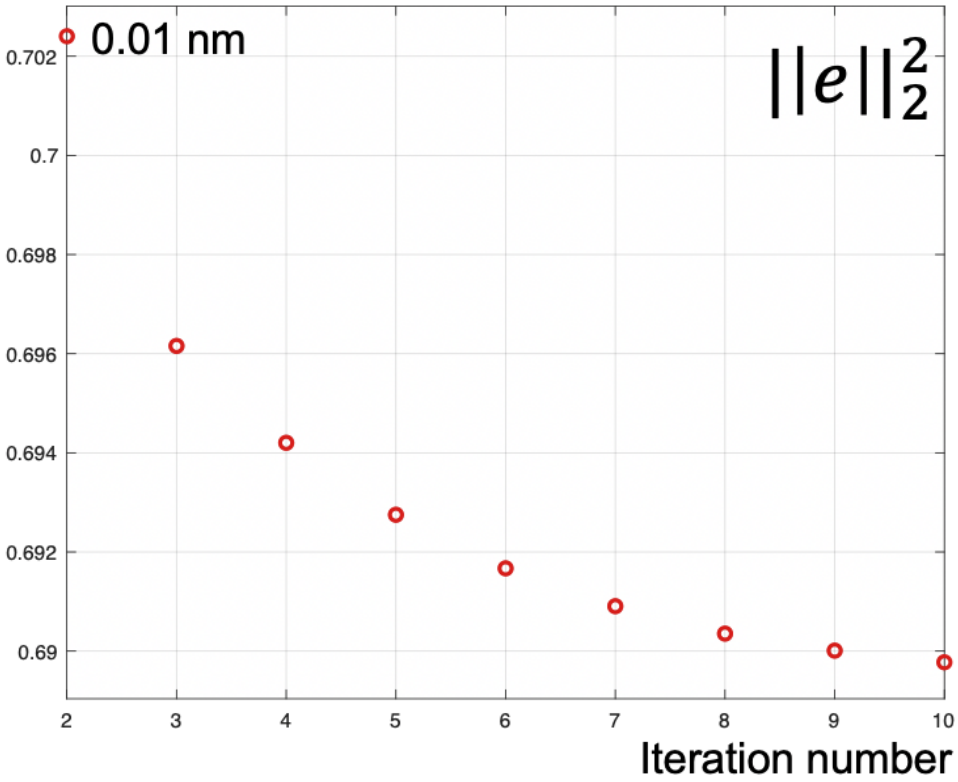

Figure 6.17: The variance of the position error signal $||e||_2^2$ is plotted versus the iteration number in this figure. The variance of the error signal is minimized with each iteration until it converges to a constant value.

eight seeking input signals u_{seek} were considered in the design process. The shortest seek is completed in 0.002 seconds, whereas, the longest seek requires around 0.014 seconds, as shown in Figure 6.2.

Figure 6.18 plots the vibration disturbance e_{dist}, the dual actuator feedforward suppression signal $e_{ff,dual}$ and the residual signal after feedforward suppression $e_{ff+dist}$ for the shortest seek in the time domain. A feedforward suppression upto 3× initially and 8× later is observed. The feedforward signal matches the gain of the vibration disturbance signal to a large extent with negative phase.

Figure 6.19 plots the residual signals after feedforward suppression for all eight seek scenarios. The initial jerk induces a resultant vibration of $\sim$ 200 nano-meters. After 0.003 seconds, the mid-range seeks have the largest residual vibration of the order of $\sim$ 80 nano-meters. Eventually, it can be observed that the longest seek is the last to die down, and all vibration scenarios being suppressed to $\sim$ 5 nano-meters.

From Eq.(6.14), we define the closed loop coupling transfer function $G_{d,i,l}(j\omega)$ for i^{th}

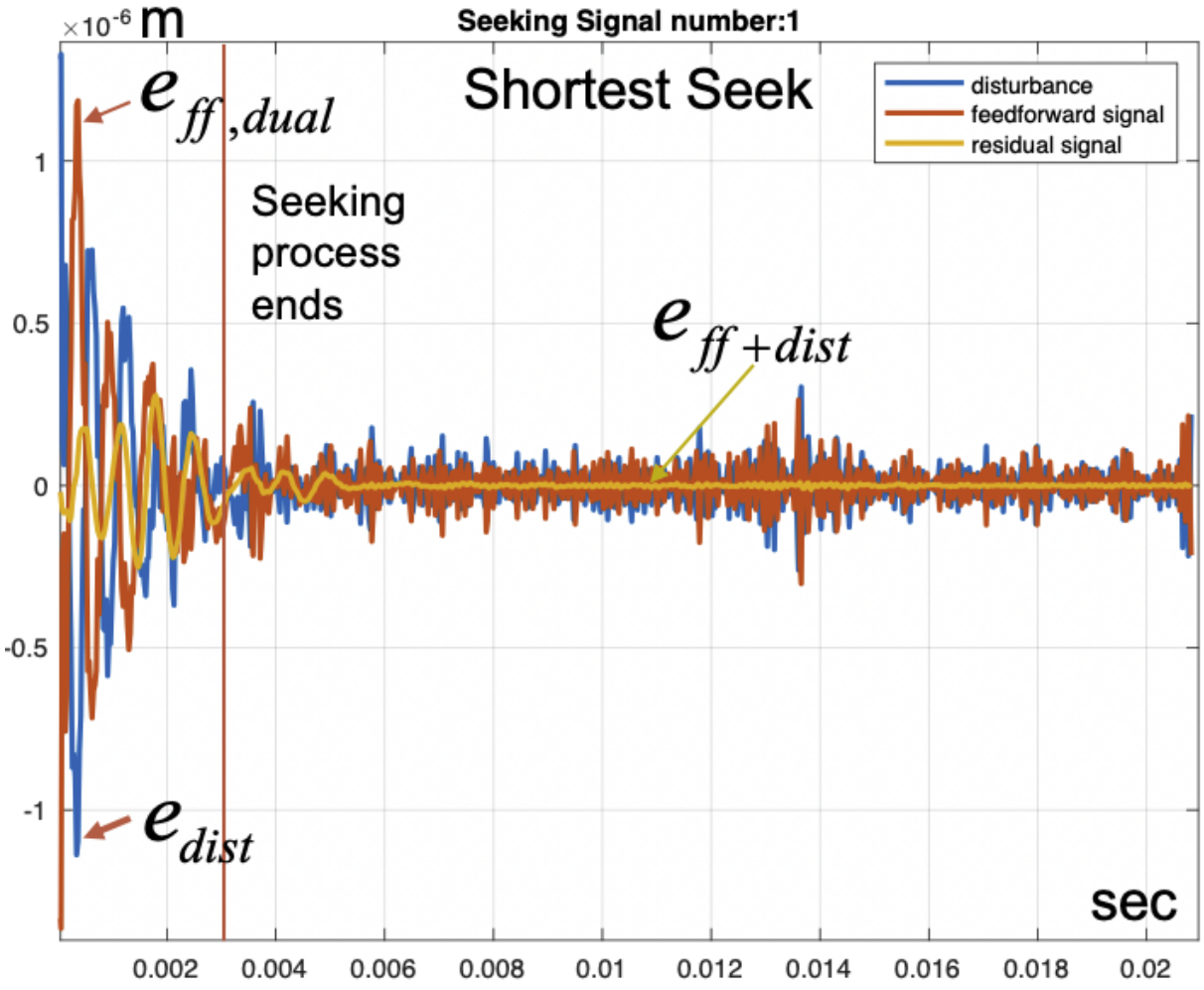

Figure 6.18: The vibration disturbance e_{dist}, the dual actuator feedforward suppression signal $e_{ff,dual}$ and the residual signal after feedforward suppression $e_{ff+dist}$ for the shortest seek is plotted in the time domain. A feedforward suppression upto 3× initially and 8× later is observed. The feedforward signal matches the gain of the vibration disturbance signal to a large extent with negative phase.

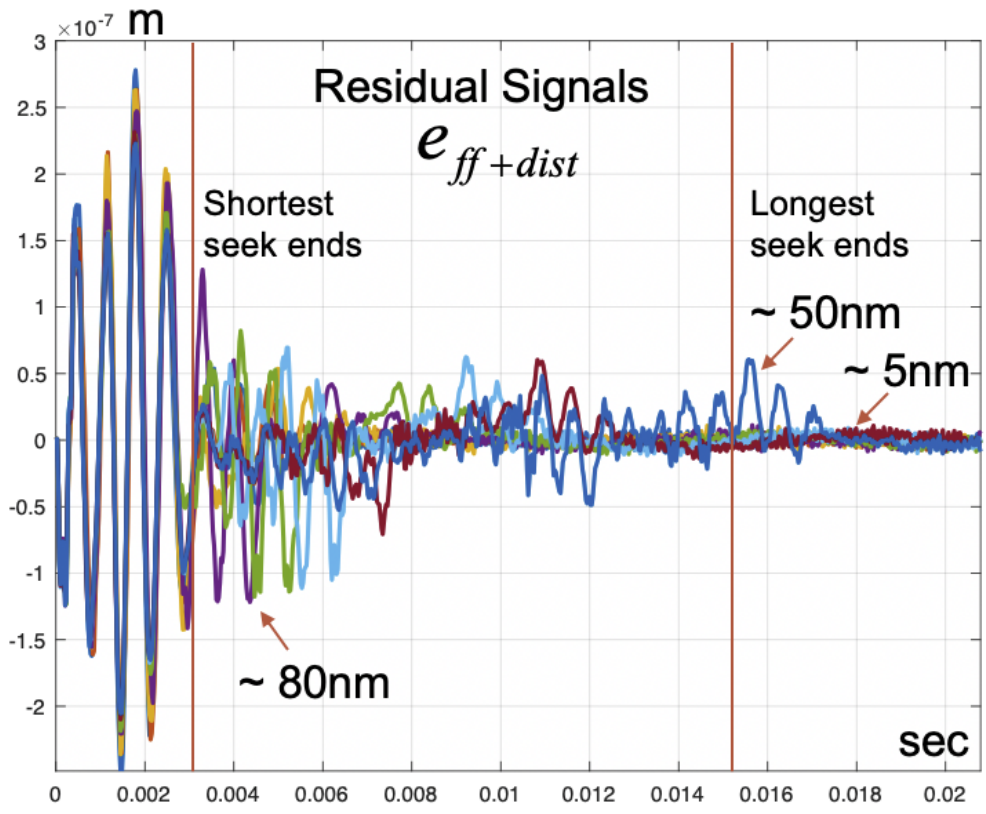

Figure 6.19: The residual signals after feedforward suppression for all eight scenarios is plotted. The initial jerk induces a resultant vibration of $\sim$ 200 nano-meters. After 0.003 seconds, the mid-range seeks have the largest residual vibration of the order of $\sim$ 80 nano-meters. Eventually, it can be observed that the longest seek is the last to die down, and all vibration scenarios being suppressed to $\sim$ 5 nano-meters.

actuator measurement and l^{th} coupling dynamics as follows:

$$G_{d,i,l}(j\omega) = E_{(r\to e),i}(j\omega)H_{d,l}(j\omega) \tag{6.31}$$

The closed loop feedforward controllers for i^{th} actuator measurement are defined as:

$$K_{cl,VCM,i}(j\omega) = E_{w_v\to e}(j\omega)K_{ff,VCM}(e^{j\omega}) \tag{6.32}$$
$$K_{cl,MA,i}(j\omega) = E_{w_m\to e}(j\omega)K_{ff,MA}(e^{j\omega}) \tag{6.33}$$

The objective of the feedforward control design is to match the closed loop coupling transfer function $G_{d,i,l}(j\omega)$ from Eq.(6.31) with the closed loop feedforward action given by Eq.(6.32) and Eq.(6.33). The closed loop feedforward control transfer function and the closed loop coupling transfer function are plotted against each other in Figure 6.20.

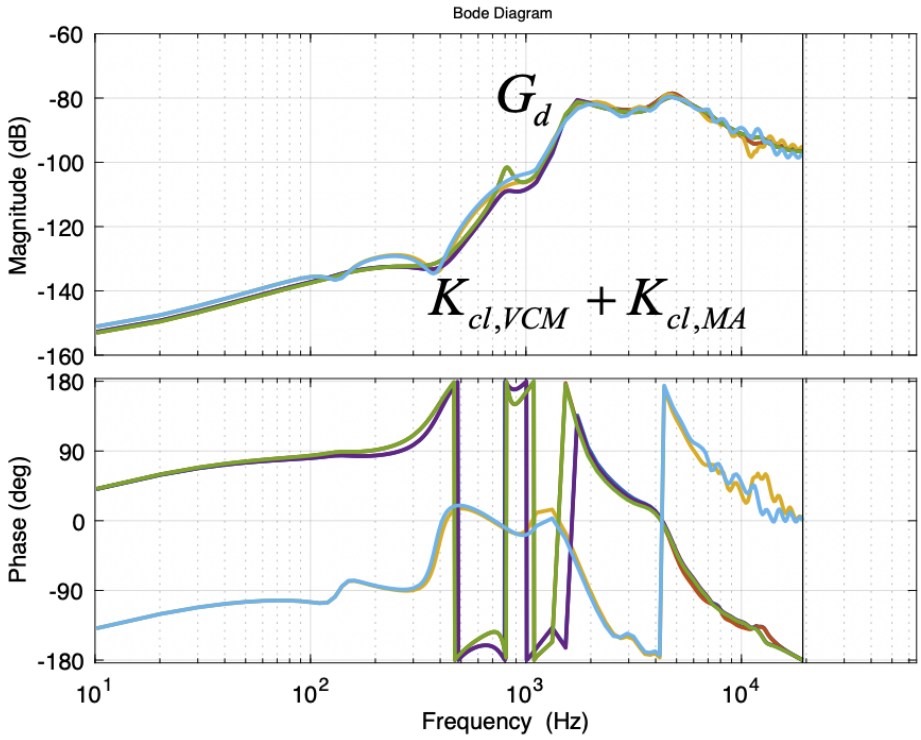

Figure 6.20: The objective of the feedforward control design is to match the closed loop coupling transfer function $G_{d,i,l}(j\omega)$ from Eq.(6.31) with the closed loop feedforward action given by Eq.(6.32) and Eq.(6.33). In this figure, we can observe that for one actuator plant data, the feedforward controllers are able to closely match $G_d(j\omega)$ for five coupling scenarios.

Alternating Iterative Approach vs Simultaneous Design Approach

The performance of the two control design approaches will be compared in this section. First, the variance of the PES e is compared versus iteration number for the two design approaches. Then, the time domain results of the feedforward suppression is compared for the two design methods.

The worst case open loop margins and bandwidths for the alternating iterative approach (AI) and the simultaneous design approach (SIM) are shown in Table 6.1

The H_2 norm of the feedback control design part of the PES e given by the following equation is plotted in Figure 6.21.

$$||e_{fb}||_2^2 \approx ||E_{(r\to e)}R||_2^2 + ||E_{(n\to e)}N||_2^2 \tag{6.34}$$

In Figure 6.21, triangle represents the simultaneous control design approach whereas, the circle represents the alternating iterative control design approach. It is observed that the feedback control design for both the approaches converge to the same value.

Scenario	$E_{r\to e}$ peak dB	GM dB	PM $degree$	ω_{GM} Hz	ω_{PM} Hz
AI	9.62	8.90	19.2	12,402	4,930
SIM	9.55	8.85	19.14	12,393	4,922

Table 6.1: Worst case open Loop stability margins and bandwidths

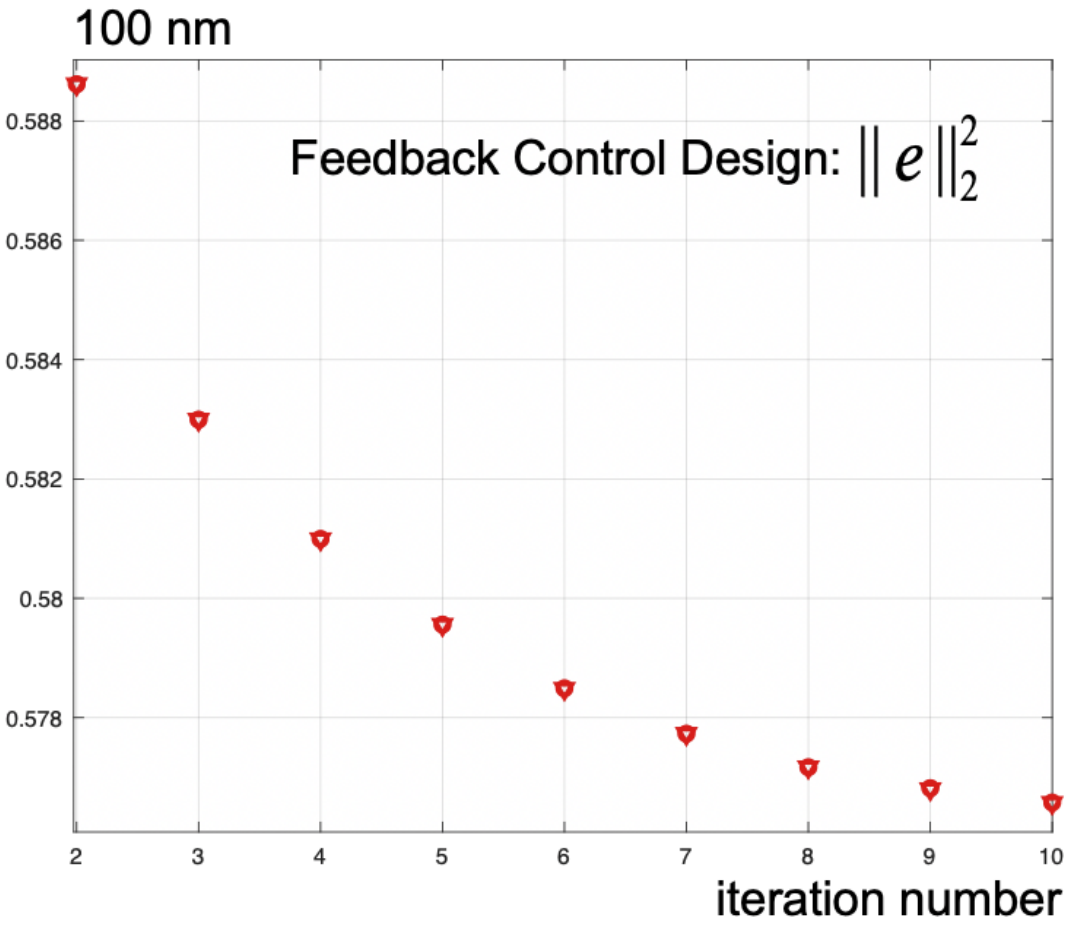

Figure 6.21: The H_2 norm of the feedback control design part of the PES e, as given in Eq.(6.34), is plotted versus the iteration number in this figure. Triangle represents the simultaneous control design approach whereas, the circle represents the alternating iterative control design approach. It is observed that the feedback control design for both the approaches converge to the same value.

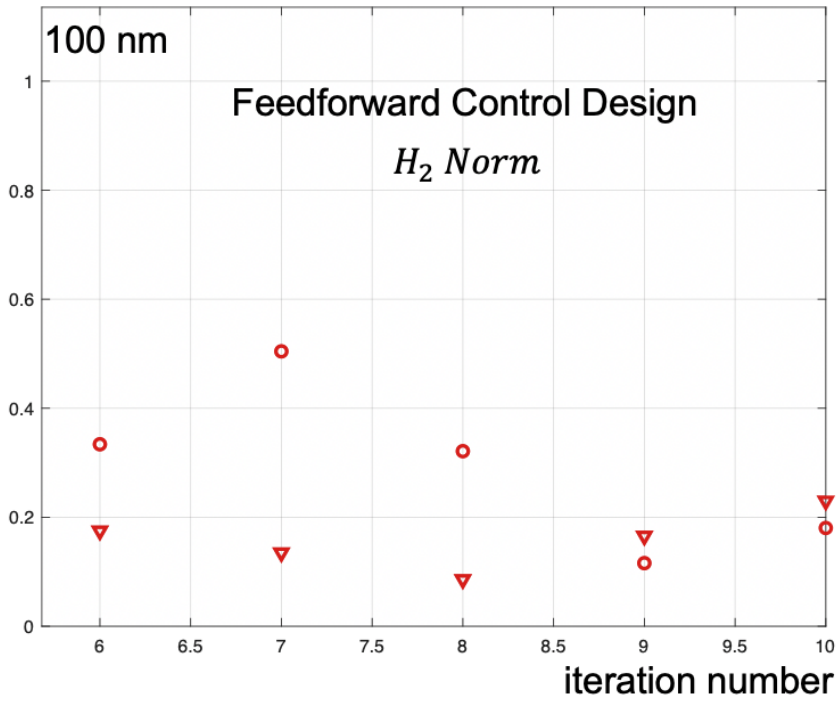

Figure 6.22: The H_2 norm of the feedforward control design part of the PES e, as given in Eq.(6.35), is plotted versus the iteration number in this figure. Triangle represents the simultaneous control design approach whereas, the circle represents the alternating iterative control design approach. It is observed that the simultaneous control design approach requires fewer iterations to converge than the alternating iterative approach. But, alternating iterative approach does slightly better.

Figure 6.22 plots the H_2 norm minimized for the feedforward control design.

$$||e_{ff}||_2^2 \approx ||(E_{(r\to e)}H_d + E_{(w_v\to e)}K_{ff,VCM} + E_{(w_m\to e)}K_{ff,MA})U||_2^2 \tag{6.35}$$

The H_2 norm of the feedforward control design part of the PES e, as given in Eq.(6.35), is plotted versus the iteration number in this figure. Triangle represents the simultaneous control design approach whereas, the circle represents the alternating iterative control design approach. It is observed that the simultaneous control design approach requires fewer iterations to converge than the alternating iterative approach. But, the two methodologies converge to the same feedforward controller.

The feedforward controllers obtained using the two approaches are plotted in Figure 6.23. Both the approaches converge to very similar feedforward controllers.

In Figure 6.24, the residual vibration for both the approaches are compared for the longest seek and the shortest seek. Ideally, the resultant residual vibration should be zero. But, as the controllers are designed for multiple frequency response measurements and due

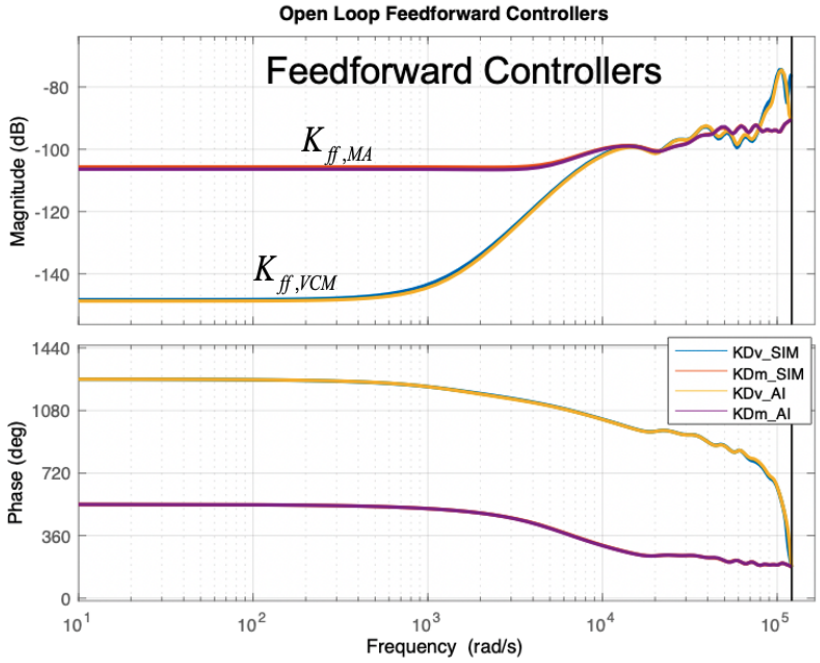

Figure 6.23: The feedforward controllers obtained using the two approaches are plotted in this figure. Both the approaches converge to very similar feedforward controllers.

to noise in the system, a perfect suppression cannot be attained. But, it is observed that the alternating iterative control design approach does slightly better than the simultaneous control design approach.

Simultaneous Design Approach for One Actuator Measurement

In this section, the time domain results for a set of one frequency response measurements of the VCM and MA, one frequency response measurement of the coupling dynamics H_d and for one seeking scenario are presented. The simultaneous feedback - feedforward data driven control design methodology obtains a feedback controller to stabilize the closed loop system and minimize the variance of the position error signal e. The feedforward controller is obtained to suppress the imparted vibration.

The feedforward controller obtained performs slightly better than the robust design scenario with multiple measurements, as shown in Figure 6.25. The primary reason for these results is that the resonant peaks considered in the coupling dynamics are close enough to be suppressed in the multiple measurements case.

In Figure 6.25, the vibration disturbance e_{dist} and the residual signal after feedforward compensation $e_{ff+dist}$ for the shortest seek is plotted, in this figure, in time domain. A feedforward suppression upto $6\times$ is observed. The seeking process ends around 0.005 seconds,

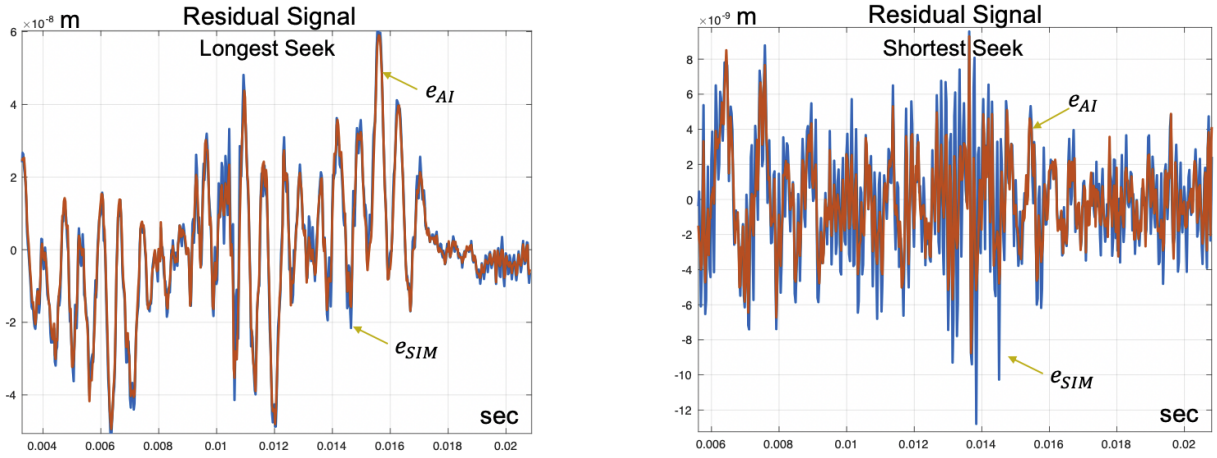

(a) Short Seek

(b) Long Seek

Figure 6.24: The residual vibration for both the approaches are compared for the longest seek and the shortest seek. It is observed that the alternating iterative control design approach does slightly better than the simultaneous control design approach to suppress the high frequency disturbance.

denoted by the vertical red line. Causal controllers are used for the feedforward suppression. These results can be further improved by considering an acausal controllers using the future information of the seeking signals for feedforward suppression. Increasing the data points used for the design process also improves the performance of the feedforward controller. The industry requirement is to achieve a suppression of $2\times$, which is comfortably achieved by the data driven feedforward controllers. To improve the suppression performance, an add-on input shaper is considered in the next chapter.

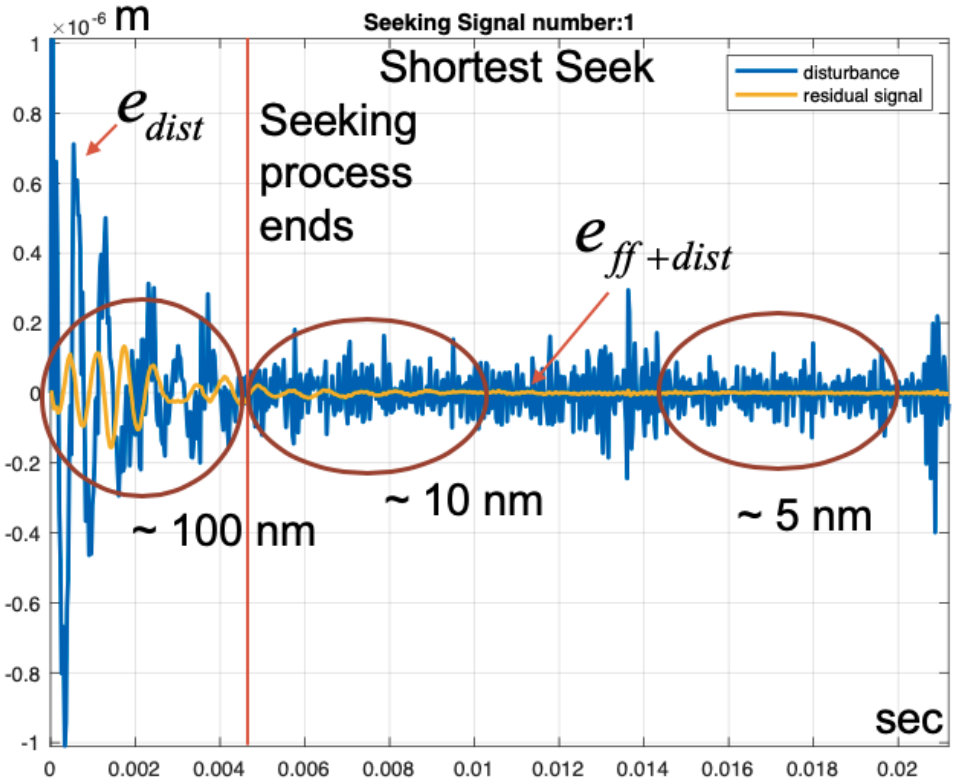

Figure 6.25: This plot is obtained for a set of one frequency response measurements for the actuators and the coupling dynamics H_d. The vibration disturbance e_{dist} and the residual signal after feedforward compensation $e_{ff+dist}$ for the shortest seek scenario is plotted, in this figure, in time domain. A feedforward suppression upto 6× is observed. The seeking process ends around 0.005 seconds, denoted by the vertical red line.

Chapter 7

Input Shaping as an add-on feedforward suppression scheme

Input shaping is an open loop time domain tool used to suppress the resonant frequencies from input signals of actuators [54, 40]. Input shapers can be used in the seeking actuator of the multi actuator drive. Seeking actuator of the multi actuator drive generates a lot of vibration during its seeking process affecting the neighboring track following actuator adversely. Input shaper reduces the generated vibration at the source, hence aiding in the feedforward suppression of the vibration signal by the track following actuator. The disadvantage of using an input shaper is that it adds a delay to the seeking process.

We consider two input shaping techniques, a zero vibration ZV input shaper and a zero vibration derivative ZVD input shaper [54, 40, 57, 61, 53]. Addition of an input shaper adds a delay to the seeking process. ZV input shaper adds a smaller delay but is less robust that the ZVD input shaper. It requires the suppressing resonant frequency to be known precisely. We present a data driven technique to locate the resonant frequency to be suppressed. Multiple frequencies can be suppressed simultaneously using an input shaper. But, each frequency adds a delay to the seeking process.

In section 7.1, the control block diagram from Figure 6.1 is shown with the addition of an input shaping block. The input shaping theory from [54, 40] is discussed in section 7.2. The residual vibration after an input shaper is used as an add-on tool to the feedforward controllers designed in chapter 6 is discussed in section 7.3.

7.1 Control Block Diagram

The input shaping tool reshapes the excitation signal causing the imparted vibration disturbance. The objective of the input shaping tool is to suppress the resonance frequencies of the coupling transfer function from the excitation signal.

In Figure 7.1, the control block diagram from chapter 6 with the addition of the input shaping block IS is shown. In this block diagram, the new seeking input signal is $u_{seek,IS}$ is

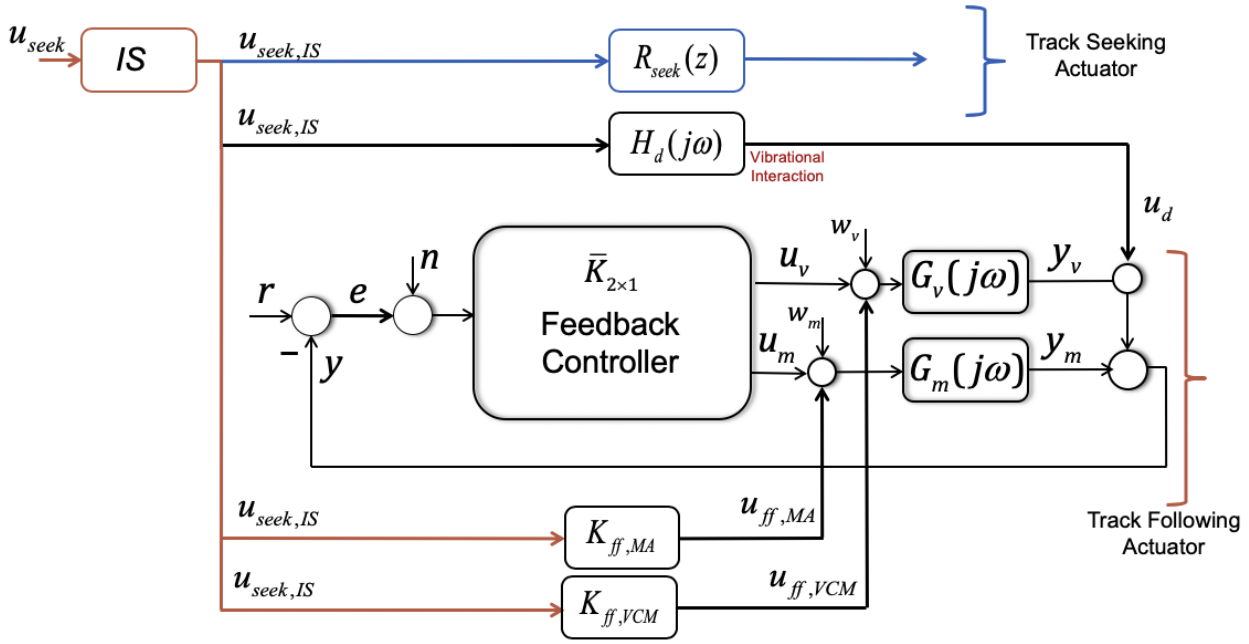

Figure 7.1: The control block diagram presented in chapter 6 with the addition of an input shaping block used to reshape the excitation signal u_{seek}

obtained using the input shaping tool. The new seeking signal does not excite the resonant frequencies of $H_d(j\omega)$. Therefore, a smaller disturbance signal u_d is imparted to the track following actuator. The input shaping tool can only suppress the resonant frequencies from the excitation signal, it cannot suppress the entire disturbance signal. The feedforward controllers $K_{ff,VCM}(z)$ and $K_{ff,MA}(z)$ are used to suppress the imparted vibration. The input shaping methodology can only act as an add-on tool to the data driven feedforward control design methodologies.

7.2 Input Shaping

Once, the feedforward controllers for VCM and MA are designed using the data driven control design methodology, an add-on input shaping tool can be designed to aid the vibration suppression process.

Input shaping is an open loop control technique to reduce vibration. It is a novel technique that works by forming an input signal that suppresses the vibration created by itself. That is, the vibration generated by the initial part of the input signal is cancelled by the vibration generated by the later part of the signal.

Any input signal can be shaped to have this property. The seeking input signal is convoluted with a carefully designed impulse train such that the resulting signal will achieve

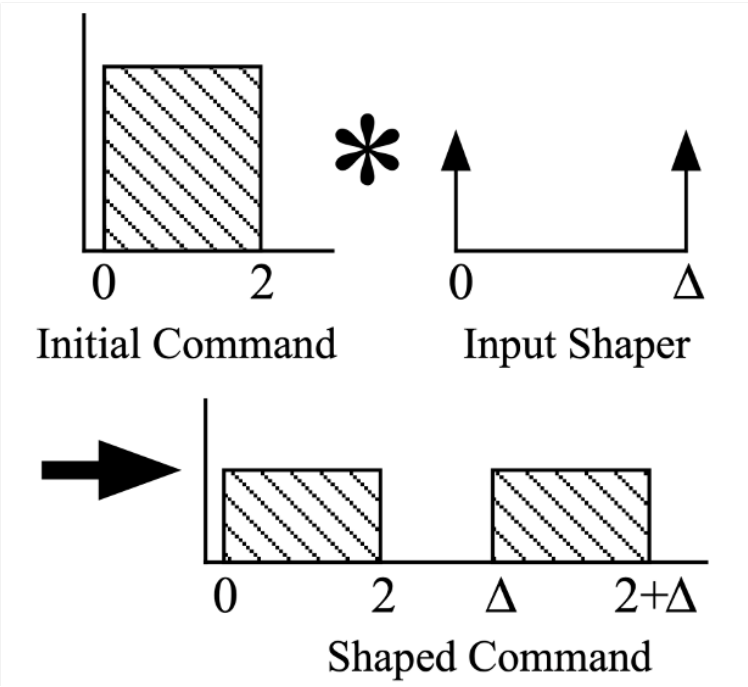

Figure 7.2: Input Shaping convolution process [61]. Here, $\Delta = \frac{2\pi}{\omega_d}$ where ω_d is the damped resonant frequency to be suppressed. Input shaping process will add a delay of Δ to the seeking process.

the required seek process and cancel the resonance vibration of the desired frequency [54]. Figure 7.2 shows the process to obtain the desired input signal after shaping.

For the purpose of input shaping we will assume the pivot timber causing vibration interaction between the seeking actuator and the track following actuator to be an under-damped second order system given by $G(z)$ in the z domain.

$$G(z) = \frac{\omega_n^2}{z^2 + 2\zeta\omega_n z + \omega_n^2} \tag{7.1}$$

Here, w_n is the resonant frequency that we want to suppress and ζ is the damping ratio.

A sequence of impulses that cause zero vibration when applied to this second order system is called an input shaper. Residual vibration obtained when a n impulse sequence is applied to the system:

$$V(\omega_n, \zeta) = e^{-\zeta\omega_n t_n}\sqrt{C(\omega_n, \zeta)^2 + S(\omega_n, \zeta)^2} \tag{7.2}$$

where,

$$C(\omega_n, \zeta) = \sum_{i=1}^{n} A_i e^{\zeta \omega_n t_i} cos(\omega_n t_i \sqrt{1-\zeta^2}) \tag{7.3}$$

$$S(\omega_n, \zeta) = \sum_{i=1}^{n} A_i e^{\zeta \omega_n t_i} sin(\omega_n t_i \sqrt{1-\zeta^2}) \tag{7.4}$$

In Eq.(7.3) and Eq.(7.4), A_i is the amplitude of the i-th impulse applied at time t_i. Our objective is to determine the impulse sequence which results in zero vibration. We will consider two input shapers.

Zero Vibration Input Shaper

Zero vibration ZV input shaper is the simplest form of an input shaper [54]. In a ZV shaper amplitudes and impulse time are obtained by solving the following equations:

$$V(\omega_n, \zeta) = 0 \tag{7.5}$$

$$\sum A_i = 1 \tag{7.6}$$

$$A_i > 0 \tag{7.7}$$

$$t_1 = 0 \tag{7.8}$$

We solve Eq.(7.5) - Eq.(7.8) for amplitudes A_i and time steps t_i for all i to obtain the impulse sequence which gives zero vibration. ZV shaper is the most simple form of an input shaper, hence the Δ delay added to the seeking process is the smallest. But, a ZV shaper is less robust to uncertainties in ω_n and ζ and does not provide good vibration suppression with uncertainties in ω_n.

Zero Vibration Derivative Input Shaper

Zero vibration derivative ZVD shaper is more robust to uncertainties in ω_n and ζ [54]. A ZVD shaper is obtained by solving the following equations:

$$V(\omega_n, \zeta) = 0 \tag{7.9}$$

$$\frac{d}{d\omega_n}(V(\omega_n, \zeta)) = 0 \tag{7.10}$$

$$\sum A_i = 1 \tag{7.11}$$

$$A_i > 0 \tag{7.12}$$

$$t_1 = 0 \tag{7.13}$$

Eq.(7.9) - Eq.(7.13) give us amplitudes and time steps such that we minimize the vibration and its derivative. ZVD shaper is more robust but also adds a larger delay Δ to the seeking process.

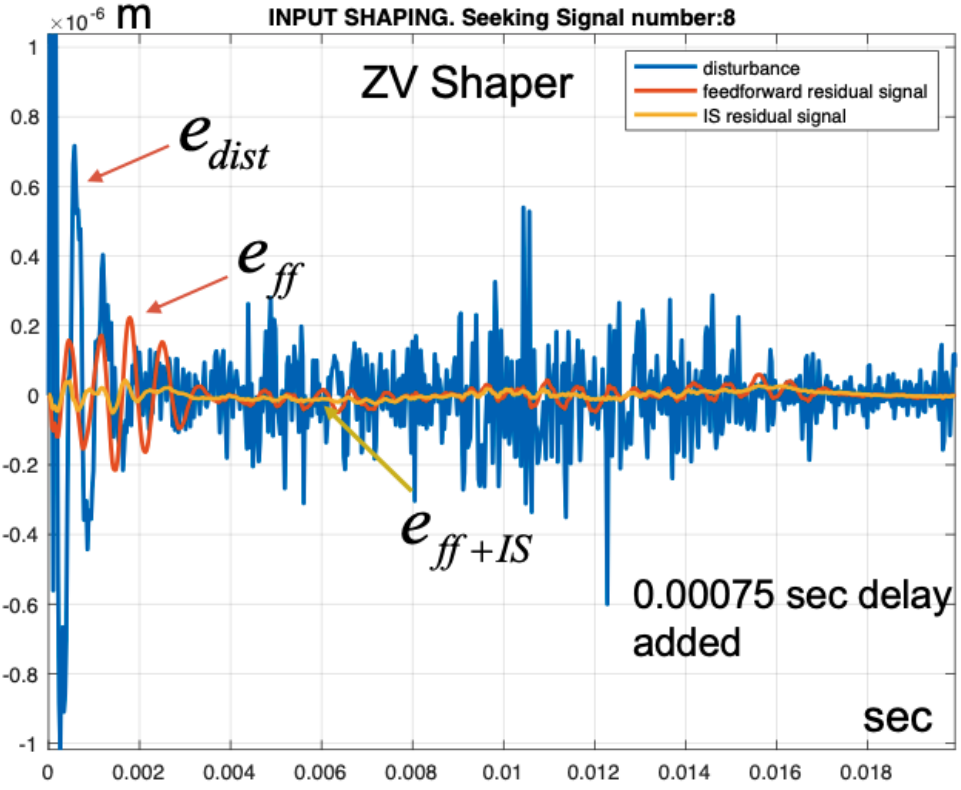

Figure 7.3: The resultant residual vibration obtained after feedforward action and ZV input shaping e_{ff+IS} is plotted versus the residual vibration obtained with only the feedforward action e_{ff} and the original vibration disturbance signal e_{dist}. The delay of ZV shaper added is 0.0007 seconds.

We implement ZV shaper and the ZVD shaper along with our SIMO data driven control methodology for multi actuator drives. We compare the performance of ZV shaper with the ZVD shaper.

7.3 Design Results

An input shaping tool will be designed for the data driven feedforward controllers obtained in chapter 6 for multiple actuator and vibration measurements. A delay is added for each resonant frequency suppressed using the input shaping tool.

Figure 7.3 plots the resultant residual vibration obtained after feedforward action and input shaping e_{ff+IS} is plotted versus the residual vibration obtained with only the feedforward action e_{ff} and the original vibration disturbance signal e_{dist}. The delay of ZV shaper added is 0.0007 seconds. The resultant residual signal obtained is less than 50 nano-meters

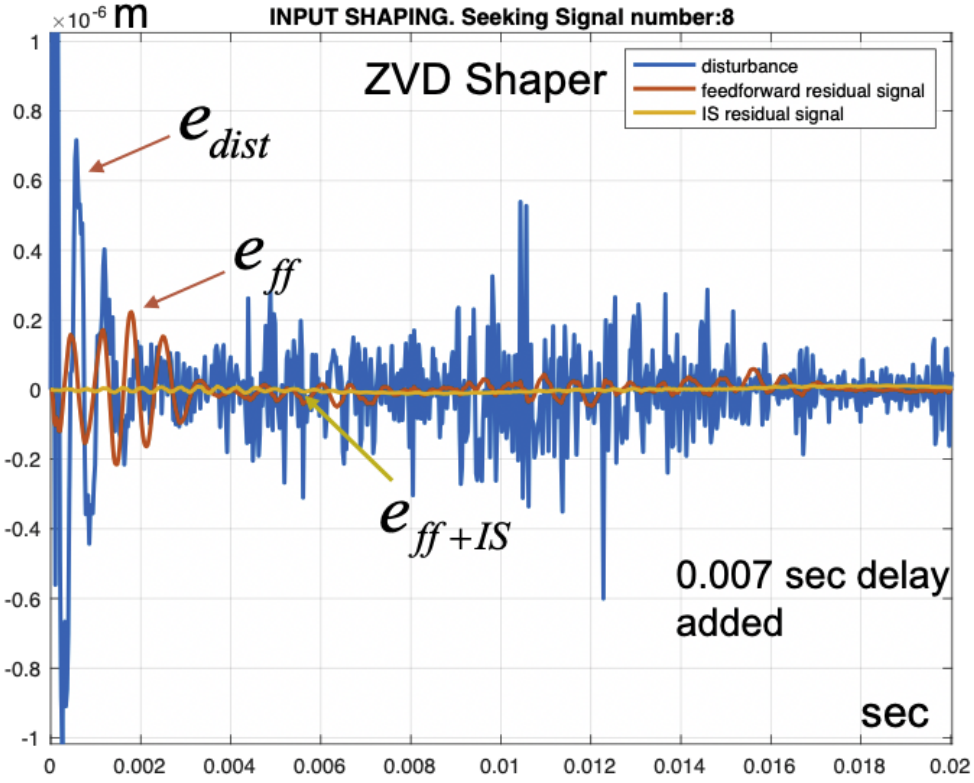

Figure 7.4: The resultant residual vibration obtained after feedforward action and ZVD input shaping e_{ff+IS} is plotted versus the residual vibration obtained with only the feedforward action e_{ff} and the original vibration disturbance signal e_{dist}. The delay of ZV shaper added is 0.007 seconds.

from the start. An additional 3× vibration suppression is achieved using a ZV shaper.

Figure 7.4 plots the resultant residual vibration obtained after feedforward action and ZVD input shaping e_{ff+IS} is plotted versus the residual vibration obtained with only the feedforward action e_{ff} and the original vibration disturbance signal e_{dist}. The delay of ZV shaper added is 0.007 seconds. The resultant residual signal obtained is less than 10 nano-meters from the start. An additional 4× vibration suppression is achieved using a ZV shaper.

Figure 7.5 plots the resultant residual vibration obtained using a ZV shaper versus the resultant residual vibration obtained using a ZVD shaper. The delay added by the ZVD shaper is 0.006 seconds more than the ZV shaper. But the suppression performance of the ZVD shaper is better than the ZV shaper. The choice between the two input shaping techniques depends on the designing constraints and acceptable delay in the track seeking process.

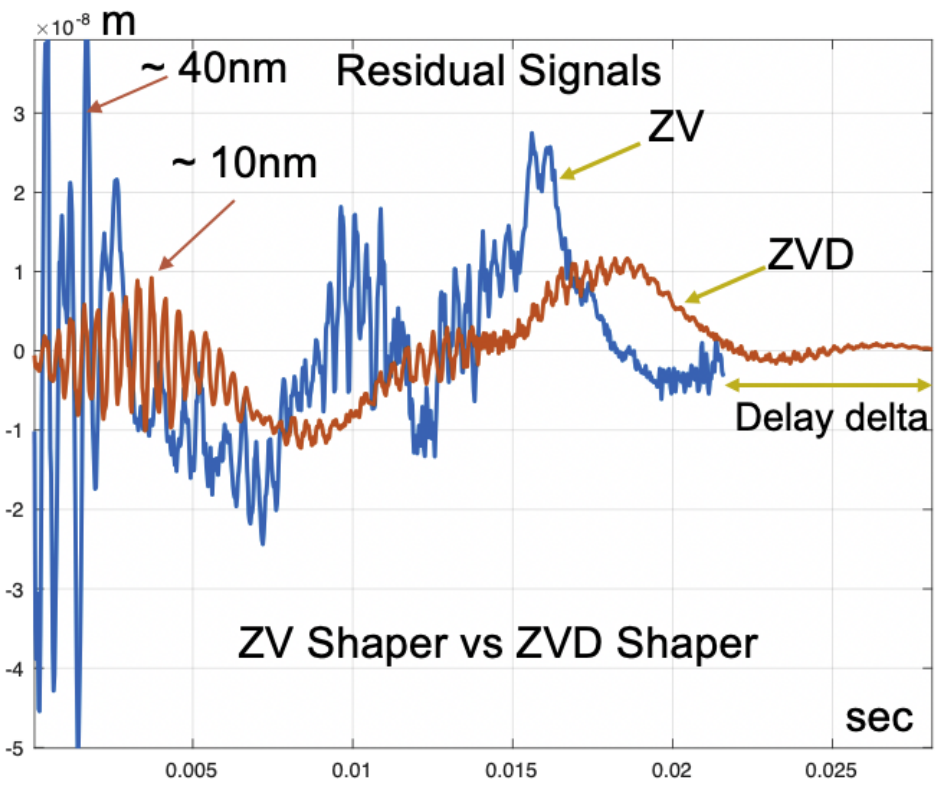

Figure 7.5: This figure plots the resultant residual vibration obtained using a ZV shaper versus the resultant residual vibration obtained using a ZVD shaper. The delay added by the ZVD shaper is 0.006 seconds more than the ZV shaper. But the suppression performance of the ZVD shaper is better than the ZV shaper.

Chapter 8

Conclusion and Future Work

8.1 Conclusion

In this dissertation, feedforward and feedback data driven control design methodologies for multi actuator drives were presented. Multi actuator drive technology was presented by Seagate in 2017. Multi actuator hard disk drive has two independent actuator arms operating on the same pivot timber. The control forces and torques generated by one actuator arm can adversely affect the performance of the second actuator arm. The objective of the data driven feedforward control design methodologies presented is to suppress the vibration interaction between the actuator arms of a multi actuator drive. The joint feedback - feedforward data driven control design methodology equips designers to obtain feedback controllers for track following design of the actuator arm as well as feedback controllers to suppress the imparted vibration simultaneously. Application of input shaping techniques is also discussed as an add-on feedforward suppression technique for the data driven feedforward control design methodology.

The data driven control design methodologies presented in this dissertation consider multiple frequency response measurements of the actuator arms, coupling transfer function imparting vibration, and the control input signals of the second actuator arm exciting the coupling transfer function. Ability to consider multiple frequency response measurements simultaneously ensures robustness of the control design. Common feedback and feedforward controllers can be generated for multiple actuator arms with similar frequency responses. Non linear behavior of an actuator can also be captured using multiple frequency response measurements.

In chapter 1, an introduction and a brief literature review of the control problems in hard disk drives was provided. The contributions of each chapter discussed in this dissertation was then discussed. Finally, some preliminary definitions relevant to the dissertation were glossed over.

In chapter 2, the structure and mechanisms of a dual stage hard disk drive and a multi actuator drive were discussed. Each actuator arm of a multi actuator drive is made up of

a dual stage servo assembly. The servo assembly comprises of a voice coil motor (VCM) and a micro actuator (MA) connected in series. The read/write head is connected to MA. The read/write head floats over a lubricated rotating disk. Each disk is made up of data tracks. The hard disk drive operates in two major modes. First, the track following mode, the read/write head follows a data track to read or write data. Second, the track seeking mode, the actuator arm sweeps through data tracks to settle onto a new desired track to begin track following. The track seeking process generates a lot of vibration, adversely affecting the performance of a neighboring actuator arm in a multi actuator drive. The control block diagram of a standard dual stage hard disk drive and a multi actuator drive was also discussed in this chapter.

In chapter 3, a data driven feedforward control design methodology was presented to design a feedforward controller to suppress vibration imparted by operation of a neighboring actuator. The control input signal of the second actuator, the frequency response measurements of the coupling interaction and the frequency response measurements of the actuator plants were used to design the controller. H_2 norm conditions were used to obtain controllers to suppress the imparted vibration (Theorem 1). H_∞ norm conditions were used to obtain initial stabilizing controllers. The H_∞ norm condition was transformed into a necessary and sufficient convex constraint (Theorem 2). Whereas, the H_2 norm condition was transformed into a locally convex objective function which was solved in an iterative manner. A mixed locally convex $H_2 - H_\infty$ norm optimization problem was formulated to design the feedforward controller to suppress the imparted vibration.

In chapter 4, feedforward controllers were designed for the track following actuator of a multi actuator drive using the data driven control design methodology from chapter 3. A sequential single-input single-output (SISO) control design methodology and a single-input multi-output (SIMO) control design methodology were presented in this chapter. In the sequential SISO approach, first a feedforward controller for VCM is designed to suppress the entire imparted vibration, then, a feedforward controller for MA is designed to suppress the residual vibration after VCM compensation. Whereas, the SIMO control design methodology designs VCM and MA feedforward controllers simultaneously.

VCM has a higher stroke but a smaller bandwidth than MA. SIMO control design methodology ensures that VCM focuses on vibration in the low frequency region and MA focuses on vibration in the high frequency region. Whereas, in the sequential SISO control design methodology VCM tries to suppress vibration across the entire frequency region. The dual stage feedforward suppression performance of the SIMO design methodology is better than the sequential SISO design methodology. But, single stage, VCM only, suppression of the sequential SISO design methodology is better than the SIMO design methodology. The sequential SISO control design methodology allows more independence to the controller order of the VCM and MA. In SIMO control design methodology, the controller order of VCM and MA needs to be the same.

In chapter 5, two joint feedback - feedforward data driven control design methodologies are presented. The objective of the data driven feedback control design is to stabilize the closed loop of the system and minimize the error of the output. H_∞ norm conditions are

used to guarantee the stability of the closed loop system and obtain an initial stabilizing controller (Theorem 3). H_2 norm objective function is used to minimize the error of the output signal (Theorem 4). According to Parseval's theorem, the total energy of the system in the frequency domain should be equal to the total energy of the system in the time domain. Therefore, H_2 norm constraints are also used to constrain the variance of signals in time domain.

The alternating iterative data driven control design methodology, alternately optimizes the feedback control design problem and the feedforward control design problem, to jointly obtain feedback controller as well as the feedforward controller for an actuator. This process allows the control design to account for the imparted vibration and corresponding feedforward suppression while designing the feedback controller. This idea is especially beneficial in systems facing constant vibration disturbance from neighboring actuators like a multi actuator drive.

The simultaneous data driven control design methodology obtains feedback as well as the feedforward controller jointly through one optimization problem (Theorem 5). The advantage of the simultaneous control design problem is the conciseness of the problem formulation achieving similar results as the alternating iterative data driven control design methodology.

In chapter 6, feedback and feedforward controllers are designed for the track following actuator of a multi actuator drive. The mixed $H_2 - H_\infty$ norm optimization problems are formulated for the feedback control design, feedforward control design and the joint feedback-feedforward control design using the simultaneous design methodology. The feedback control design results show that the closed loop transfer functions meet the H_∞ norm constraints posed. It was also observed that the variance of the position error signal of the read/write head was minimized with each iteration until the variance converged. The time domain simulations of the closed loop vibration affecting the position of the read/write head and the feedforward signal suppressing the vibration for multiple seeking scenarios were shown in this chapter. It was observed that a feedforward suppression upto $8\times$ was observed for most parts meeting the industry requirements with a good margin.

The performance of the feedback control design and the feedforward control design was compared for the alternating iterative approach and the simultaneous control design approach. Both the approaches converged to the same feedback controllers. But, the performance of the alternating iterative feedforward controller was slightly better than the feedforward controller obtained using the simultaneous control design approach. The time simulations of the feedforward suppression showed that the alternating iterative feedforward suppression achieved five percent more vibration suppression in the high frequency region. The feedforward controllers obtained for the simultaneous control design and the alternating iterative control design varied slightly in the high frequency region. Overall, both approaches performed well meeting the industry requirements with a fair margin.

In chapter 7, input shaping techniques were discussed as an add-on tool to the data driven feedforward controllers. A zero vibration (ZV) input shaper [54] and a zero vibration derivative (ZVD) input shaper [54] were used to reshape the input signal of the seeking

actuator arm exciting the coupling vibration transfer function and imparting disturbance to the track following actuator arm of the multi actuator drive. Input shaping suppresses certain frequencies from the excitation signal ensuring that the resonant frequencies of the coupling transfer function are not excited. The disadvantage of this approach is that it adds a slight delay to the seeking process, by extending the seeking input signal. The input shaper cannot be used independently as it does not suppress the bias and other frequencies of the vibration spectrum. Only a handful frequencies can be chosen to be suppressed to ensure the added delay is as small as possible. A frequency search is conducted across the frequency response of the coupling transfer function to choose the frequencies to be suppressed while adding the slightest delay as possible.

The ZVD input shaper is more robust to variations in the suppressed frequencies than the ZV input shaper. But, the ZV input shaper adds smaller delay than the ZVD input shaper. It is upon the designer to choose the number of frequencies to be suppressed and which input shaper to be used. In the results shown in chapter 7, two resonant frequencies were suppressed.

Finally, feedback and feedforward controllers for the multi actuator drive were obtained using the joint feedback - feedforward data driven control design methodology, and an add-on input shaper was designed to aid the feedforward suppression. The data driven control design methodology was obtained for multiple frequency response measurements of the track following actuator and coupling vibration and, multiple excitation signals simultaneously.

8.2 Future Work

The data driven control design methodology was obtained for multiple frequency response measurements simultaneously in chapter 3 and 5. A good extension to this theory is designing a clustering technique to obtain clusters of similar frequency response measurements. One common feedforward and feedback controllers can be designed for each cluster. Sometimes, the coupling vibration might change under certain temperature or physical conditions. The clustering technique can be coupled with a control switching technique to ensure smooth controller operation.

The online computational capabilities of devices is increasing now a days, allowing more complex operations and design online. As the data driven control design technique obtains one common controller for multiple actuator arms simultaneously, it cannot perfectly suppress the imparted vibration. An online low order adaptive feedforward controller or an online low order model predictive control can be designed to suppress any residual vibration.

The feedforward data driven methodology uses the frequency response of the excitation signal during the design process. Traditionally, adaptive controllers require an accelerometer to obtain vibration signals in real time. But, for the multi actuator drives, the excitation signal is known as the control input signal of the neighboring actuator. Hence, allowing the use of future excitation inputs to design a non-causal adaptive controller.

Bibliography

[1] D. Abramovitch and G. Franklin. "A brief history of disk drive control". In: *IEEE Control Systems* 22.3 (2002), pp. 28–42.

[2] V Agarwal and R Cloke. "Using an external spiral servo write to write spiral reference patterns to a disk to facilitate writing product servo bursts to the disk". In: (2006). US Patent 6,992,848.

[3] S. K. Aggarwal et al. "Micro-actuators for high density disk drives". In: *Proceedings of the 1997 American Control Conference (Cat. No.97CH36041)*. Vol. 6. 1997, 3979–3984 vol.6.

[4] A. Al Mamun et al. "Dual stage actuator control in hard disk drive - a review". In: *IECON'03. 29th Annual Conference of the IEEE Industrial Electronics Society (IEEE Cat. No.03CH37468)*. Vol. 3. 2003, 2132–2137 Vol.3.

[5] T. Atsumi et al. "Triple-stage-actuator system of head-positioning control in hard disk drives". In: *2012 Digest APMRC*. 2012, pp. 1–2.

[6] Takenori Atsumi et al. "Vibration Servo Control Design for Mechanical Resonant Modes of a Hard-Disk-Drive Actuator". In: *Jsme International Journal Series C-mechanical Systems Machine Elements and Manufacturing - JSME INT J C* 46 (Sept. 2003), pp. 819–827. DOI: 10.1299/jsmec.46.819.

[7] O. Bagherieh. "Estimation, Identification and Data-Driven Control Design for Hard Disk Drives". https://escholarship.org/uc/item/0998n097. PhD thesis. University of California, Berkeley, 2017.

[8] Omid Bagherieh, Prateek Shah, and Roberto Horowitz. "Application of Mixed H2/H infinity Data Driven Control Design to Dual Stage Hard Disk Drives". In: *DSCC/ASME* 51913 (2018), V003T35A002. DOI: 10.1115/DSCC2018-9094. URL: http://dx.doi.org/10.1115/DSCC2018-9094.

[9] Alexandre Bazanella, Lucíola Campestrini, and Diego Eckhard. *Data-driven Controller Design: The H2 Approach*. Jan. 2012. DOI: 10.1007/978-94-007-2300-9.

[10] Leo L. Beranek, István L. Vér, and Louis R. Quartararo. "Noise and Vibration Control Engineering: Principles and Applications". In: 2014.

[11] Allan J Connolly et al. "The design of LQG and H/sub/spl infin//controllers for use in active vibration control and narrow band disturbance rejection". In: *Proceedings of 1995 34th IEEE Conference on Decision and Control*. Vol. 3. IEEE. 1995, pp. 2982–2987.

[12] Western Digital Corp. *Three Technologies that make HDD Magic*. July 2016. URL: https://blog.westerndigital.com/hdd-magic-20tb-18tb/.

[13] Western Digital. *History of Innovation*. 2020. URL: www.westerndigital.com/company/innovations/history.

[14] Jiagen Ding, M Tomizukas, and H Numasato. "Design and robustness analysis of dual stage servo system". In: *Proceedings of the 2000 American Control Conference. ACC (IEEE Cat. No. 00CH36334)*. Vol. 4. IEEE. 2000, pp. 2605–2609.

[15] Quoc Tran Dinh et al. *Combining Convex-Concave Decompositions and Linearization Approaches for solving BMIs, with application to Static Output Feedback*. 2011. arXiv: 1109.3320 [math.OC].

[16] "Dual-stage servo systems and vibration compensation in computer hard disk drives". In: *Control Engineering Practice* 15.3 (2007). Selected Papers Presented at the Third IFAC Symposium on Mechatronic Systems (2004), pp. 291–305. ISSN: 0967-0661.

[17] R Ehrlich et al. "Hard disk drives having self-written servo burst patterns". In: (2003). US Patent 6,519,107.

[18] N. K. GUPTA. "Frequency-shaped cost functionals - Extension of linear-quadratic-Gaussian design methods". In: *Journal of Guidance and Control* 3.6 (1980), pp. 529–535. DOI: 10.2514/3.19722.

[19] T. Hara and M. Tomizuka. "Multi-rate controller for hard disk drive with redesign of state estimator". In: *Proceedings of the 1998 American Control Conference. ACC (IEEE Cat. No.98CH36207)*. Vol. 5. 1998, 3033–3037 vol.5.

[20] Cyril M. Harris. "Handbook of Acoustical Measurements and Noise Control". In: 1979.

[21] D. Hernandez et al. "Dual-stage track-following servo design for hard disk drives". In: *Proceedings of the 1999 American Control Conference (Cat. No. 99CH36251)*. Vol. 6. 1999, 4116–4121 vol.6.

[22] D. Hernandez et al. "Dual-stage track-following servo design for hard disk drives". In: *American Control Conference*. Vol. 6. Proceedings of 1999. IEEE. 1999, pp. 4116–4121.

[23] Guido Herrmann and Guoxiao Guo. "HDD dual-stage servo-controller design using a mu-analysis tool". In: *Control Engineering Practice* 12.3 (2004). Benchmarking Modelling and Control in Wastewater Treatment, pp. 241–251. ISSN: 0967-0661.

[24] R. Herzog. "Active Versus Passive Vibration Absorbers". In: *Journal of Dynamic Systems, Measurement, and Control* 116.3 (Sept. 1994), pp. 367–371.

[25] IBM. *IBM 350 disk storage unit*. 1956. URL: www.ibm.com/ibm/history/exhibits/storage/storage_350.html.

[26] Olsen J. *Hard Drives: How Do They Work?* 2020. URL: blogs.umass.edu/Techbytes/2017/04/04/hard-drives-how-do-they-work/.

[27] A. Karimi and C. Kammer. "A data driven approach to robust control of multivariable systems by convex optimization". In: *Automatica* 85.85 (2017), pp. 227–233.

[28] A. Karimi, A. Nicoletti, and Y. Zhu. "Robust H-infinity controller design using frequency domain data via convex optimization". In: *International Journal of Robust and Non Linear Control* (2016).

[29] V. Kasavajhala. "Sold state drive vs. hard disk drive price and performance study". In: *Proc. Dell Tech. White Paper* (2011).

[30] Peter Konstanzer et al. "Recent Advances in Eurocopter's Passive and Active Vibration Control". In: (May 2).

[31] Nan Liu, Jinglin Zheng, and David B. Bogy. "Thermal flying-height control sliders in hard disk drives filled with air-helium gas mixtures". In: *Applied Physics Letters* 95.21 (2009), p. 213505. DOI: 10.1063/1.3268468.

[32] P Lueng. "Process of silencing sound oscillations". In: (1936). US Patent 2,043,416.

[33] A.A. Mamun et al. *Hard Disk Drive: Mechatronics and Control*. Automation and control engineering. CRC Press, 2007. ISBN: 9781351829335. URL: https://books.google.com/books?id=PjR4tgEACAAJ.

[34] MATLAB. *version 9.10.0 (R2016b)*. Natick, Massachusetts: The MathWorks Inc., 2016.

[35] John B Moore and D Lewis Mingori. "Robust frequency-shaped LQ control". In: *Automatica* 23.5 (1987), pp. 641–646.

[36] APS MOSEK. *The MOSEK optimization toolbox for MATLAB manual. Version 7.1.(revision 28)*. 2015.

[37] Computer History Museum. "The First Disk Drive: RAMAC 350". In: *Revolution Exhibit* (2011).

[38] Prasanth B. Nair and Andrew J. Keane. "Passive Vibration Suppression of Flexible Space Structures via Optimal Geometric Redesign". In: *AIAA Journal* 39.7 (2001), pp. 1338–1346.

[39] Huy Nguyen, Omid Bagherieh, and Roberto Horowitz. "Settling Control of the Triple-Stage Hard Disk Drives Using Robust Output Feedback Model Predictive Control". In: *DSCC/ASME* 50701 (2016), V002T18A006. DOI: 10.1115/DSCC2016-9831. URL: http://dx.doi.org/10.1115/DSCC2016-9831.

[40] Q.C. Nguyen and NQO H.Q.T. "Input shaping control to reduce residual vibration of a flexible beam". In: *Journal of Computer Science and Cybernetics* 32 (June 2016), pp. 75–90.

[41] H. Numasato and M. Tomizuka. "Settling control and performance of a dual-actuator system for hard disk drives". In: *IEEE/ASME Transactions on Mechatronics* 8.4 (Dec. 2003), pp. 431–438. ISSN: 1083-4435. DOI: 10.1109/TMECH.2003.819999.

[42] Jinwen Pan, Prateek Shah, and Roberto Horowitz. "DSP Implementation of a Direct Adaptive Feedfoward Control Algorithm for Rejecting Repeatable Runout in Hard Disk Drives". In: *ISPS2016-9615* (June 2016).

[43] Jinwen Pan et al. "Triple-Stage Track-Following Servo Design for Hard Disk Drives". In: Oct. 2016, V002T18A004. DOI: 10.1115/DSCC2016-9770.

[44] Seagate Technology PLC. *Multi Actuator Technology: A New Performance Breakthrough*. [Online; posted December-2017]. Dec. 2017. URL: blog.seagate.com/homefeatured/multi-actuator-technology-a-new-performance-breakthrough/.

[45] M. A. Rahman and A. Hossain. "Design and Analysis of Servo Controller in Triple-Stage Hard Disk Drive Servo System". In: *2017 2nd International Conference on Electrical Electronic Engineering (ICEEE)*. 2017, pp. 1–4.

[46] Prateek Shah and Roberto Horowitz. "Active Vibration Rejection in Multi Actuator Drives: Data Driven Approach". In: *Dynamic Systems and Control Conference* Volume 3 (2019). DOI: 10.1115/DSCC2019-8983. eprint: https://asmedigitalcollection.asme.org/DSCC/proceedings-pdf/DSCC2019/59162/V003T17A002/6455757/v003t17a002-dscc2019-8983.pdf. URL: https://doi.org/10.1115/DSCC2019-8983.

[47] B. Shahsavari, J. Pan, and R. Horowitz. "Adaptive rejection of periodic disturbances acting on linear systems with unknown dynamics". In: *2016 IEEE 55th Conference on Decision and Control (CDC)*. 2016, pp. 1243–1248.

[48] Behrooz Shahsavari. "Direct and indirect adaptive feedforward repetitive control of servo systems". PhD thesis. UC Berkeley, 2015.

[49] Behrooz Shahsavari et al. "Adaptive repetitive control design with online secondary path modeling and application to bit-patterned media recording". In: *IEEE Transactions on Magnetics* 51.4 (2015), pp. 1–8.

[50] Behrooz Shahsavari et al. "Adaptive repetitive control using a modified filtered-x lms algorithm". In: *Dynamic Systems and Control Conference*. Vol. 46186. American Society of Mechanical Engineers. 2014, V001T13A006.

[51] Behrooz Shahsavari et al. "Limits of Performance in Systems with Periodic Irregular Sampling and Actuation Rates". In: *IFAC Proceedings Volumes* 46.5 (2013). 6th IFAC Symposium on Mechatronic Systems, pp. 347–354. ISSN: 1474-6670. DOI: https://doi.org/10.3182/20130410-3-CN-2034.00087. URL: http://www.sciencedirect.com/science/article/pii/S1474667015362376.

[52] W. M. Siebert. *Circuits, Signals and Systems*. Cambridge, MA: MIT Press, 1986, pp. 410–411.

[53] T. Singh and W. Singhose. "Input shaping/time delay control of maneuvering flexible structures". In: *Proceedings of the 2002 American Control Conference (IEEE Cat. No.CH37301)*. Vol. 3. 2002, 1717–1731 vol.3.

[54] W.E. Singhose, Warren Seering, and M. Singer. "Input Shaping for Vibration Reduction With Specified Insensitivity to Modeling Errors". In: *Proc. Japan-USA Symp. Flexible Automation* 1 (Jan. 1996).

[55] Cisco Systems. "Amount of data actually stored in data centers worldwide from 2015 to 2020 (in exabytes)". In: *Statista - the statistics portal* (2017).

[56] T. T. Tay, J. B. Moore, and R. Horowitz. "Indirect adaptive techniques for fixed controller performance enhancement". In: *International Journal of Control* 50.5 (1989), pp. 1941–1959.

[57] A. Tzes and S. Yurkovich. "An adaptive input shaping control scheme for vibration suppression in slewing flexible structures". In: *IEEE Transactions on Control Systems Technology* 1.2 (1993), pp. 114–121.

[58] Shang-Chen Wu and Masayoshi Tomizuka. "An iterative learning control design for self-servowriting in hard disk drives". In: *Mechatronics* 20.1 (2010), pp. 53–58.

[59] L. Yi and M. Tomizuka. "Two-degree-of-freedom control with robust feedback control for hard disk servo systems". In: *IEEE/ ASME transactions on mechatronics* 4.1 (1999), pp. 17–24.

[60] Fu-Ying Huang et al. "Active damping in HDD actuator". In: *IEEE Transactions on Magnetics* 37.2 (2001), pp. 847–849.

[61] Azdiana Yusop. "Input shaping for vibration-free positioning of flexible systems". In: (Jan. 2001).

[62] Kemin Zhou, John C. Doyle, and Keith Glover. *Robust and Optimal Control*. USA: Prentice-Hall, Inc., 1996. ISBN: 0134565673.